

Realization of radiobiological *in vitro* cell experiments at conventional X-ray tubes and unconventional radiation sources

Elke Beyreuther

September 2010

Realization of radiobiological *in vitro* cell
experiments at conventional X-ray tubes and
unconventional radiation sources

Der Fakultät für Chemie und Physik
der Technischen Universität Bergakademie Freiberg
genehmigte

DISSERTATION

zur Erlangung des akademischen Grades
doctor rerum naturalium
Dr. rer. nat.,
vorgelegt

von Dipl. -Nat. Elke Beyreuther
geboren am 24.06.1981 in Meissen

Gutachter: Prof. Dr. Michael Schlömann, Freiberg
Prof. Dr. Sepp Unterricker, Freiberg
Prof. Dr. Wolfgang Enghardt, Dresden

Tag der Verleihung: 10.09.2010

IN DER WISSENSCHAFT GLEICHEN WIR ALLE NUR DEN KINDERN, DIE AM RANDE DES WISSENS HIE UND DA EINEN KIESEL AUFHEBEN, WÄHREND SICH DER WEITE OZEAN DES UNBEKANNTEN VOR UNSEREN AUGEN ERSTRECKT.

Sir Isaac Newton (1643-1727)

Contents

Abbreviations	iii
List of figures	v
List of tables	vi
Abstract	vii
1 Introduction	1
2 Photon energy dependence of the relative biological effectiveness of X-rays	3
2.1 Background	3
2.2 Sources of X-radiation	5
Radiation source ELBE	5
Generation of bremsstrahlung	5
Quasi-monochromatic channeling X-rays	7
2.3 Dosimetric characterization	8
Terms and conditions for <i>in vitro</i> cell irradiations	9
Ionization chambers	10
Thermally stimulated exoelectron emission dosimeters	11
Radiochromic EBT films	12
2.4 Radiobiological characterization	13
Human mammary epithelial cells	13
Micronucleus assay	14
Determination of chromosomal aberrations	15
Immunofluorescence detection of DNA double-strand breaks	18
2.5 Realization and results	21
Investigation of a TSEE dosimetry system for determination of dose in a cell monolayer	23
Cell irradiation setup and dosimetry for radiobiological studies at ELBE	37
Relative biological effectiveness of 25 and 10 kV X-rays for the induction of chromosomal aberrations in two human mammary epithelial cell lines	53
DNA double-strand break signaling: X-ray energy dependence of residual co-localized foci of γ -H2AX and 53BP1	65
3 <i>In vitro</i> cell irradiation experiments with laser-accelerated electrons at JETI	79
3.1 Background	79
3.2 Laser wake field acceleration of electrons (LWFA)	81
3.3 Dosimetric and radiobiological characterization	82
Dosimetry with the Faraday Cup	83

First systematic radiobiological experiments	84
3.4 Application and first results	87
Establishment of technical prerequisites for cell irradiation experiments with laser- accelerated electrons	89
Laser particle acceleration for radiotherapy: A first radiobiological characterization of laser accelerated electrons	103
4 Discussion	109
5 Literature	119
Acknowledgments	129

Abbreviations

γ -H2AX	Phosphorylated form of the histone H2AX
53BP1	Tumor protein p53 binding protein 1
ATCC	American Type Culture Collection
ATM	Ataxia telangiectasia mutated
BeO	Beryllium oxide
BESSY	Berliner Elektronen-Speicherring Gesellschaft für Synchrotronstrahlung
BNC	Binucleated cell
BrdU	5-Bromo-2'-deoxyuridine
CA	Chromosomal aberration
CB	Conduction band
CIS	Cell irradiation system
CPA	Chirped pulse amplification
CR	Channeling radiation
DAPI	4',6-Diamidino-2-phenylindol, fluorescence dye
DMEM	Dulbecco's Modified Eagle Medium
DNA	Deoxyribonucleic acid
DSB	Double-strand break
EDTA	Ethylenediaminetetraacetic acid
ELBE	Electron Linac for beams with high Brilliance and low Emittance
ESRF	European Synchrotron Radiation Facility
FACS	Fluorescence activated cell sorting
FITC	Fluorescein, fluorescence dye
FPG	Fluorescence plus Giemsa staining
FWHM	Full width at half maximum
FZD	Forschungszentrum Dresden-Rossendorf
IAEA	International Atomic Energy Agency
IC	Ionization chamber
ICRP	International Commission on Radiological Protection
ICRU	International Commission on Radiation Units and Measurements
JETI	Jena Titanium:Sapphire laser system
LET	Linear energy transfer
LINAC	Linear electron accelerator
LWFA	Laser wake field acceleration
MEBM	Mammary epithelial basal medium
MN	Micronucleus / Micronuclei
p53	Tumor protein 53
PE	Plating efficiency
R ²	Coefficient of determination

Abbreviations

RBE	Relative biological effectiveness
RBE _M	Maximum low-dose RBE
SD	Standard deviation
SE/SEM	Standard error/of the mean
SF	Surviving fraction
SM-LWFA	...	Self-modulated laser wake field acceleration
SSK	German Commission on Radiological Protection (Strahlenschutzkommission)
TL	Thermoluminescence
TSEE	Thermally stimulated exoelectron emission
TxRed	Texas Red, fluorescence dye
VB	Valence band

List of figures

2.1	Floor plan of the ELBE facility	6
2.2	Bremsstrahlung and channeling X-ray production	7
2.3	Thermally stimulated exoelectron emission	11
2.4	Configuration of GafChromic® EBT dosimetry films	13
2.5	Formation of micronuclei	14
2.6	Cell cycle of eukaryotic cells	15
2.7	Formation of dicentric chromosomes	16
2.8	Formation of centric rings	17
2.9	Chromosomal deletions: formation and classification	17
2.10	Harlekin chromosomes observed in 184A1	18
2.11	Organization of eukaryotic chromosomes	19
2.12	Cellular signaling cascade following DSB incidence	20
2.13	Glow curves of the tested TSEE detectors	28
2.14	Time of irradiation response of TSEE detector type I, system I	29
2.15	Saturation and dose response of TSEE detector type I, system I	30
2.16	Fading effect for TSEE detector type IV	31
2.17	Gas flow dependence of the TSEE system response	32
2.18	Schematic drawing of the radiation physics cave at ELBE	41
2.19	Cell irradiation system at ELBE	42
2.20	Dose beam profile and the meander shaped track for dose homogeneity	43
2.21	Positioning of cell samples at the ELBE photon beam	44
2.22	Calibration curve for GafChromic® EBT films	45
2.23	Dose homogenization with 34 MV bremsstrahlung	47
2.24	Dose response curves for 34 MV bremsstrahlung and 200 kV X-rays	49
2.25	Energy dependent yields of excess fragments induced in 184A1 and MCF-12A	60
2.26	Dicentric chromosomes and centric rings in dependence on X-ray energy	61
2.27	Co-localized foci of γ -H2AX and 53BP1 detected in cell line 184A1	70
2.28	Time courses of co-localized foci after irradiation	72
2.29	X-ray energy dependent dose-effect curves for residual co-localized foci	74
3.1	Depth dose profiles of different charged particles	80
3.2	Laser wake field acceleration of electrons	82
3.3	Schematic illustration of the colony formation assay	85
3.4	Schematic drawing of the experimental setup at JETI	96
3.5	Exemplary dose distribution over the beam diameter and the cell area	97
3.6	Comparison of the actual doses and number of laser pulses applied	98
3.7	Online parameters vs. absolute doses for JETI electrons	99
3.8	Online vs. absolute dose delivered by laser-accelerated electrons	107
4.1	Illustration of the LET and its resultant consequences on DNA level	112

List of tables

2.1	Sensitivity of the studied TSEE detectors	31
2.2	Reproducibility of the TSEE detectors compared to a reference	33
2.3	Influence of the irradiation medium on TSEE detectors response	34
2.4	Effective dose rate and dose homogeneity in the region of interest	48
2.5	Yield of chromosomal aberrations observed in cell line 184A1	58
2.6	Yield of chromosomal aberrations observed in cell line MCF-12A	59
2.7	Regression coefficients and low dose RBE for excess fragments	62
2.8	Dose response of dicentric chromosomes and centric rings	63
2.9	Parameters of the photon spectra transmitted through different slide materials . . .	71
2.10	Residual co-localized foci in dependence on dose and time post irradiation	73
2.11	Fit parameters of the 24 hours dose response of residual co-localized foci	74
2.12	RBE determined on basis of the 24 hour dose responses	75
3.1	Beam parameters of conventional and laser based particle accelerators	81
3.2	Actual parameters of the laser system and the electron beam at cell position	97
4.1	RBE values determined for the various biological effects and X-ray energies	109

More than hundred years after the discovery of X-rays different kinds of ionizing radiation are ubiquitous in medicine, applied to clinical diagnostics and cancer treatment as well. Irrespective of their nature, the widespread application of radiation implies its precise dosimetric characterization and detailed knowledge of the radiobiological effects induced in cancerous and normal tissue. Starting with *in vitro* cell irradiation experiments, which define basic parameters for the subsequent tissue and animal studies, the whole multi-stage process is completed by clinical trials that translate the results of fundamental research into clinical application. In this context, the present dissertation focuses on the establishment of radiobiological *in vitro* cell experiments at unconventional, but clinical relevant radiation qualities.

In the first part of the present work the energy dependent biological effectiveness of photons was studied examining low-energy X-rays (≤ 50 keV), as used for mammography, and high-energy photons (≥ 20 MeV) as proposed for future radiotherapy. Cell irradiation experiments have been performed at conventional X-ray tubes providing low-energy photons and 200 kV reference radiation as well. In parallel, unconventional quasi-monochromatic channeling X-rays and high-energy bremsstrahlung available at the radiation source ELBE of the Forschungszentrum Dresden-Rossendorf were considered for radiobiological experimentation. For their precise dosimetric characterization dosimeters based on the thermally stimulated emission of exoelectrons and on radiochromic films were evaluated, whereas just the latter was found to be suitable for the determination of absolute doses and spatial dose distributions at cell position. Standard ionization chambers were deployed for the online control of cell irradiation experiments. Radiobiological effects were analyzed in human mammary epithelial cells on different subcellular levels revealing an increasing amount of damage for decreasing photon energy. For this reason, the assumed photon energy dependence was reconfirmed for a cell line other than human lymphocytes, an important finding that was discussed on the 2007 Retreat of the German Commission on Radiological Protection.

After successful finalization of the photon experiments the focus of the present dissertation was directed to the realization of *in vitro* cell irradiation experiments with laser-accelerated electrons. This research was carried out in the frame of the project onCOOPTics that aims on the development of laser-based particle accelerators, which promise accelerators of potentially compact size and more cost-effectiveness suitable for a widespread medical application, especially for high precision hadron therapy. The unique properties, i.e., the ultrashort bunch length and resultant ultrahigh pulse dose rate, of these unconventional particle accelerators demand for extensive investigations with respect to potential effects on the dosimetric and radiobiological characterization. Based on the experiences gained at ELBE first experiments on the radiobiological characterization of laser-accelerated electrons have been performed at the Jena Titanium:Sapphire laser system. After beam optimization, a sophisticated dosimetry system was established that allow for the online control of the beam parameters and for the controlled delivery of dose to the cell sample. Finally, worldwide first systematic *in vitro* cell irradiation experiments were carried out resulting in a reduced biological effectiveness for laser-accelerated electrons relative to the 200 kV X-ray reference, irrespectively on the biological effect and cell lines examined. These successful results are the basis for future *in vivo* studies and experiments with laser-accelerated protons.

1 Introduction

“On a new kind of rays“ - the famous report published in 1896 by Wilhelm Conrad Röntgen does not just announce the discovery of the “X-radiation“, but also introduce the first medical application by showing a radiography of his wife’s hand on a photographic plate [103]. More than one hundred years later X-rays and other kinds of ionizing radiation are omnipresent in medicine, used for diagnostic purposes and radiotherapeutic treatment as well. However, improvements and further technological developments are still conceivable, for example by introducing new radiation qualities that promise the reduction of radiation side-effects or the enhancement of the tumor control rate. Before a new radiation quality can be applied in medicine their radiobiological effects on cancer and normal tissue have to be investigated in detail. Starting with *in vitro* cell irradiation experiments, which are followed by tissue and animal studies and completed by clinical trials that translate the results of the fundamental research into medical application. Therefore, the radiation qualities of interest have to met several interdependent requirements in order to allow for radiobiological studies:

- (i) the development, supply and adjustment of an adequate radiation source,
- (ii) their precise physical and dosimetric characterization and
- (iii) the determination of its radiobiological effectiveness by means of an appropriate biological object and effect.

A characteristic feature of radiobiological studies is the examination of one radiation quality (X) in comparison to a reference (R) in order to determine the *Relative Biological Effectiveness* (RBE), which is defined as the inverse ratio of the absorbed doses (D) producing the same effect (E) [57]:

$$(1) \quad RBE = \frac{D_R}{D_X} \Big|_{E_X=E_R}.$$

Main reasons for this approach are the elimination of influences arising from the diversity of biological samples, fluctuations of the biological response and varying experimental, i.e., environmental, conditions. On the other side, there exists a large amount of experimental and epidemiological data about the radiogenic cancer risk of high-energy γ -radiation, which is recommended as reference by the International Commission on Radiological Protection (ICRP) [57]. In consequence, photons in this energy range, either provided by ^{60}Co γ -emitter (1.17 and 1.33 MeV) or ordinary $\cong 200$ kV X-ray tubes, are used as reference radiation. Keeping in mind that 200 kV X-rays are twice as effective as high-energy γ -rays, it is essential for every declaration of the RBE to specify the appropriate reference radiation source.

In practice, radiobiological studies are performed as two-armed studies investigating the same biological effect for the examined and the reference radiation source in parallel. Hence, the requirements (i-iii) have to be fulfilled for both radiation qualities. Moreover, the concept of RBE requires a sufficient number of targets irradiated under similar conditions (e.g., beam properties, irradiation

geometry, environmental conditions etc.) at both radiation qualities in order to overcome the varying radiosensitivity of biological objects. Whereas this requirement might not be the crucial factor for *in vitro* cell studies, it may be a problem for animal experiments or clinical trials. Consequently, *in vitro* studies are not only the first step for the establishment of a new radiation quality, but also an important step for the definition of experimental conditions of the subsequent ones.

Taken into account these aspects, two issues, both dealing with the realization of *in vitro* cell irradiation experiments at conventional X-ray tubes and unconventional radiation sources of potential medical interest, were studied in the present dissertation:

- Photon energy dependence of the relative biological effectiveness of X-rays.
- Establishment of *in vitro* cell irradiation experiments with laser-accelerated electrons.

The research work of the present dissertation was carried out in the context of the project “Radiation induced cell damage“ at the Institute of Radiation Physics of the Forschungszentrum Dresden-Rossendorf (FZD) in a close cooperation with the **OncoRay** - Center for Radiation Research in Oncology. OncoRay is a joint institution of the FZD, the Dresden University of Technology and the university hospital Carl Gustav Carus combining their physical, biological and medical knowhow for radiation research in oncology, for example for tumor diagnostics and treatment.

The examination of the photon energy dependence of the RBE was a continuation of a research project that was initiated several years ago aiming primarily on the investigation of the RBE of low-energy X-rays. In the framework of the present dissertation the research on this particular topic was continued, but extended with regard to the applied energy range and radiation sources, to the selective improvement of the dosimetry and to the establishment and investigation of a second human cell line as well as the analysis of further biological effects. The background, methods and results associated with the realization of this multidisciplinary work are described in section 2.

After the successful finalization of the first issue, the research of the present dissertation was concentrated on a completely new scientific question: the development of laser-based ion accelerators for radiotherapeutic application. For this reason, the joined project onCOOPTics was started in 2007 aiming on both the technological development of the new laser technology and on the physical and biological characterization of the generated particle beams. The multidisciplinary research linked with the project onCOOPTics is carried out by two research centers - OncoRay in Dresden, responsible for the comprehensive characterization and future clinical implementation of this new radiation quality, and **ultra optics** in Jena, responsible for the technological development of the laser system and the auxiliary equipment. In this context, section 3 of the present dissertation comprises the completion of the requirements (i-iii) mentioned above for the realization of radiobiological experiments with laser-accelerated electrons. The results obtained for the investigation of the photon energy dependence of the RBE of X-rays and during the establishment of *in vitro* cell irradiation experiments with laser-accelerated electrons are discussed in section 4.

2 Photon energy dependence of the relative biological effectiveness of X-rays

2.1 Background

In 2002 the German Parliament opted for the introduction of a nationwide mammography screening program in Germany and started a continuing cost-benefit discussion on the general application of mammography. At the same time, the group of Frankenberg *et al.* [32] published their controversial study on the biological effectiveness of mammographic X-rays. Analyzing neoplastic transformations of CGL1 human hybrid cells as one type of DNA damage, this group found an RBE of about 4 comparing 29 kV X-rays and conventional 200 kV photons as reference. Taken into account the implications for the radiation risk estimation, especially for mammography, this high RBE value was discussed critically. Moreover, the whole experiment of Frankenberg *et al.* was repeated and reevaluated [40, 45] in order to validate their finding. And indeed, values significantly higher than one were confirmed for 29 kV X-rays compared to 220 kV X-rays [40], a $^{90}\text{Sr}/^{90}\text{Y}$ radioactive source and a simulated atomic bomb spectrum [45], respectively. Furthermore, the analysis of several *in vitro* studies [41, 68, 75, 86, 93, 108, 112, 113, 119] lead also to the conclusion that soft X-rays are more effective per unit dose than higher energy photons. Contrary to these findings is the photon energy independent radiation weighting factor (w_R) of 1 as specified by the ICRP [56], which presumes that photons of all energies will cause similar radiation effects in the considered tissue or organ. Systematic investigations on the photon energy dependence of the RBE were performed so far by analyzing chromosomal aberrations induced in human lymphocytes by monochromatic synchrotron X-rays in the energy range of 1.83 - 40 keV [41, 68, 108, 112]. The obtained chromosomal aberrations were considered relative to those induced by 200 kV X-rays or MeV photons as reference revealing RBE values inversely proportional to the photon energy, i.e., increasing for decreasing energy [48]. The maximum RBE was found at 6.9 keV, whereas the further reduction of the photon energy results in a minimum at 2.1 keV [108] and a significant rise for energies below [48]. The most likely explanations for this finding are the range and local energy deposition of the generated secondary electrons in irradiated matter (section 4).

In the framework of the ongoing discussion on the radiation risk of mammographic X-rays a close cooperation between the research project “Radiation induced cell damage“ at the Institute and Division of Radiation Physics at the Forschungszentrum Dresden-Rossendorf (FZD) and the OncoRay group “Radiobiology of normal tissues and radiation protection“ of the Medical Faculty Carl Gustav Carus at the Dresden University of Technology was initiated. Combining the physical and dosimetric knowhow of the FZD project with the radiobiological expertise of the hospital group, the primary aim of this cooperation was the investigation of the relative biological effectiveness of low-energy X-rays utilizing the soft X-ray (10 and 25 kV) as well as the 200 kV X-ray reference tube of the Medical Faculty. At first, the radiation effects of 25 kV X-rays were investigated in

human fibroblasts and human keratinocytes showing a slightly enhanced RBE relative to 200 kV X-rays. After the successful implementation of a precise dosimetry for the challenging ultra-soft X-rays radiobiological studies have been performed with 10 kV X-rays. Although this X-ray energy is not relevant for clinical purposes, due to their strong attenuation in air and even more in tissue, 10 kV X-rays were chosen for systematic reasons and due to their mean energy of ≈ 7 keV close to the energy of the maximum RBE. Furthermore, the human mammary breast epithelial cell line MCF-12A was established in accordance to the underlying scientific question. Based on these requirements radiobiological studies aiming on the determination of the relative biological effectiveness for 10 kV and 25 kV X-rays relative to 200 kV X-rays were performed analyzing the cellular survival and the induction of micronuclei in MCF-12A [74, 75]. Parallel to the investigation of low-energy X-rays the project “Radiation induced cell damage“ focused also on the feasibility of radiobiological *in vitro* experiments at the radiation source ELBE (Electron Linac for beams with high Brilliance and low Emittance) of the FZD (section 2.2.1). ELBE delivers electron beams of up to 40 MeV, which can be deployed to generate secondary radiation of radiobiological interest, like neutrons, high-energy bremsstrahlung and quasi-monochromatic channeling X-rays [34]. Mainly the development of the latter was of special interest for radiobiological experimentation, since tunable quasi-monochromatic X-rays in the energy range of 10 - 100 keV [3, 73] will allow for a detailed and systematic investigation of the relative biological effectiveness of X-rays.

Within the scope of the present dissertation, the investigation of the relative biological effectiveness of low-energy X-rays with conventional X-ray tubes was pursued but extended by the establishment of a second human mammary epithelial cell line (section 2.4.1). Furthermore, two additional radiation effects, chromosomal aberrations (sections 2.4.3, 2.5.3) and DNA double-strand breaks (DSB) (sections 2.4.4, 2.5.4), were analyzed providing information on the radiation damage on sub-cellular level. In addition to these radiobiological experiments the technological development of the channeling X-ray source (section 2.2.3) was also advanced. Moreover, selective improvements of the challenging dosimetry of soft X-rays have been achieved by evaluating different types of dosimeters for the precise determination of the absolute dose administered to a cell monolayer: the detection of thermally stimulated exoelectron emission (TSEE) (sections 2.3.3, 2.5.1) and the application of radiochromic EBT films (sections 2.3.4, 2.5.2). Beside low-energy X-rays, the research on the photon energy dependence of the RBE of X-rays was also focused on high-energy photons of up to 34 MV. Photons of this and even higher energies (≈ 50 MV) are better focusable to narrow pencil beams of a few centimeter in diameter [123] allowing for the idea of a scanned photon beam, which may be of benefit for high-precision radiotherapy. In the present work the ELBE electron beam was used to generate high-energy photons of up to 34 MV (section 2.2.2) by means of bremsstrahlung production. Optimized with respect to the physical and dosimetric properties required for radiobiological experiments, e.g., sufficient beam spot size and adequate dose rate, high-energy photons of 20 MV and 34 MV were deployed later on for radiobiological *in vitro* cell irradiation experiments analyzing the induction of micronuclei (section 2.4.2, 2.5.2).

The following sections outline the basic principles and background information required to under-

stand but not mentioned in the publications (section 2.5) that comprises the experimental studies performed in the context of the present dissertation. According to the consecutive requirements for radiobiological experimentation given above section 2.2 includes the different radiation sources, 2.3 their dosimetric and 2.4 their biological characterization. Finally, in section 2.5, the realization and the results of the different studies are presented in the corresponding publications.

2.2 Sources of X-radiation

In dependence on the underlying scientific question three different radiation sources were applied in the present work to study the relative biological effectiveness of X-rays in dependence on photon energy. Irradiations with 10 kV and 25 kV soft X-rays as well as with the 200 kV X-ray reference were performed with conventional X-ray tubes provided at the “Klinik und Poliklinik für Strahlentherapie und Radioonkologie“ of the university hospital Carl Gustav Carus. By contrast, the generation of unconventional high-energy bremsstrahlung and quasi-monochromatic channeling X-rays demand for high-energy electrons available at the radiation source ELBE.

Radiation source ELBE

The radiation source ELBE of the Forschungszentrum Dresden-Rossendorf [30, 34] provides monoenergetic continuous wave electron beams with energies up to 40 MeV and average currents up to 1 mA at a micropulse repetition rate of 13 MHz [30]. The beam may be applied either directly for radiation experiments or for the production of secondary radiation such as bremsstrahlung (continuous photon spectrum), quasi-monochromatic channeling X-rays, neutrons or positrons [30]. The floor plan of the ELBE accelerator hall with associated experimental rooms is shown in Figure 2.1. Concerning radiobiological experiments, two types of secondary radiation, both are produced in the radiation physics cave of ELBE (Layout, cf. section 2.5.2), have to be considered:

- High-energy bremsstrahlung where the available photon energies extend from the keV region up to the electron beam energy.
- Quasi-monochromatic X-rays in form of channeling radiation which offers the possibility for more detailed investigations of the photon energy dependence of the RBE.

Generation of bremsstrahlung

Generally, bremsstrahlung is produced by focusing accelerated electrons on a (usually metallic) target. During the stopping process, the incoming electrons successively lose small portions of their kinetic energy due to ionization of the medium or large portions of energy due to inelastic scattering from target atoms what results in the emission of bremsstrahlung photons. Ionization losses are converted to heat (99 %), while bremsstrahlung photons of sufficient energy may partially escape the target and form a forward directed cone of polychromatic radiation. Whereas the energy of a single bremsstrahlung photon depends on the momentum transfer to the target atoms, i.e., on the interaction distance between electron and atomic nucleus (Fig. 2.2a).

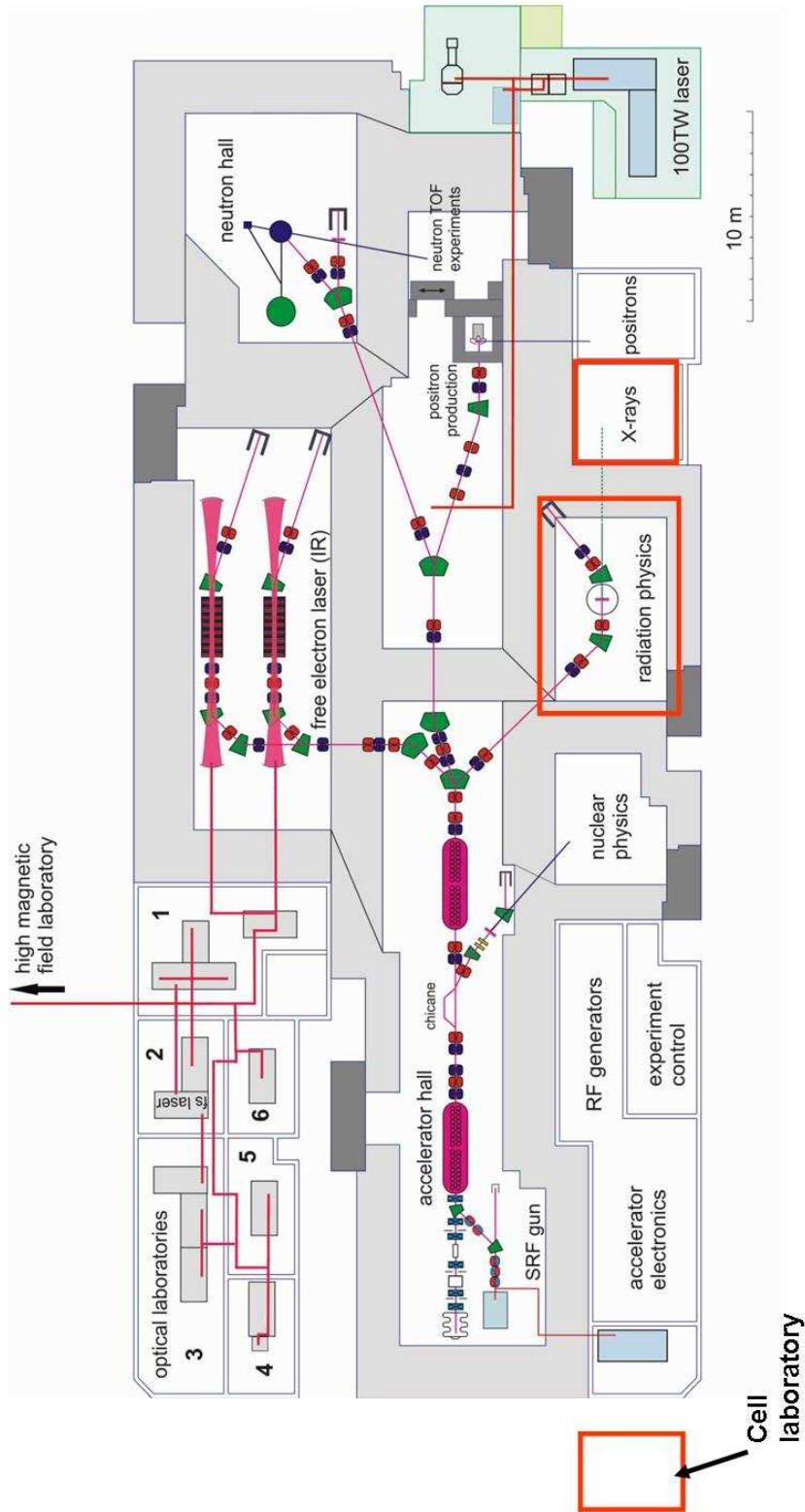


Figure 2.1: Floor plan of the ELBE facility showing the accelerator hall, the hall of the free-electron lasers (FEL) with associated optical laboratories, the 100 TW laser laboratory and different caves for experiments with photon, neutron and positron radiation. Radiobiological experiments are carried out in the radiation physics cave, in the X-ray laboratory, where the 200 kV reference source is placed, and in the cell laboratory situated aside from the accelerator complex (all framed in red) [30].

Collisional ionization of medium atoms due to expelling of electrons from inner atomic shells leads, additionally to bremsstrahlung, to the emission of characteristic X-rays because the vacancies are filled up by electron transitions from outer atomic shells to inner ones. The excess of binding energy is radiated into full solid angle in form of characteristic X-rays (Fig. 2.2a). Therefore, the continuous bremsstrahlung spectrum is superimposed by characteristic X-ray lines of the target material.

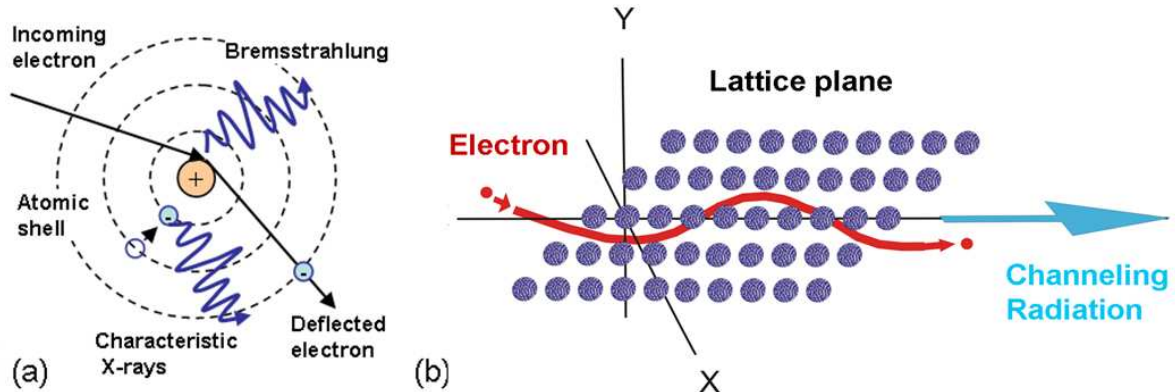


Figure 2.2: a) Generation of bremsstrahlung and characteristic X-rays by interaction of the incoming electrons and the target material atoms. b) Production of quasi-monochromatic X-rays by electron channeling through a diamond crystal.

Comparing the bremsstrahlung production in conventional X-ray tubes and at ELBE differences occur just in the target material, the filtration and the electron energy applied. For example, tungsten targets are used in the X-ray tubes and a thin aluminum foil was deployed at ELBE to generate bremsstrahlung, respectively. Furthermore, the production of bremsstrahlung at ELBE was accompanied by the transmission of high-energy electrons (≤ 34 MeV) through the aluminum target. Although separated from the photon beam by means of a deflecting dipole magnet and absorption in the beam dump, these electrons might contribute to radiation background, e.g., by bremsstrahlung production in the beam line walls. In contrast, electrons in the keV range are stopped in the thick target material of an X-ray tube. The realization and results of the experiments with high-energy bremsstrahlung at ELBE are presented in section 2.5.2, detailed information on the X-ray tubes are given in sections 2.5.3 and 2.5.4 together with the associated radiobiological findings.

Quasi-monochromatic channeling X-rays

Channeling radiation (CR) is generated by relativistic charged particles at traveling through a single crystal along a periodic structure, i.e., a crystallographic axis or plane. At ELBE, relativistic electrons transmit a diamond single crystal of thickness 40 - 200 μm along an appropriate crystallographic plane, e.g., the (110) plane (Fig. 2.2b). At sufficiently small entrance angles of the beam electrons with respect to the crystallographic planes considered, they are trapped into the attractive average planar potential and forced to an oscillatory motion along this plane through the crystal. During this so-called channeling process, which is similar to an accelerated sine-like motion, the trapped beam electrons emit CR photons. Since the velocity of the electrons is approximately

that of light, the energy of CR is shifted according to the Lorentz transformation into the X-ray domain, and the rather intense quasi-monochromatic photon flux is also directed into a forward cone. Furthermore, the photon energy of CR can easily be tuned within an energy range of about 10 - 100 keV by only changing the energy of the electron beam (range: $\approx 8 - 40$ MeV).

For medium electron energies available at ELBE the description of the channeling process given above is not complete to deduce all characteristic features of CR, because their quantum nature has been neglected so far. In reality, the mentioned transverse oscillations are only allowed at given frequencies. This means that the trapped electrons occupy only discrete bound channeling states. Consequently, the emission of quasi-monochromatic CR lines has to be understood as resulting from transitions between these bound states. At defined beam properties, even a selective occupation of energy levels is feasible, which leads to an increase of the intensity of dedicated CR lines [3, 129].

The present work aims at the development and adjustment of the CR source to facilitate *in vitro* cell irradiations with monochromatic instead of polychromatic X-rays in order to investigate the dependence of the RBE on the photon energy in detail (section 2.5.2). Such experiments might of course also be performed at synchrotron radiation facilities, e.g., at the ESRF (European Synchrotron Radiation Facility) in Grenoble or at BESSY (Berliner Elektronen-Speicherring Gesellschaft für Synchrotronstrahlung) in Berlin. The compact size and availability at reasonable costs promise, however, several advantages of CR sources compared with large synchrotrons. The complete equipment required for a CR source, an electron injector, an acceleration cavity and a goniometer chamber for crystal positioning and adjustment, may fit into a 10 - 15 m long laboratory, whilst an electron storage ring, for example at the ESRF, has a circumference of 844 m.

2.3 Dosimetric characterization

According to the requirements (i-iii) listed above for radiobiological experimentation the next step includes the precise physical and dosimetric characterization of the different radiation qualities. In the context of the present dissertation, the term dosimetry includes the very precise determination of the absolute dose delivered to a few micrometer thick adherent cell monolayer inside a cell culture vessel. Otherwise, the experiment conditions at the radiation source ELBE (section 2.3.1) demand for an online dose monitoring and the measurement of the spatial dose distribution over the cell covered area. Whereas the former allows for the control of the irradiation, i.e. the delivery of prescribed doses, the latter is necessary to reveal potential dose deviations. Moreover, the high attenuation of soft X-rays through the cell culture vessel bottom has also to be considered.

Three types of dosimeters were evaluated for the different dosimetric requirements in the present work. Standard ionization chambers (IC) (section 2.3.2) offer the unique feature of an online dose readout and are calibrated for absolute photon dosimetry. However, IC provide the integrated dose over a sensitive volume that usually exceed the volume of a cell. In consequence, ionization chambers were deployed in the present work for the online control of the ELBE experiments, measuring the direct beam exposure as well as the radiation background in the radiation physics cave. An exception was the precise dosimetric characterization of soft X-rays, where the soft X-ray chamber was used to determine the absolute dose at cell position under consideration of the varying cell sample

geometries (sections 2.5.3 and 2.5.4). In addition, TSEE detectors and radiochromic films were considered for absolute dosimetry at ELBE and for the measurement of spatial dose distributions in different radiation fields. TSEE detectors offer the main advantage of a just few nanometer thick sensitive volume at the surface enabling the sampling of spatial dose distributions not only laterally but also as depth dose distributions within the $\approx 10 \mu\text{m}$ thick cell monolayer (section 2.3.3). Furthermore, the TSEE detectors allow for the measurement of absolute doses at interfaces and of dose gradients, especially for ultra-soft X-rays after transmission through the cell culture vessel bottom. The radiochromic films (section 2.3.4) in turn are easy to handle and available in flexible and large sizes, suitable for the measurement of spatial dose distributions of extended and variable beam spots. Both, the TSEE detectors as well as the radiochromic films are feasible for the retrospective determination of absolute doses administered to a cell monolayer.

Terms and conditions for *in vitro* cell irradiations

The precise dosimetric characterization of the varying radiation qualities used in the present work demands for the consideration of their specific physical and technical properties, like photon beam attenuation and intensity variations of the ELBE beam, respectively.

Regarding the soft X-rays, the beam attenuation in different materials play an important role for the determination of absolute doses administered to a cell monolayer adherent on a cell culture vessel bottom. That means, especially for 10 kV X-rays, that both, the influence of the vessel bottom as well as dose rate deviations arising from small variations of the bottom thickness were taken into account [73]. For all X-ray energies GEANT4 simulations [35] and dosimetric measurements were performed in parallel in order to understand the influence of different materials, namely glass and plastic, on the photon spectra (cf. section 2.5.4). Moreover, the cell samples were irradiated upside down at the vertical beam (from above) to minimize the material in and the influence on the X-ray spectra (sections 2.5.3, 2.5.4).

At ELBE, the photon beam attenuation might also be a challenge for the experimentation with quasi-monochromatic channeling X-rays, whereas for high-energy bremsstrahlung photons this influence can be neglected. However, some practical limitations for radiobiological experiments at ELBE arise from the radiation protection directives and the reproducibility of the beam parameters. Concerning the first, the directives demand for a waiting period of 20 minutes after switching off the beam before entering the radiation physics cave and exchanging the cell samples. In consequence, the irradiation procedure as practiced at conventional X-ray tubes, where cell samples that were currently not irradiated are stored outside the experimental room and exchanged individually, was not reasonable. To overcome this limitation a cell irradiation system (see section 2.5.2) was constructed that allows the storage and remote-controlled irradiation of up to 27 cell samples of different sample geometry. The second limitation for radiobiological experimentation at ELBE is related to the intensity of the ELBE electron beam that might shift during and between the experiments and cause intensity or dose rate variations of the secondary radiation (CR and bremsstrahlung). By contrast, photon beams with stable and reliable properties are delivered at conventional X-ray tubes allowing for the precise delivery of prescribed doses to the cell target by control of the irradiation

time. In order to compensate for potential dose rate variations at ELBE, the dose delivery has to be monitored during irradiation and the administered doses have to be determined for each cell sample individually. The first requirement was fulfilled with the help of a Farmer ionization chamber (section 2.3.2), that was positioned on beam axis behind the cell samples providing an online dose signal relative to the absolute dose delivered to the cells (section 2.5.2). However, since the Farmer IC is not applicable for the determination of absolute doses at cell position (see above), a second dosimeter has to be implemented in order to fulfill this necessary requirement for dose-effect curves and RBE determinations. Therefore, two dosimeters based either on the thermally stimulated emission of exoelectrons (section 2.3.3) or on the coloring of radiochromic films (section 2.3.4) were evaluated for the measurement of absolute doses under the given experimental conditions.

Another challenge at ELBE is the varying and sometimes quite high radiation background in the radiation physics cave. Main reasons are beam loss during tuning and optimization, bremsstrahlung necessarily produced whenever an electron interacts with matter and tertiary radiation produced by photo nuclear reactions, e.g., (γ, n) , (γ, p) of higher energy photons with matter. During the cell irradiation, the background was monitored with a Farmer IC and a neutron dosimeter positioned next to the cell samples (section 2.5.2). Supplementary cell samples (controls) were prepared, but not irradiated, in order to determine the impact of the radiation background, the ambient conditions and the whole procedure on the cell and the examined biological effect.

Ionization chambers

Ionization chambers are in principle two electrodes of opposite polarity, which surround an ionizable medium, mostly gas. Subsequent to radiation incidence the gas molecules are ionized and the generated charged particles (ions and electrons) move to the appropriate electrodes and an ionization charge proportional to the exposed radiation dose is measurable. The detection sensitivity and working energy range of an IC depend substantially on the applied gas (e.g., He, H₂, N₂, O₂, air) and its pressure, on the size of the sensitive volume and the sensitivity of the electronic. Furthermore, the chambers have to be constructed in such a way that either the secondary electron equilibrium or the Bragg-Gray principle is fulfilled. The former presumes that the same number of electrons with identical energy distribution enter and exit the sensitive volume. The latter, most frequently applied for higher energy particles, demand for ionization chambers being small enough to avoid influences on the secondary particle flux and its energy distribution.

Generally, the various types of ionization chambers are widely-used as standard dosimeters for medical purposes providing absolute doses and the possibility of dose monitoring during radiotherapy. In the present work, three different types of IC were applied for the dosimetric characterization of differing radiation qualities. A soft X-ray IC with a small sensitive volume of 0.02 cm³, a very thin flat beryllium entrance window and an applicable photon energy range of 10 to 100 kV was applied for 25 kV and 10 kV X-ray dosimetry. Whereas the 200 kV reference radiation and bremsstrahlung photons of higher energy were characterized by a semi flex (sensitive volume: 0.3 cm³, photon energy range: 30 kV - 50 MV) and a Farmer ionization chamber (sensitive volume: 0.6 cm³, photon energy range: 30 kV - 50 MV). Corrected for ambient air temperature and pressure as well as the different

cell sample and experiment geometries, the IC provide the absolute dose or dose rate in water or air. However, the integration over a sensitive volume that usually exceeds the size of a cell provides rather a relative dose signal than the measurement of the absolute dose administered at cell position. The practical implementation of the different types of IC in the framework of the present dissertation as well as the necessary corrections due to various sample and experiment geometries are described in detail in sections 2.5.2 to 2.5.4.

Thermally stimulated exoelectron emission dosimeters

The method of exoelectron emission dosimetry is based upon the electronic band structure of semiconductors and the dose dependent emission of electrons from the near surface region. Concerning a solid with lattice structure, the potentials of the periodical arranged atoms and of the quasi-free electrons form spatio-periodical potentials whose energy differences are so small, that continuous bands arise. Those bands emerging from overlapping orbitals of the bonded valence electrons are abstracted to the valence band (VB); whereas the conduction band (CB) comprise those states with free electron movement and conduction. Both bands are separated by the band gap, which is in principle not allowed for electrons. The width of the band gap and the occupation of the two bands classify a solid material as isolator, semiconductor or electric conductor.

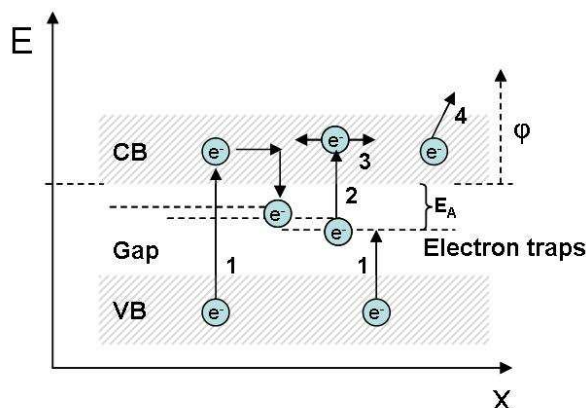


Figure 2.3: Processes that result in the emission of exoelectrons: VB electrons were excited by radiation incidence and trapped into deep acceptor levels (1) either directly from the VB or from an intermediate CB level. Subsequently, thermal stimulation that exceed the activation energy E_A lead to electron release from the traps (2) and increase the electron conduction (3) in the CB. Some of these electrons overcome the work function (φ) and were emitted as exoelectrons from the crystal surface (4).

Concentrating on semiconductors, their band gap, i.e., the gap energy, is low enough that electrons from the VB can enter the CB for example by thermal excitation. As result, the excess electrons in the CB will contribute to intrinsic electron (n-) conduction, whereas the remaining holes in the VB cause hole or p-type conduction. Both types of conduction can be amplified by appropriate doping of the semiconductor material. Additional electron acceptor or donor levels in the band gap will increase the conductivity of the semiconductor. For the emission of exoelectrons, a necessary requirement is the existence of deep electron acceptor levels positioned in the band gap near the

lowest energy level of the CB (Fig. 2.3).

Electrons excited from the valence to the conduction band, e.g., by means of ionizing radiation, are trapped into these deep acceptors with a certain probability. The further supply of energy by thermal or optical stimulation will result in the release of trapped electrons, i.e., stored energy, back into the CB. Here, they contribute to electron conduction, but they also have a certain temperature dependent probability to overcome the electron work function (φ) and to escape from the crystal surface [50]. As the temperature is increased the density of the released electrons changes proportional to the distribution of electron traps in the band gap. Flat traps are exhausted by lower temperatures than deeper ones, whereas optical stimulation will simply release the electrons from flat traps.

In the present work a Geiger-Müller counter was utilized to detect the released electrons and glow curves, i.e., the electron number in dependence on temperature, determined for five types of beryllium oxide TSEE detectors (section 2.5.1). These detectors promises several advantages for the dosimetry of *in vitro* cell irradiation experiments. Since the sensitive volume is at the detector surface and just a few nanometers thick TSEE detectors rather provide the spatial dose distribution at cell position than other dosimeters with sensitive volumes on a micrometer to millimeter scale, like IC. Moreover, TSEE detectors are suitable for the measurement of dose gradients, e.g., caused by the strong beam attenuation of ultra-soft X-rays in the cell monolayer, and for dose determination at interfaces. For these reasons, different types of TSEE detectors were evaluated with respect to their basic physical properties, like dose and time response and saturation, and to their applicability for *in vitro* cell irradiation experiments (section 2.5.1).

Radiochromic EBT films

The third type of dosimeter established and tested for the dosimetric characterization of the various radiation qualities examined in the present work are GafChromic® EBT films, which were developed for radiotherapy. The dose determination with radiochromic films is based on a polymerization process in the active film layer (Fig. 2.4) following radiation incidence. This polymerization results in a color change, from light to dark blue in the case of EBT films, the darker the higher the absorbed radiation dose. Irradiated films as well as the unirradiated controls are digitized (cf. section 2.5.2) and the shade of blue is converted to dose using a predetermined calibration curve. The scanning procedure, the calibration and the software analysis were adopted for our requirements from previously published protocols (e.g., [21]), that is, the calibration was performed with reference radiation sources appropriate for our interests (sections 2.5.2, 3.4.1).

EBT films are self-developing after irradiation and easy to cut to any size and shape required, a feature that enables the substitution of the cell monolayer in the cell culture vessel in order to determine the dose delivered to the cells after transmission, for example of the ELBE photon beam, through the plastic bottom. Moreover, as stated by the manufacturer, EBT films are energy independent in the range of 30 keV to several MeV for electrons and photons and applicable for doses of up to 8 Gy [59]. Beside absolute dosimetry, EBT films were also deployed to monitor the dose homogeneity over different radiation fields, for example at conventional X-ray tubes (sections

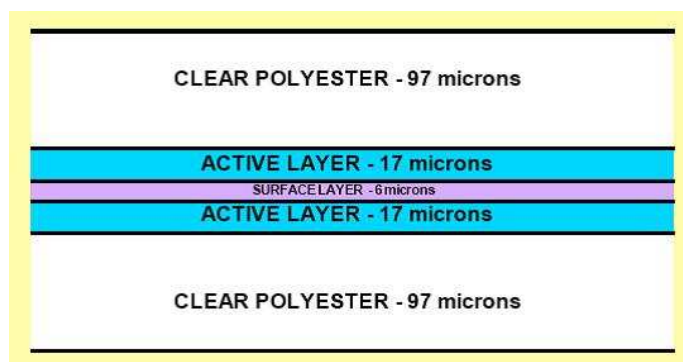


Figure 2.4: Configuration of GafChromic® EBT dosimetry films [59].

2.5.3, 2.5.4) or for high-energy bremsstrahlung photons at ELBE. The latter is of high importance, since horizontal and vertical shifts of the ELBE beam and with it dose inhomogeneities over the cell monolayer cannot be excluded. Therefore, in addition to the retrospective dose information given by EBT films, Farmer IC were implemented into the ELBE setup to allow for dose monitoring and irradiation control during the experiment (section 2.5.2). Considering soft X-rays absolute dosimetry with EBT films was not indicated, because of the low-energy limit (30 keV) recommended by the manufacturer and the increasing dose uncertainties below.

2.4 Radiobiological characterization

Following dosimetric characterization the different radiation qualities could be examined with respect to their radiobiological properties, i.e., their relative biological effectiveness. The cell type used in the present work was of human mammary epithelium origin (section 2.4.1) chosen due to the underlying scientific question on the radiation risk of mammographic X-rays. Information on the biological effectiveness were gained by analyzing biological effects on different cellular and subcellar level. Therefore, an important and well-established assay is the determination of the cellular survival following radiation incidence, which is of special interest for the radiotherapeutic application of radiation and is mostly investigated in parallel to other effects. In the present work, this assay is part of the second issue presented in section 3. For the characterization of X-rays, the micronucleus test (section 2.4.2) and the analysis of chromosomal aberrations (section 2.4.3) provide information on the radiation induced damage on chromosomes, whereas the immunofluorescence detection of signaling molecules was deployed to indicate DNA double-strand breaks (section 2.4.4).

Human mammary epithelial cells

So far, most of the studies realized to determine the RBE of mammographic X-rays and its underlying photon energy dependence have been performed with peripheral human lymphocytes (e.g., [41, 68, 108, 113]). These studies provide essential information on the radiosensitivity of circulating blood cells, which are inevitably irradiated during radiotherapy or -diagnostics. However, with regard to mammography two human mammary gland epithelial cell lines, namely 184A1 and MCF-

12A (section 2.5.3), have been chosen in the present work in order to investigate the biological effects of low energy X-rays.

Micronucleus assay

For the first *in vitro* cell irradiation experiments at the high-energy photon beam at ELBE the induction of micronuclei (MN) as an easy to handle and economic method was chosen to analyze the biological effectiveness (section 2.5.2). Micronuclei (Fig. 2.5a) originate from two basic phenomena - chromosome breakage, i.e., the formation of acentric fragments by means of ionizing radiation, or the dysfunctioning of the mitotic apparatus, which results in the lagging of whole chromosomes or chromatids during mitosis [92]. However, parts of the DNA are not incorporated in the daughter cell nuclei and remain as micronuclei in the cytoplasm of undivided cells. For the analysis of MN, the cells have to be blocked after the first nucleus division but before a subsequent cell division (Fig. 2.5a) to prevent the exclusion of micronuclei [92]. Hence, binucleated cells (BNC) are formed that contain the MN.

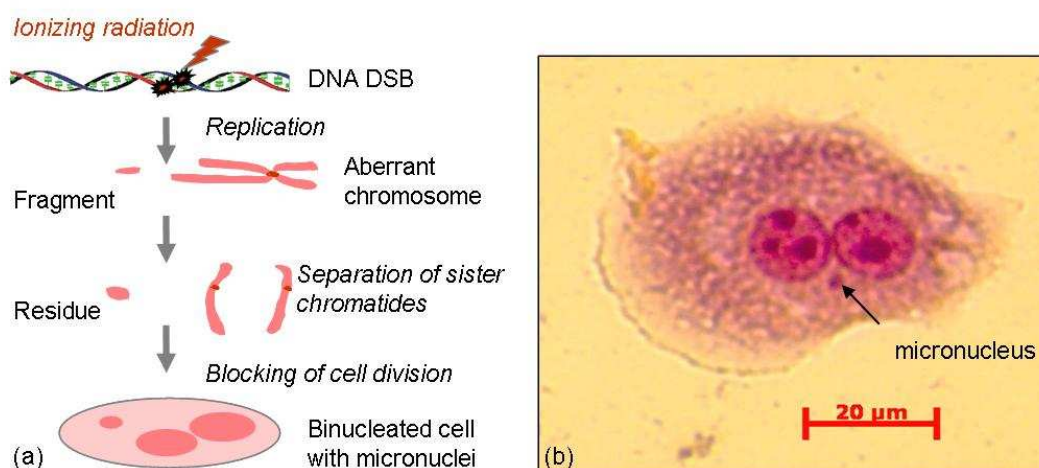


Figure 2.5: a) Process of micronuclei formation following ionizing radiation incidence. b) Binucleated cell of the human mammary epithelial cell line 184A1 exhibiting one micronucleus induced by 3 Gy irradiation with 34 MV bremsstrahlung.

Regarding the ELBE experiments with high-energy bremsstrahlung, the cell preparation starts with the plating one day before irradiation in order to assure cell adherence. Shortly before the experiment the culture vessels were completely filled with medium and sealed with Parafilm to avoid medium depletion as consequence of the upright positioning of the cell samples during the experiment. The samples, each equipped with an EBT dosimetry film, were positioned in special designed sample holders (section 2.5.2) and irradiated consecutively, at which some remain unirradiated to control the influence arising from the radiation background and the ambient conditions. After irradiation, the cells were treated in accordance to the protocol published by Fenech [77] and adopted for the human mammary epithelial cells used in the present work. The cell medium was exchanged to one containing 2 $\mu\text{g}/\text{ml}$ cytochalasin B, that prevent cell but not nucleus division, and the cells were

incubated for 72 hours at normal culture conditions (section 2.5.3). Subsequently, they were washed in 0.9 % NaCl, fixed with ice cold methanol and stained with 5 % Giemsa solution in water. One exemplary BNC possessing one micronuclei is shown in Figure 2.5b.

The analysis of the MN was performed under a light microscope applying the identification and scoring criteria defined by Fenech [77]. Briefly, a BNC has to possess two nuclei of approximately equal size, with not more than six micronuclei, whereas fine nucleoplasmic bridges between and a slight overlap or touching of MN are allowed. In addition, a micronucleus is defined, when its diameter is between 1/16 and 1/3 of that of the cell nucleus, it is non-refractile and not linked to the cell nucleus via a nucleoplasmic bridge. At least, the MN may overlap the boundaries of the cell nucleus. Taken into account these definitions, the MN were analyzed in dependence on radiation dose. The corresponding RBE value was obtained by comparing the dose response curves of 34 MV bremsstrahlung and the 200 kV X-ray reference (section 2.5.2).

Determination of chromosomal aberrations

Irreparable damages and structural changes induced in the DNA, e.g., by ionizing radiation, might cause a loss of replication capability and consequently cell death. However, since the radiation doses delivered during mammography are too low to cause cell death, the investigation of inheritable DNA damages is of capital importance. Mutations and a reduced genetic stability in daughter generations are potential consequences. Therefore, the induction and heredity transmission of these damages have to be quantified, especially for mammographic X-rays, in order to allow for risk estimation of acute and late radiation effects. Such early radiation effects were determined in the present work by analyzing chromosomal aberrations within the first cell cycle after irradiation (section 2.5.3). Chromosomal aberrations (CA) are chromatin damages induced by ionizing radiation or other mutagens that are observable on chromosomes, the condensed form of chromatin during mitosis (Fig. 2.6).

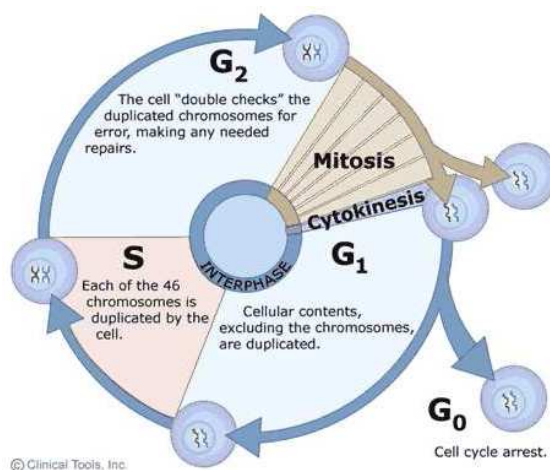


Figure 2.6: Normal cell cycle of an eukaryotic cell [128].

In general, CA originated from DNA DSB, which were misrejoined or cause the separation of chromatin [54], and can be classified in structural and numerical aberrations. The latter, the numerical

aberrations or the deviation from the normal chromosome number, were not analyzed in detail in the present work but were used to exclude cells with an abnormal chromosome set. Structural CA are distinguished in chromosome- and chromatid-type aberrations according to the number of chromatids affected. Chromosome-type aberrations are subdivided into deletions and exchange aberrations,

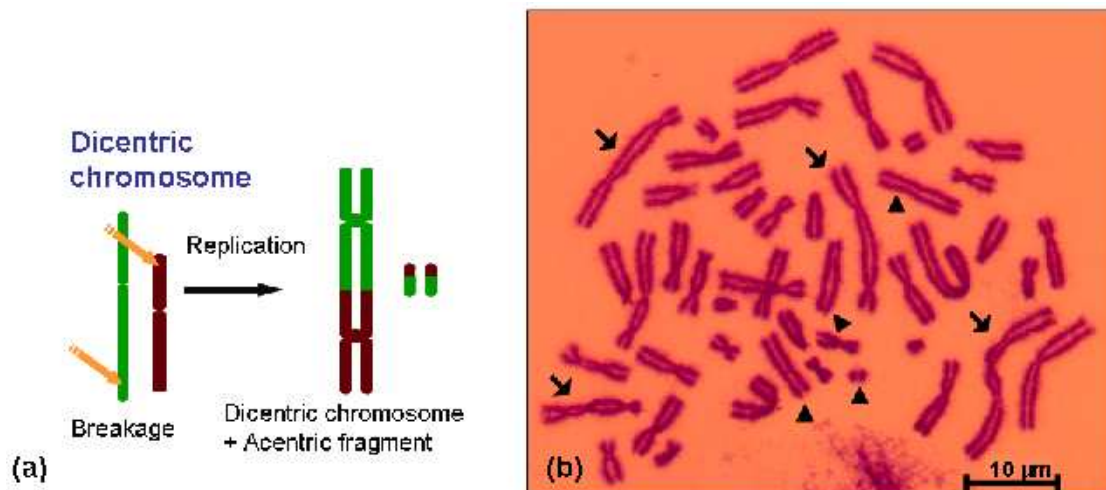


Figure 2.7: a) Possible mechanisms for the formation of dicentric chromosomes as example for chromosomal exchange aberrations [54]; b) Mitotic cell of cell line MCF-12A irradiated with 5 Gy of 10 kV X-rays and containing four dicentric chromosomes (arrows) and its associated fragments (triangles).

whereas the latter includes interchanges between at least two chromosomes and intrachanges within one chromosome. The chromosomal or chromosome-type aberrations most frequently used for radiobiological analysis, e.g., [41, 68, 108, 112, 113], and retrospective biological dose determination [54] are dicentric chromosomes, which represent one type of interchange aberration. As outlined in Figure 2.7a, dicentric chromosomes arise from the misrejoining of two broken chromosomes during DSB repair, whereas the remaining chromatin fragments can also be rejoined forming an associated acentric fragment. Hence, one dicentric and one acentric fragment observed in an examined cell are counted together as one CA. One example is shown in Figure 2.7b, where 4 dicultrics with its associated fragments were detected in the human mammary epithelial cell line MCF-12A. Additionally, the joining of more than two chromosomes is also possible, forming for example tricentric chromosomes that are accompanied by two acentric fragments.

The second type of chromosome-type aberration analyzed is the centric ring, which arise from an exchange or adjoined broken ends of the same chromosome (Fig. 2.8). Again, an associated fragment is formed by rejoining the two remaining fragments.

A third chromosome-type aberration are deletions, which are distinguished in terminal and interstitial deletions according to the position of the chromatin loss. Terminal deletions arise from DNA DSB and separation of chromatin next to the telomeric region of the chromosome, whereas interstitial deletions are caused by at least two DNA DSB within the same chromosome (Fig. 2.9). However, as these different types of deletions can not be differentiated by means of the applied Giemsa, i.e., homogeneous, chromosome staining, all deletions or acentric fragments, not associated

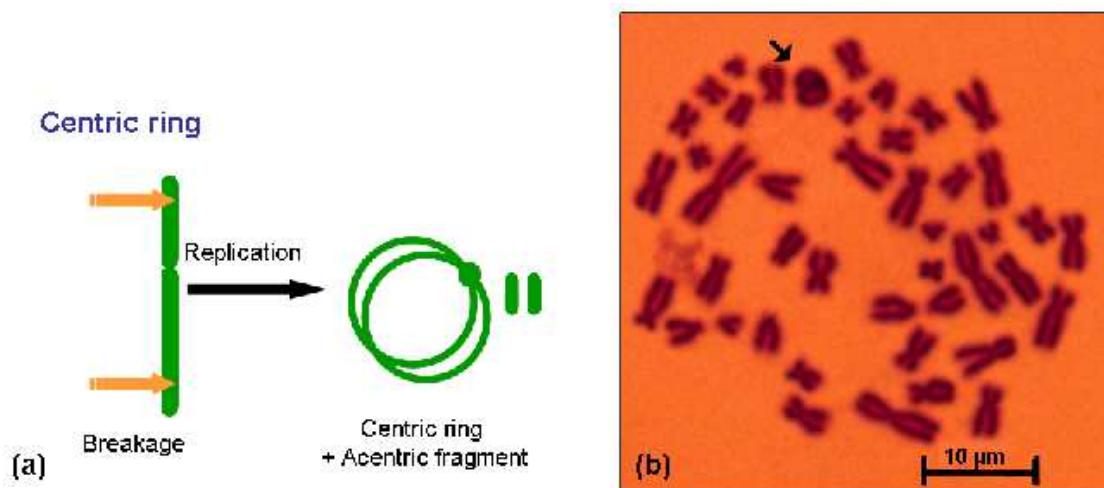


Figure 2.8: a) Formation of a centric ring chromosome after irradiation [54]; b) Mitotic cell of 184A1 exhibiting one centric ring (arrow) but without the appendant acentric fragment. The cell was irradiated with 5 Gy of 10 kV soft X-rays.

with an exchange aberration, were summarized as excess fragments in the present work.

The analysis of chromosomal aberration was performed with human mammary epithelial cells arrested in the first mitosis after irradiation in order to obtain the primary radiation damage unaffected by subsequent cell divisions. This requirement is fulfilled by cell synchronization and irradiation in G₀-phase, an appropriate incubation time and the arrest of mitotic cells with colcemid. At first, the

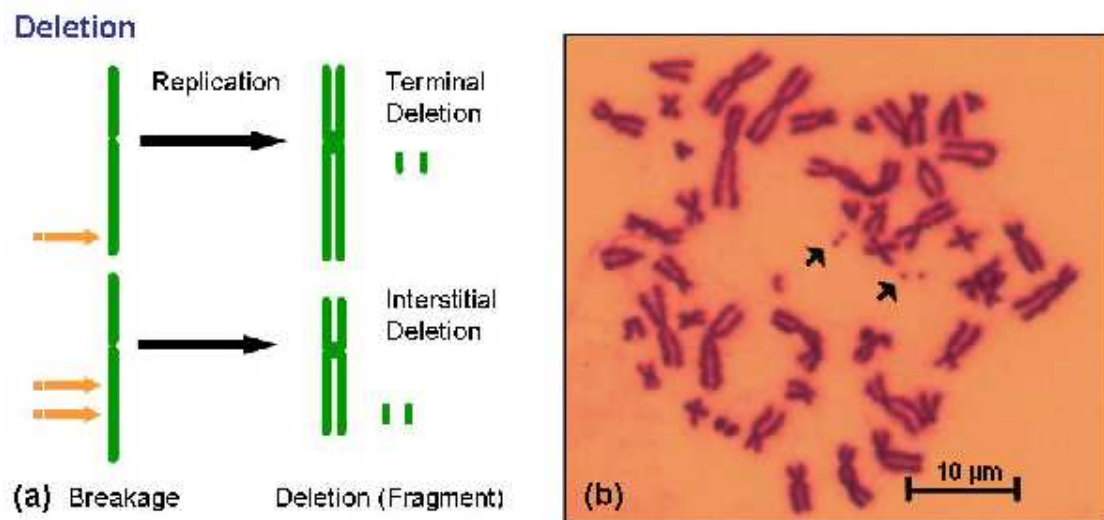


Figure 2.9: Chromosomal deletions a) Classification [54]; b) Excess fragments (arrows) observed in cell line 184A1 irradiated with a dose of 3 Gy of 10 kV soft X-rays.

cells were synchronized by means of confluent growing, that is, about one hundred percent coverage of the cell culture vessel bottom with cells. Due to this unfavorable condition the contact inhibition of the epithelial cells is activated and the cells were arrested in G₀-phase (Fig. 2.6). After irradiation

tion the cells were released from G₀-phase by subcultivation and incubated under normal growth conditions until they enter the first mitosis. At least, the cellular toxin colcemid, which permits the formation of spindle fibers during metaphase, was added for the last two to three hours of the incubation time. Consequently, the sister chromatids cannot be divided and the cells were arrested in mitosis (metaphase) enabling the analysis of CA.

The efficiency of cell arrest in the first mitosis was controlled by determining the number of cell cycles that the mitotic cells have passed after irradiation. For this, the method of fluorescent plus Giemsa staining, as described by Perry and Wolff [95], was applied. Cell samples, prepared and irradiated simultaneously to the examined probes, were incubated with bromodeoxyuridine (BrdU) a thymidin analogue which is taken up preferentially in the DNA during replication. After irradiation and incubation, the cells were harvested, stained and exposed to 254 nm UV light, that causes the photolytic degradation of DNA with embedded BrdU (section 2.5.3). Following Giemsa staining, the degraded DNA appears in light and intact DNA in dark purple, whereas one sister chromatid appears in light purple if both DNA strands were degraded. Taken into account the semi-conservative replication of human DNA, chromosomes with light purple chromatids have necessarily passed at least one mitosis. Hence, the number of so-called “Harlekin-chromosomes“ (Figure 2.10), that posses one light and one dark purple sister-chromatid, should be insignificant for cells being in the first metaphase.



Figure 2.10: Harlekin chromosomes observed in cell line 184A1 after incubation for 72 hours indicating that the mitotic cell has already passed the first cell cycle.

Immunofluorescence detection of DNA double-strand breaks

DNA DSB are accepted to be the most harmful DNA lesion induced by ionizing radiation. Although, the vast majority of DSB is repaired by non-homologous end-joining, homologous recombination or single-strand annealing, some non- or even mis-repaired DSB remain in the cell. In consequence, remaining DSB or resultant chromosomal aberrations and other chromatin mis-arrangements might influence the cellular survival and the genomic stability of daughter generations. A sensitive method

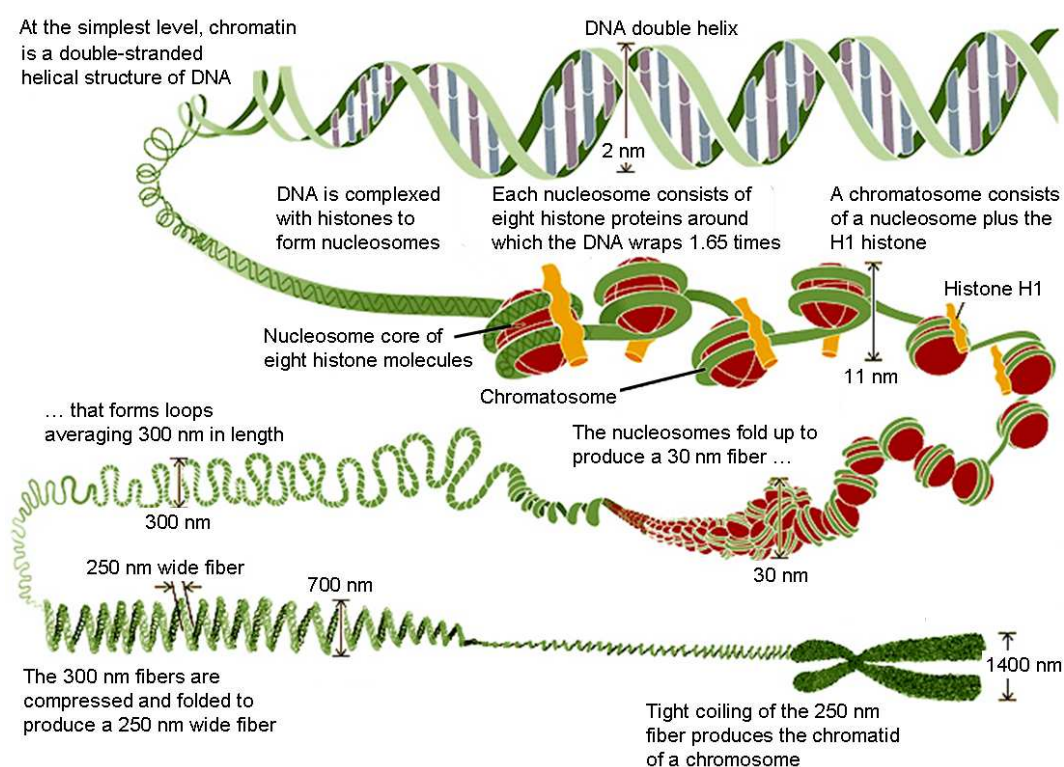


Figure 2.11: Organization of the chromosomes - starting from the DNA double-helix, which is wrapped around nucleosomes each consisting of eight histone molecules and linked by histone H1. The arrangement of nucleosomes as well as the DNA around forms the so-called chromatin, which becomes visible as chromosomes during mitosis (Schematic drawing adopted from [88]).

to quantify DNA double-strand breaks is based on the cellular DSB signaling pathway (Fig. 2.12) and the proteins involved, respectively. Following DSB induction, several proteins are activated, recruited and accumulated at the DNA DSB, whereas two of them, the phosphorylated histone H2AX and the protein 53BP1, are often used for the quantification of DSB (e.g., [2, 104, 106]). Regarding the eukaryotic chromatin in detail its organization in several levels is evident (Fig. 2.11). The double-stranded DNA is wrapped around a histone core, which consists of eight histones, two of each histone family H2A, H2B, H3 and H4 [104], forming the nucleosomes the basic units of chromatin. Sharing the highly conservative histone folding motif [62], but differing in the N- and C-terminal tails, each histone family is subclassified, e.g., the family H2A is divided in H2AX, H2A1-H2A2 and H2AZ [104]. The most famous member of this family is the histone H2AX, which represents approximately 2 - 25 % of the whole family H2A in mammals [104]. As demonstrated by Rogakou *et al.* [104] the histone H2AX becomes rapidly phosphorylated at the C-terminal of the serine 139 residue in consequence of radiation induced DNA DSB. The phospho-form of H2AX, also referred to as γ -H2AX, appears on either side of a DNA double-strand break and ranges over a total of 2×10^6 base pairs, thus involving 0.03 % of the chromatin per DSB [104]. The maximum amount of phosphorylated H2AX is achieved in less than 10 minutes after irradiation providing a sensitive and rapid method to detect DNA DSB. Therefore, the accumulation of hundreds of phos-

phorylated histone H2AX molecules at each DSB have to be visualized as so-called “ γ -H2AX foci” by fluorescence staining. In the present work, this was realized by a specific antibody binding at serine 139 residue of γ -H2AX, where the phosphate moiety is added, and the subsequent binding of a fluorescence dye.

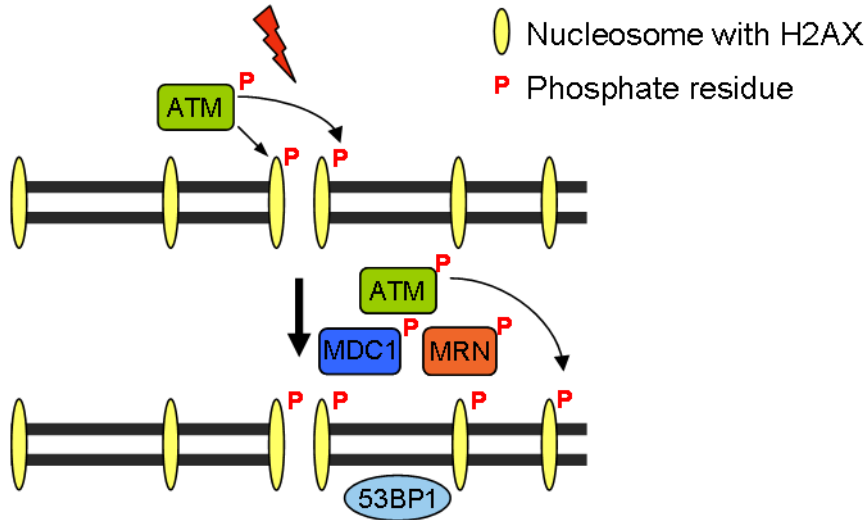


Figure 2.12: Part of the cellular DSB signaling cascade focusing on γ -H2AX and 53BP1: Initially the histone H2AX becomes phosphorylated by activated ATM (Ataxia Telangiectasia Mutated). Subsequently, the signaling protein MDC1 (Mediator of DNA damage checkpoint 1) and the MRN complex (Mre11/Rad50/NBS1) are recruited to the DSB leading to further activation of ATM. The generated feedback loop result in further phosphorylation of H2AX and chromatin modifications necessary for the recruitment of 53BP1 to the DNA DSB. Downstream this initial signaling cascade activated cell cycle checkpoints provide time for DNA repair or leading to the induction of apoptosis (Redrawn and modified from Kinner *et al.* [62]).

One limitation that arise by using the detection of γ -H2AX alone is its cell cycle dependent expression [53, 79]. Possible alternatives are the usage of synchronized cells or the co-detection of a signaling protein downstream of the pathway that is also located at the DNA DSB. The *tumor protein p53 binding protein 1* or shortly 53BP1, was identified as a good candidate for such co-detection or co-localization in experiments by Rappold *et al.* [99]. Following ionizing radiation, the 53BP1 proteins, normally homogeneously distributed over the nucleoplasm, are redistributed and accumulated at the position of the induced DNA DSB [99]. Moreover, 53BP1 is activated by ATM phosphorylation [2] and is necessary to accumulate p53 (tumor protein 53) [130], which regulates for example the functioning of cell cycle checkpoints. In the present work, an antibody was selected that bind to the region around serine 25, again the position where the phosphate moiety is added. For analysis, only co-localized foci of both proteins, γ -H2AX and 53BP1, were used to quantify DNA DSB (section 2.5.4).

2.5 Realization and results

1. Investigation of a TSEE dosimetry system for determination of dose in a cell monolayer
2. Cell irradiation setup and dosimetry for radiobiological studies at ELBE
3. Relative biological effectiveness of 25 and 10 kV X-rays for the induction of chromosomal aberrations in two human mammary epithelial cell lines
4. DNA double-strand break signaling: X-ray energy dependence of residual co-localized foci of γ -H2AX and 53BP1

Investigation of a TSEE dosimetry system for determination of dose in a cell monolayer

Anna Lehnert, Elke Beyreuther, Elisabeth Lessmann and Jörg Pawelke

Institute of Radiation Physics, Forschungszentrum Dresden-Rossendorf, P.O. Box 510119, D-01314 Dresden, Germany

Corresponding author:

Anna Lehnert

Institute of Radiation Physics

Forschungszentrum Dresden-Rossendorf

P.O. Box 510119

D-01314 Dresden, Germany

Fon: +49 351 260 3657

Fax: +49 351 260 3700

E-mail: A.Lehnert@fzd.de

Radiation Measurements 42:1530-37(2007)

DOI: 10.1016/j.radmeas.2007.03.007

www.elsevier.com/locate/radmeas

ABSTRACT

A prototype system for radiobiological studies has been investigated. It is based on thermally stimulated exoelectron emission (TSEE) detectors and can be used for precise determination of the absorbed dose in a live cell monolayer of several μm thickness. In the present study, five types of BeO detectors, different in structure and method of production, were tested in combination with a Geiger-Müller counter. The dose response and dose range, reproducibility and long-time stability of response, as well as the applicability in a simulated cell culture environment have been studied. The dose response was found to be linear over two orders of magnitude and limited by the counter resolution. However, by a variation of detector sensitivity, the whole dose range of interest for radiobiological experiments can be covered. The irradiation in a simulated cell environment was successful only for one detector type. The system performance was found to be limited by the variation in the system response for time periods longer than several hours, therefore, it is suitable for absolute dose measurement with calibrated detectors if reproducible laboratory conditions are provided.

Keywords: TSEE, Exoelectron emission, BeO; Geiger-Müller counter, Dosimetry, Cell monolayer

I. INTRODUCTION

Thermally stimulated exoelectron emission (TSEE) is a well-known phenomenon. Its theoretical description is based on the band model of solids. The excitation by external irradiation results in trapping of electrons near the bottom of the conduction band. As a result of a thermal stimulation, the electrons may overcome the work function and leave the crystal surface (exoelectron emission). Although optical stimulation of exoelectron emission is possible, the thermal stimulation is much more efficient [76]. The exoelectrons are in both cases emitted from the detector surface, however, the thermal stimulation can bring in motion also electrons from the depth of the material. At increasing temperature, it results in maxima of the electron emission at distinct temperatures, which are characteristic for the investigated material (glow curve). The use of TSEE detectors in dosimetry is based on the relation between radiation dose and the glow curve. The mathematical description of the glow curve in the frame of the Randall and Wilkins model [50] is similar to the theoretical description of the thermoluminescent (TL) glow curves and allows to calculate the depth of the energy levels. Although a TSEE detector has several advantages over the widely used TL detectors, no commercially available systems exist and its application in dosimetry is seldom. One of its main advantages is the surface-based origin of the phenomenon, since the exoelectrons have an escape depth of less than 10 nm [66]. This makes such a dosimeter very attractive in the cases where a small sensitive volume is desired, such as detection of low-penetrating β -radiation and low-energy X-rays as well as for studying highly inhomogeneous radiation fields at the interface of different materials [19, 100] or in the dose build-up region of high-energy photon beams.

The most common materials used for TSEE dosimetry are ionic crystals such as alkali halides or oxides. One widely used detector material is BeO, because of its physical stability, thermal conductivity and insolubility in water. Its low atomic number of about 7.1 approximates the mean atomic number of tissue, making it especially suitable for application in personal dosimetry. A method introduced by Kramer, based on mixing of BeO with sufficient amount of graphite powder to improve conductivity, results in a linear dose response of the detector over 8 orders of magnitude [64]. This method has been further developed and improved to obtain optimal detector properties [50, 63]. The experimental investigations with BeO have proved its applicability for γ - and β -dosimetry, showing a low dependence on photon [67] or electron energy [66] and linearity of dose response over a large dose range [24]. These are additional advantages when compared with the widespread TL detectors. A superconducting electron linear accelerator of high brilliance and low emittance (ELBE) is under operation at Forschungszentrum Dresden-Rossendorf since January 2003. The relativistic electron beam with variable time structure and energy up to 40 MeV is used to drive various kinds of secondary radiation sources. Among all, *in vitro* radiobiological studies with high-energy bremsstrahlung as well as with channeling X-rays, tunable in the range 10 - 100 keV, are being performed. The goal of the present study was to investigate a prototype system for precise determination of the absorbed dose in a live cell monolayer of several μm thickness. The advantage of a small sensitive volume of the TSEE detector based on BeO could be useful in soft X-rays dosimetry, as well as for studying dose build-up effects of high-energy bremsstrahlung radiation. In addition, for the determination of the absolute dose and dose inhomogeneity in the cell, a tissue-equivalent dosimeter which could be irra-

diated in a real cell growth environment, e.g., in liquid, was desirable. On the other hand, the TSEE detectors could be used for the routine monitoring of the absorbed dose in the cell monolayer, where an easy to handle calibrated dosimeter with small sensitive volume and stable response was required.

II. EXPERIMENTAL SETUP AND DETECTORS

The prototype TSEE detector system was based on an open gas flow Geiger-Müller counter, with a point anode and working gas methane of higher than 99.5 % purity. The gas flow was controlled by an oil-bubble system, where the gas flowed through an oil container and produced bubbles with a certain frequency. A microphone connected by a pipe to the oil container registered the sound signal from the bubbles. The amplitude and the duration of the pulses were observed on an oscilloscope whereas a gas filter prevented oil drops from entering the measuring head of the counter. The measuring head had two positions, either above a β^- -source used as a reference or above a heating plate. In the first case, electrons emitted by the source were registered, whereas in the second case the exoelectrons were emitted during the annealing of the detector on the heating plate. The heating rate was controlled by a thermocouple. The detector, being the emitting cathode, was placed behind a circular aperture. The point anode consisted of a gold sphere of 0.27 mm diameter, located at the end of a short gold wire of 0.1 mm diameter. The emitted exoelectrons were accelerated by a high voltage of up to + 5 kV applied to the anode and produced an electron avalanche.

Two prototype systems differing in pulse collection and data acquisition were tested (both from Dr. Holzapfel Messgerätelabor, Teltow, Germany). For system I, the signal, extracted from the high voltage, was applied to a plotter and the glow curve was plotted during acquisition. This system was available from the beginning of the experiments, and due to promising results, later system II was introduced. For system II, a guard ring served as an electrode to pick up the counting pulses. The electronic hardware in this case consisted of an interface (comprising the high voltage unit, power supply for the heater and an amplifier) and plug-in cards for controlling and data acquisition with a PC. Using dedicated software, the heating rate and the high voltage could be changed and the data stored in ASCII-format. In the present study, five types of BeO detectors, different in structure and method of production, were tested. The dose response and dose range, reproducibility and long-time stability of response, as well as applicability in a simulated cell culture environment were studied. The common materials for all detector types were the exoelectron emitter BeO, as well as the graphite substrate, serving as an electrical conductor. The production methods have been developed and all detectors (except detectors type IV) were produced by Dr. Holzapfel Messgerätelabor, Teltow, Germany.

Detectors type I: First, graphite pellets (1.5 mm thick discs of about 12.5 mm outer diameter, with an inner concentric deepening of 0.5 mm and radius of about 4.3 mm) were covered with an Au layer of approximately 300 nm thickness by vapor deposition. A Be layer of about 120 nm thickness was vapor deposited and subsequently oxidized. The gold layer served for electrical and mechanical stabilization of the BeO layer. For highest sensitivity of the detectors, the optimal conditions were oxidation in air at 1 mbar pressure and a temperature of 1450°C. Additional increase of the sensitivity was obtained by the reduction procedure in methane atmosphere at 5 mbar pressure and

temperature of 800°C (Holzapfel, private communication). The effective area of the detector was 43 mm².

Detectors type II: The dimensions of the graphite substrate were 12.0 × 12.0 × 0.5 mm³. The detectors were produced by the upper procedure, but without the Au layer. For mechanical stability of the detectors, they were mounted in a round Al holder. The effective detector area was 144 mm².

Detectors type III: They were basically identical with the detectors type II, but without the Al holder, therefore, special care for handling was necessary. The effective area in this case was the same as for detectors type II.

Detectors type IV: The graphite pellets were 1.0 mm thick discs of 17 mm outer diameter, with an inner concentric deepening of 0.5 mm and a radius of 5.0 mm. The BeO was brought on the surface in the form of water suspension with a defined concentration and the water was evaporated by heating at about 50°C without any further treatment. The effective area was 79 mm².

Detectors type V: The graphite substrate (about 11 × 11 mm², thickness 0.5 or 1 mm) was covered with a Be suspension of defined concentration in alcohol. After evaporation, the layer was oxidized at 1400 - 1500°C. The effective area was 140 mm².

The properties of the detectors were studied after irradiation with γ - and β^- -sources: ⁹⁰Sr (activity 410 kBq or 20 MBq), ⁵⁵Fe (nominal activity 130 kBq or 37 MBq), ²²Na (activity 58 kBq), ¹³⁷Cs (dose rate in water 0.1 mGy/min at 53.7 cm source-detector distance). The reference sources were ¹⁴C (activity about 3 kBq) and ⁶³Ni (activity about 2.5 kBq).

III. RESULTS

Working point of the Geiger-Müller counter

For both counters, operated at the same methane flow rate, the working point was set to be 4.0 kV. For system II, the increase of the high voltage was connected with a change in the pulse height distribution. A noise peak in the distribution was observed at channel number about 224, corresponding to about 4.4 V (the pulses in the range 0.4 - 5 V were registered), regardless of the electron source (a reference source or a TSEE detector). Its height was found to increase with increasing high voltage and to deteriorate the counter performance at voltage higher than about 4.1 kV. Since it was found to be at the same position even after exchange of the anode, the reason for it was probably in the electronics of the data acquisition system. However, as presented further, the noise peak was only one of the factors influencing the whole system performance and its contribution could be neglected. It was not excluded in any of the further evaluations.

Glow curves

The glow curves of all detector types are presented in Figure 2.13. The irradiations were performed with the same ⁹⁰Sr source, and the heating rate was 3°C/s. The source-detector distance of about 7 mm was optimized by the reader count rate and a reasonable irradiation time and was varying by less than 0.5 mm for the different detector types. A difference in the glow curves was observed as a result of the difference in the production method, but most often there was one main peak in the range 200 - 400°C, which makes dosimetric application convenient. Since both the number of

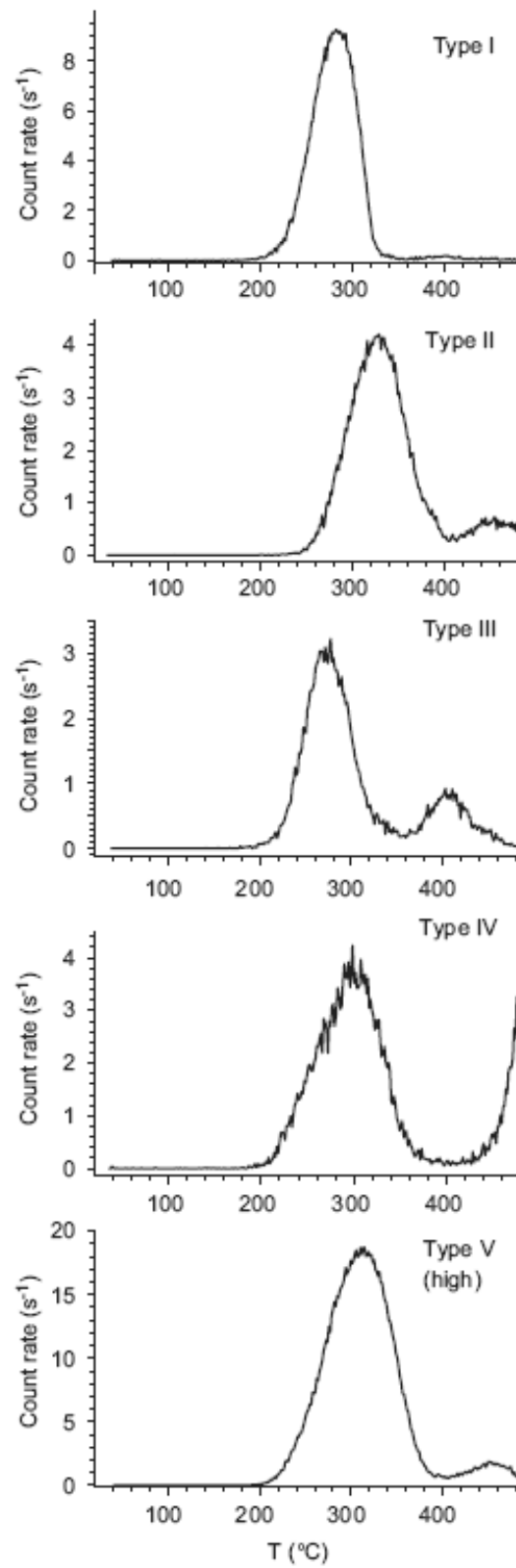


Figure 2.13: Glow curves of all tested detector types. Detector type V of high sensitivity is presented. Different scales of the ordinates are used for better presentation.

counts in the peak range of the glow curve and the total number of counts are proportional to the dose, they both can be used as a dosimetric signal. In the frame of the Randall and Wilkins model [50], a numerical evaluation of the sample glow curves, presented in Figure 2.13, was performed to calculate the energetic distance from the trap levels to the bottom of the conductivity band. The obtained values for all the detectors are in the realistic range 0.5 - 1.2 eV.

Dose range of the TSEE system

The dependence of the number of TSEE counts on the time of irradiation, or, respectively, dose, has been studied for both systems and different sources. In Figure 2.14, the detector response in dependence on irradiation time for two different sources is shown.

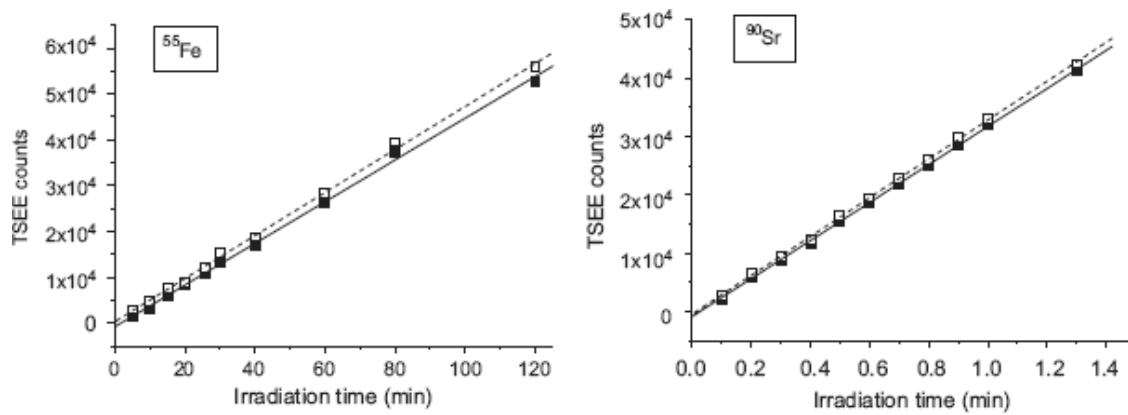


Figure 2.14: Time of irradiation response of detector type I, system I. The solid squares represent the peak range of the glow curve (20 - 370°C) with the corresponding linear fit (solid line). The open squares represent the whole range (20 - 520°C) with the corresponding linear fit (dash line). Left panel: ^{55}Fe irradiation. Right panel: ^{90}Sr irradiation.

As seen from the figure, the linearity of response is held both for soft X-rays and for β -rays. It was observed also after irradiation with the ^{137}Cs source and other types of detectors. This makes calibrated detectors useful for dose determination. However, after longer irradiation times, a plateau in the count number was observed for detectors type I, II and III for both systems, which could result either from saturation of the detector response, or from the limited pulse rate resolution of the counter. This was proved by comparing the response of two different detectors after irradiation with the same source at the same irradiation geometry. The results of irradiation with a ^{90}Sr source for system I, detectors type I, are presented in Figure 2.15 (left). Although both samples have different sensitivity, reproduced by the different slopes of the linear ranges of the curves, the saturation of response was achieved at the same count number, about 5×10^5 total number of counts. Saturation at a similar number of counts was also observed for system II. Therefore, saturation due to limited counter resolution was concluded. In order to determine the dose range, corresponding to the count rate range of the TSEE systems, a ^{137}Cs source, calibrated to dose rate in water of 0.1 mGy/min at a 53.7 cm distance from the source, was used. The response for detector type I and system I, shown in Figure 2.15 (right), after irradiation with the ^{90}Sr source was scaled to fit the response curve

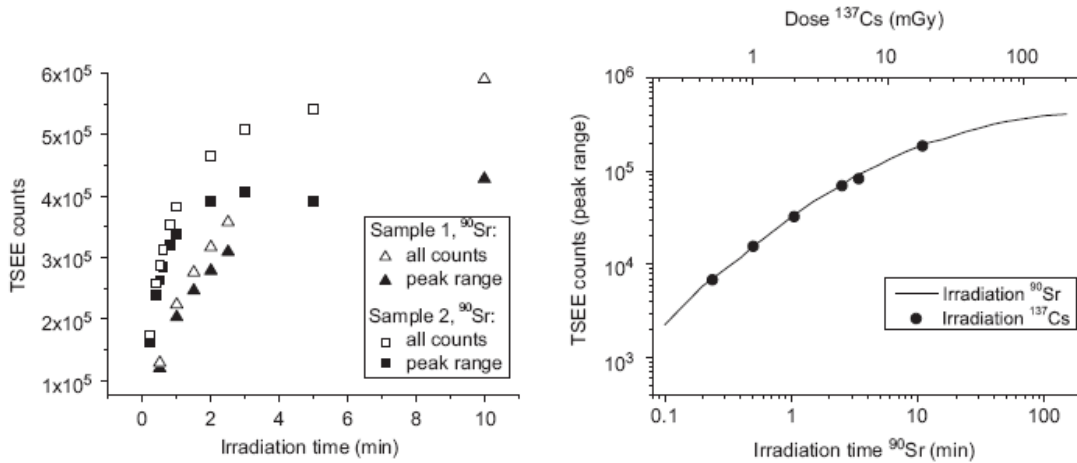


Figure 2.15: Left: saturation of system I response, measured for two samples of detector type I after irradiation with ⁹⁰Sr. Right: dose response of detector type I, system I. The measured response after irradiation with ⁹⁰Sr is shown by the solid line. The solid circles represent the response after irradiation of the same detector with a calibrated ¹³⁷Cs source.

after ¹³⁷Cs irradiation for the same number of counts. This procedure is not equal to a “calibration” of the ⁹⁰Sr source, since the difference in detector response to both radiation qualities is unknown. The dose range of system I was obtained to be 2 orders of magnitude. The upper limit, defined by the counter saturation, was about 10 mGy, and the lower limit was defined by the statistical error of the count number. This upper value is far from the reported saturation limit of the detectors of up to 10 Gy [66], and the entire sensitivity range is far from the dose range necessary for cell irradiation experiments, which is usually 0.1 - 10 Gy. This is a serious problem for dose monitoring during irradiation. A shift in the TSEE system sensitivity could be achieved by manipulation of the read-out system (counter geometry, gas flow), which however, would result in a rather small increase of the upper response limit. A decrease of the detector sensitivity by orders of magnitude can be reached by decreasing detector size, but since a 10-fold decrease of the detector radius, resulting in 100 times sensitivity decrease, would result in a detector size less than 1 mm², it would lead to difficulties in the production and handling of such detectors. Another possibility would be to decrease the size of the detector read-out area. This method was tested using a grid over the detector, but it resulted in a decreased stability of response. Therefore, another method of detector production was used and detector types IV and V, produced by sedimentation, were tested. Although detectors type IV can be produced in very simple laboratory conditions, their testing proved that no big variation in sensitivity could be achieved. A fading effect was observed, expressed in several orders of magnitude drop of the response to irradiation before reaching a plateau over the first days after production (Fig. 2.16). The detector response was evaluated immediately after irradiation with a ⁹⁰Sr source, and the procedure was repeated on several consecutive days. Such changes in response were not observed for any other detector type. For detectors type V, which were produced in a similar way, several orders of magnitude difference in sensitivity was achieved by variation of the BeO amount during production, and the sensitivity was proved to be stable with time. The dose

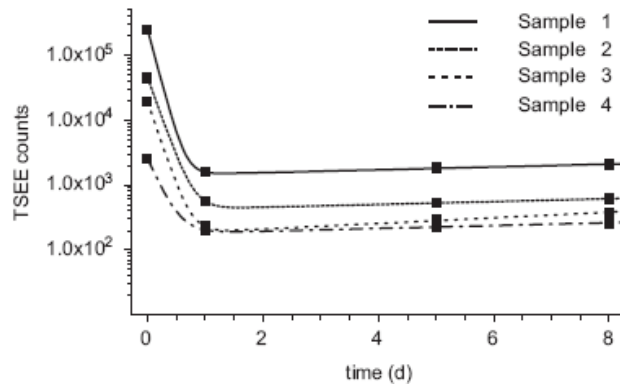


Figure 2.16: Fading effect for detector type IV (a single detector response is represented by closed symbols, fitted by a two-parameter exponential model for better presentation.)

ranges possible to be measured with the tested TSEE detector types are presented in Table 2.1. For detector types II - V, since no measurement with the calibrated ^{137}Cs source was performed, the dose range was obtained under the assumption that the response ratio of all detectors to the irradiation with the ^{137}Cs and the ^{90}Sr source was identical. In order to obtain the upper dose limit, a saturation of the counting system was assumed to occur at 5×10^5 counts. As seen from Table 2.1, the variation in sensitivity for detector type V was sufficient to achieve upper dose limits reasonable for cell irradiations.

Detector type	Sensitivity (counts/mGy)	Upper dose limit (mGy)
I, System I	14250	35
I, System II	7595	66
II	4883	102
III	6247	80
IV	5548	90
V (Low)	48	1.0×10^4
V (Medium)	6246	80
V (High)	29870	17

Detector types II - V have been studied only with system II.
For detector type V, detectors of low, medium and high sensitivity were tested.

Table 2.1: Sensitivity of all studied detector types

Reproducibility of detector response

The measured reproducibility of detector response depends, on one hand, on the system parameters, such as the stability of the high voltage, temperature and gas flow rate, and on the other hand, on the detector intrinsic properties, on the reproducibility of the irradiation parameters and the read-out geometry. Since the measurements were performed at a source-detector distance of several mm, careful detector positioning was necessary. For each system, the detectors were placed in the same source holder and irradiated so that the position and orientation of the detector surface to the

source was always the same to exclude the influence of the inhomogeneity of the BeO layer. The uncertainty of the irradiation time measurement was ± 1 s.

A parameter which could influence the stability of the system response is the gas flow rate. A linear increase in the counting efficiency with increasing gas flow rate was observed for the TSEE count rate, whereas for irradiation with the reference source, an opposite dependence was observed (Fig. 2.17). The reason for this could be the difference in the energy of the registered electrons. Whereas the maximal energy of the electrons emitted by the reference source ^{63}Ni was 67 keV, the exoelectrons have energies less than 5 eV [26], so it is possible that an increase of the gas flow results in an opposite effect on the effectiveness of electron counting. However, due to insufficient information about the geometry and electronics of this prototype system, the effect cannot be studied in detail. Due to the strong gas flow dependence of the count rate, the gas flow was kept constant and controlled regularly during experiment series. The intrinsic reproducibility of the readout system at

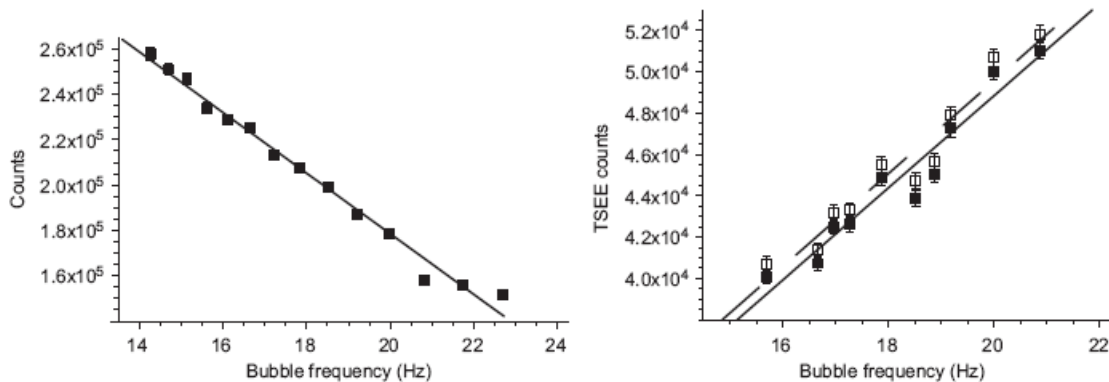


Figure 2.17: Gas flow dependence of the TSEE system response. Left panel: reference source. Right panel: TSEE detector type I, where the solid squares represent the peak range of the glow curve (192 - 360°C) with the corresponding linear fit (solid line) and the open squares represent the whole range (20 - 520°C) with the corresponding linear fit (dash line).

constant temperature and gas flow rate can be derived from the reproducibility of the count rate of the reference source, where the standard deviation (SD) was found to be better than 1 %. It is presented in Table 2.2 together with the reproducibility of all detector types for irradiation with the ^{90}Sr source. The measurement and subsequent cooling of the detectors was repeated at least 10 times in a row, and the total numbers of exoelectron counts as well as in the region of the main glow curve peak were evaluated. The best reproducibility of response was observed for detector type I, which follows the expected behavior due to the presence of a mechanically and electrically stabilizing Au layer. The reproducibility of response for detectors type IV was measured after stabilization to be about 10 % (SD), which can be attributed to the method of production by simple sedimentation of BeO. The comparison of both used systems, performed for detector type I, shows the better stability of system II properties, due to the improved high voltage stability and temperature control. However, these measurements do not reflect the fluctuation of the system response during routine work over weeks or months. Variations of up to 20 % were found within one week by reference source measurements, without any change of the setup or environmental conditions.

Detector type	System	Number of experiments	Reproducibility (SD)	
			Peak counts %	Total counts %
None (reference source)	II	19	ND	0.64
I	I	25	1.29	1.23
	II	12	0.95	0.97
II	II	13	2.45	2.37
III	II	12	2.33	2.16
IV	II	10	10.50	13.34
V	II	10	6.91	6.55

Table 2.2: Reproducibility of response for reference source and TSEE detector irradiation, presented as the SD relative to the mean value

Dose measurement in a simulated cell environment

The irradiation of living cells is complicated by the requirement of optimal environmental conditions, and especially by the presence of appropriate liquid (e.g., cell culture medium) covering the cells. Therefore, the application of TSEE detectors for dose sampling in the conditions of real cell environment and the study of interface effects would require irradiation in the presence of liquid. All studied detector types were tested for applicability for this purpose. The tested liquids were water, propanol and cell medium, whereas water and propanol were chosen for their simplicity of chemical composition. The irradiation in water resulted in big and inconsistent variations of the detector response. The irradiation in cell culture medium resulted in a complete change of the glow curve and inadequate detector response, caused probably by the influence of the organic constituents on the electric properties of the irradiated surface, however, no irreversible change of the detector response was observed. Finally, propanol was chosen as a working medium, its fast evaporation allowing immediate evaluation of the glow curve. The summary of the detector performance is presented in Table 2.3. First, a well-known problem for detectors based on surface excitations is the tribo effect, expressed in detection of a signal after a contact of the surface with any material without irradiation. The induction of the tribo effect was checked by wetting the detectors with propanol. An irradiation was performed before wetting as well as after evaporation of the propanol. No change of the detector response, which would point at a tribo effect, was observed (see Table 2.3, column 2). As a second step, the study of the influence of the liquid during irradiation on detector response was performed. The source was placed directly on the detector if it was not coming in contact with the sensitive layer of the detector, otherwise a holder was used, and this setup was placed in a vessel with liquid. The reproducibility of detector response for irradiation in propanol was checked with a ^{22}Na source.

The thickness of the liquid layer enclosed between the source and the detector was 1 - 3 mm. The reproducibility of response of all detector types was proved to be worse compared to irradiation in air (cf. Table 2.2). In addition, the plausibility of detector response after irradiation in propanol was checked with the ^{22}Na source using the same geometry. The positron decay of ^{22}Na leads to annihilation radiation at 511 keV in addition to the decay γ -line at 1275 keV. From the photon mass

attenuation coefficient for these energies and for the distances used in the experimental setup, a decrease in photon intensity due to attenuation and scattering in the liquid layer of 1 - 2 % is expected. The results presented in Table 2.3, column 4, show that for all detector types except detector type I the ratio of the responses after irradiation in air and propanol is higher than expected. A ^{55}Fe soft X-ray source was used for comparison, and in this case the change in response was expected to depend strongly on detector geometry and follow the attenuation of the soft X-rays in the propanol layer of 2.3 - 2.8 mm thickness. The range of response ratios after irradiation in air and propanol with the ^{55}Fe source was calculated assuming a rather large positioning error, resulting in a source to detector uncertainty of ± 0.5 mm and is shown in column 5. As seen from the last column in Table 2.3, the measured response ratio is in the predicted range.

Detector type	Response ratio propanol wetting ^{90}Sr	Reproducibility in propanol (%) ^{22}Na	Response ratio air to propanol ^{22}Na	Response ratio air to propanol ^{55}Fe	
				Calc.	Meas.
I	1.00 ± 0.05	13.3	0.92 ± 0.08	27 - 87	32 ± 24
II	1.02 ± 0.07	11.7	1.18 ± 0.09	33 - 110	59 ± 9
III	ND	21.7	1.26 ± 0.19	54 - 176	131 ± 11
IV	ND	21.8	1.6 ± 0.2	ND	ND
V	ND	17.8	1.4 ± 0.3	ND	ND

The response ratio was calculated as the ratio of the mean values for the TSEE peak from 3 to 12 experiments and is shown together with the corresponding 95 % confidence interval for easier comparison. The reproducibility is presented as the SD relative to the mean value for the TSEE peak range.

Table 2.3: Influence of the irradiation medium on TSEE detectors response

IV. CONCLUSIONS

The studied TSEE detector systems clarify the potential of TSEE detectors for determination of dose in complicated cases. The obtained results show that the detector response depends on the structure and method of production, however, a stable response in laboratory conditions can be easily achieved. This makes them suitable for measurement of dose in thin layers as well as of dose inhomogeneity at material interfaces. Due to the different structure and method of production, the detectors were found out to differ in mechanical stability and handling convenience, sensitivity and reproducibility of response. This results in a difference in their applicability for absolute dose determination and dose monitoring. Although the electrical properties of detector type I are improved by the Au layer, the presence of a high-Z material alters the secondary electron distribution and makes absolute dose determination in cells questionable. However, due to its stability of response, after calibration in the corresponding radiation field, this detector could be used for dose monitoring. On the other hand, the simple composition and preparation procedure of detector type IV makes it attractive for absolute dose determination in cells, but an extra fragility of the BeO layer has been observed. The detectors type V were found to combine the advantages of detectors type I - III, due to the stability of the BeO layer, and on the other hand to show variable sensitivity, like detectors type IV. Since the best reproducibility with SD of less than about 2 % was obtained for detectors

type I - III, they can be used in cases, when high precision is necessary. The dose range, in which the studied TSEE system can be used, was found to be limited by the counter resolution, but by a variation of detector sensitivity, the whole dose range of interest for radiobiological experiments can be covered. This makes the system suitable for dose measurement with calibrated detectors during routine irradiation. However, its performance is limited by the variation in the system response for time periods longer than several hours. The irradiation in a simulated cell environment was successful only for detectors type I, however, this type is least tissue-equivalent. Although the TSEE detectors could be of big interest for dosimetry at the ELBE X-ray source, it requires improvement to become suitable for precise dose determination. Furthermore, independence of the response on dose rate has to be proved, since the time structure of the ELBE radiation source allows variability of dose rate by several orders of magnitude.

ACKNOWLEDGMENTS

We express our gratitude to Dr. G. Holzapfel for the helpful discussions and the response to the specific requirements of our task in the detectors production. We thank Dr. J. Lesz for the technical support and M. Sommer for the assistance in the experimental work at the Technische Universität Dresden.

Author contributions

Study concept and design A.L., J.P.; Experimental studies A.L., E.B., E.L.; Data acquisition A.L., E.B.; Data analysis A.L.; Literature research A.L.; Manuscript preparation A.L.; Manuscript editing J.P., E.B.; Guarantor of integrity of the entire study J.P.; Manuscript review was carried out by all authors.

Cell irradiation setup and dosimetry for radiobiological studies at ELBE

Karl Zeil^a, Elke Beyreuther^a, Elisabeth Lessmann^a, Wolfgang Wagner^a and Jörg Pawelke^{a,b}

^a Institute of Radiation Physics, Forschungszentrum Dresden-Rossendorf, Dresden, Germany

^b OncoRay, Center for Radiation Research in Oncology, Medical Faculty Carl Gustav Carus, University of Technology Dresden, Dresden, Germany

Corresponding author:

Karl Zeil

Institute of Radiation Physics

Forschungszentrum Dresden-Rossendorf

P.O. Box 510119

D-01314 Dresden, Germany

Fon: +49 351 260 2614

Fax: +49 351 260 3700

E-mail: K.Zeil@fzd.de

Nuclear Instruments and Methods in Physics Research Section B:

Beam Interactions with Materials and Atoms 267(14):2403-10(2009)

DOI: 10.1016/j.nimb.2009.04.15

www.elsevier.com/locate/nimb

ABSTRACT

The radiation source ELBE delivers different types of secondary radiation, which is used for cell irradiation studies in radiobiological research. Thereby an important issue is the determination of the biological effectiveness of photon radiation as a function of photon energy by using low-energetic, monochromatic channeling radiation (10 - 100 keV) and high-energetic bremsstrahlung (up to 40 MV). Radiobiological studies at the research facility ELBE demand special technical and dosimetric prerequisites. Therefore, a cell irradiation system (CIS) has been designed, constructed and installed at the beam line. The CIS allows automatic irradiation of a larger cell sample number and the compensation of spatial inhomogeneity of the dose distribution within the beam spot. The recently introduced GafChromic® EBT radiochromic film model has been used to verify the cell irradiation dose deposition achieving a dose uncertainty of $< 5\%$. Both, the installed cell irradiation system and the developed dosimetric procedure based on the use of the EBT film have been experimentally tested at ELBE. The biological effectiveness of 34 MV bremsstrahlung with respect to 200 kV X-rays from a conventional X-ray tube has been determined. An RBE value of 0.75 has been measured in good agreement with literature.

Keywords: Radiobiology, Cell irradiation, Dosimetry, Radiochromic film

PACS: 87.53.-j; 87.53.Bn; 87.55.-N; 07.85.Fv; 29.20.Ej; 41.60.-m

I. INTRODUCTION

The basic device of the radiation source ELBE [30, 34] is a superconducting electron linear accelerator which provides an electron beam of high brilliance and low emittance with maximum electron energy of 40 MeV and a high average beam current of 1 mA. The electron beam is used for the production of different types of secondary radiation which are applied for several research topics. The primary electrons can also be used for experiments.

The different types of radiation are applied for radiobiological research as one important issue. There the determination of the biological effectiveness of ionizing photon radiation as a function of photon energy [48, 74, 75] represents a major scientific objective. Very intense, low-energetic, quasi-monochromatic, and energy tunable (10 - 100 keV) channeling radiation (CR) is generated by channeling of relativistic electrons in diamond crystals [129] at the radiation physics beam line at ELBE. Additionally, high-energetic bremsstrahlung of up to 40 MV photon energy can be delivered. The presented work is part of radiobiological studies which are related to photon radiation applied in medical application such as mammography screening and radiotherapy. In order to compare radiation qualities, the relative biological effectiveness (RBE) has to be introduced. It is defined by the fraction of the dose delivered by a reference radiation quality to the dose delivered by a given radiation quality, whereas both radiation qualities are responsible for the same biological effect. The general basis of radiobiological experiments is RBE determination by measuring of dose-effect curves for *in vitro* cell systems.

Usually radiobiological studies are performed on conventional high-voltage X-ray tubes or medical acceleration facilities. Both sources deliver broad polychromatic bremsstrahlung with a high photon flux. Thus, therapeutic dose values (few Gy per daily fraction) can be delivered in a sufficiently small irradiation duration (dose rate ≈ 1 Gy/min) to be independent from repairing processes in human cells. Due to the high reproducibility of beam parameters of conventional radiation sources, a large number of samples can be irradiated in stable conditions in order to cope with the biological diversity. Considering the dosimetry, a standardized radiation field is used. All changes in the radiation geometry resulting in differences of beam absorption, scattering or dose build up effect are taken into consideration by applying tabled correction factors. In practical irradiation experiments, cell samples are irradiated at a vertical beam and the delivered dose is controlled by presetting a certain irradiation duration.

Cell irradiation experiments at the research facility ELBE demand special technical prerequisites which mainly arises from the use of the intense CR. The intensity and the pointing of the ELBE beam show temporal variations which have to be monitored and taken into account. But also the complex tuning and optimization of the flexible electron beam line by the operators has to be mentioned. Both influence the reproducibility of irradiation experiments. Moreover, the ELBE beam provides a very small divergence, which leads to an increased spatial inhomogeneity of the dose distribution within the beam spot. For this reason the dose has to be measured for each irradiated sample. As a basic and cost efficient instrument self-developing radiochromic film dosimeters (model GafChromic® EBT Prototype A, henceforth referred to as EBT) have been used. Their high spatial resolution, low energy dependence and near tissue-equivalence make them highly suitable

for measurements of dose distributions in a wide photon energy range and in radiation fields with high dose gradients [13, 59, 91]. The EBT films were applied to quantitatively measure the dose delivered to each individual cell sample and online dose rate measurement (ionization chambers) was applied for experimental control.

For the reason of radiation protection regulations after switching off the beam, the cell samples can be taken out of the experiment room only after a waiting time of 20 min. Thus, the irradiation of a larger sample number requires an automatized irradiation procedure for which a cell irradiation system (CIS) has been designed, constructed and installed at ELBE. Spatial inhomogeneity of the dose distribution within the beam spot can be compensated by a special motion feature of the CIS in the case where simple beam scattering methods are not possible (limited intensity and strong attenuation of low-energetic CR). Supplementary, the CIS allows the use of various sample sizes with different geometries according to the biological endpoint to be investigated. For testing a procedure to spatially homogenize the delivered dose over the area of a single cell sample, the EBT films have been applied. In the following the installed cell irradiation setup at ELBE and the developed dosimetric procedure based on the use of the EBT film will be presented. Finally, first experimental results demonstrating the feasibility of the developed methods will be discussed in detail.

II. IRRADIATION SETUP AT ELBE

The elements of the radiation physics beam line at ELBE and the design of the CR source have already been described in detail in [89, 129]. A schematic drawing of the beam line parts essential for the radiobiological studies is shown in Figure 2.18. The electron beam is focused into the target chamber where different target positions are available. The generation of highly intense CR with photon energies in the range of 10 to 100 keV is realized by introducing diamond crystals (40...200 μm thick) [129]. High-energetic, polychromatic bremsstrahlung up to 40 MV is produced by insertion of foils made of aluminum for practical reasons. After passing the target chamber, the photon beam is separated from the electrons by a bending magnet. The photon beam leaves the beam line through a vacuum window of beryllium (19 mm in diameter, 100 μm thick) and is available for experiments at the irradiation site where the cell irradiation system (CIS) is situated. Along the beam line, two electron beam position monitors (BPM) are installed in front of the target area and in the beam dump for beam setting and electron beam current determination. Further beam monitoring devices especially dedicated to electron beam transmission measurements in CR experiments are discussed in [89].

It should be mentioned that incomplete electron beam transmission to the beam dump due to scattering of electrons to the walls of the beam line [90] results in an uncontrolled source of bremsstrahlung and neutron background. Due to variations in the beam setting in conjunction with unavoidable electron scattering in the target and, correspondingly, with production of background radiation, the measurement of the electron beam current is not sufficiently sensitive for estimation of photon flux at the irradiation site. Therefore, ionization chambers or alternatively photodiodes placed down the cell sample are used to measure the primary photon flux and to control cell irradiation experiments.

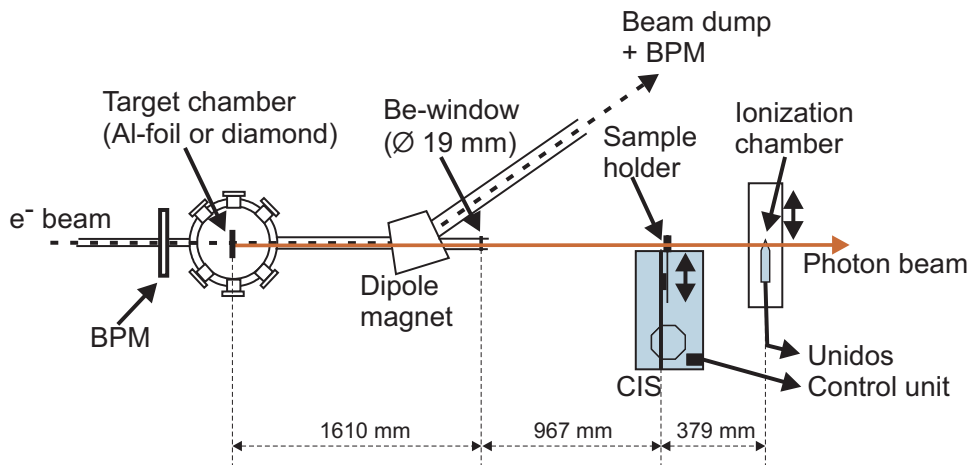


Figure 2.18: Schematic drawing of the irradiation site and beam line elements essential for radiobiological studies in the radiation physics cave at ELBE.

Cell irradiation system

An automated irradiation system for extensive routine use including user-friendly operation has been designed and constructed in collaboration with IFE-Automatisierungs GmbH and Intronik (both Dresden, Germany). It allows the irradiation of a larger number of cell samples by taking into account geometrical and spectral peculiarities of the radiation source and special cell culture conditions [73], respectively. For illustration, a picture of the CIS is shown in Figure 2.19. The CIS consists of a sample supply unit, a control unit and a personal computer. To prevent radiation damages to the control unit, it is placed outside the irradiation site. From the PC console, placed also outside the irradiation room and connected to the control unit, the irradiation procedure is software controlled. Up to 27 cell samples can be positioned in the turnable stack box, transported to the beam position and irradiated separately with a given dose value. To provide defined environment conditions during the irradiation procedure until the moment the samples can be returned to the cell laboratory (about 2 h), the stack box is covered with a plastic lid. Furthermore, a vessel is situated below the samples which can be filled with ice or water at a certain temperature depending on the requirements of the studied biological endpoint. Several cell sample geometries are manageable. All of them can be transported and irradiated from the same stack box (illustrated right in Fig. 2.19). The motion of the samples into starting position is provided by two axis, one moves horizontally and the other along the elevator. Both are independently driven by stepper motors. The angle between both axis amounts to 52.5° . This aims at a maximum distance between the beam position and the stack box in order to minimize the influence of background radiation on the cell samples remaining in the stack box. A changeable beam aperture allows additional flexibility in the irradiation geometry, particularly in the case of low-energetic photons.

Scanning procedure for dose homogenization

Despite the low electron beam emittance, the photon beam exhibits a significant divergence. This is due to the spread of the electron beam in the target which strongly depends on target thickness

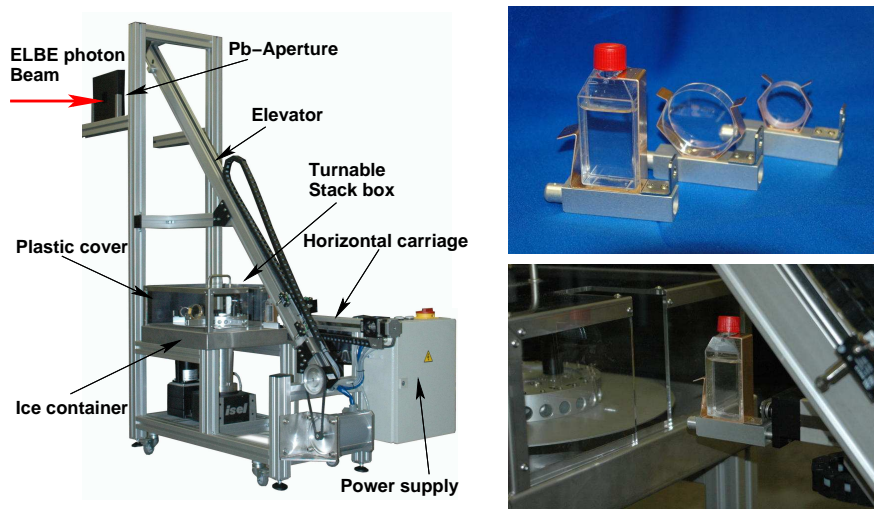


Figure 2.19: View of the cell irradiation system (left). Presentation of the cell sample holders with different geometry (top-right) and operation of the horizontal carriage (bottom-right).

and electron energy. Additionally, photon scattering on parts of the beam line and associated beam attenuation leads to a confined beam spot in the plane perpendicular to the beam axis. The spot size corresponds to the diameter of the beryllium vacuum window (see Fig. 2.18). At the cell sample position, which is situated in a distance of 96.7 cm to the vacuum window and 257.6 cm to the production target, the spot has a diameter of about 30 mm. Inside this spot the dose rate is not uniformly distributed.

In order to compensate for beam non-uniformities, in radiation therapy flattening filters are used. There, a uniform dose distribution is ensured by energy dependent absorption in the filter medium which is not suitable for radiobiological studies with low-energetic photons of several keV due to strong intensity attenuation.

Since a scanning option of the ELBE photon beam is not supported, the sample has to be moved. This is realized by a scanning feature of the CIS. The samples are moved in the plane perpendicular to the primary beam direction providing equal dose delivery to each cell of the sample. In the present CIS design, the scanning movement is controlled by a list of user-defined coordinates (scanning program) in order to take into account any cell sample geometry. A schematic drawing of a scanning trajectory used in this study is shown right in Figure 2.20. The trajectories mainly consist of a multiple of horizontal lines with a certain gap in between and a certain length according to the geometry of the cell sample, but any trajectory is conceivable. By the use of spiral scanning tracks, the homogenization effect can be increased [5]. For the reason of simplification, this kind of trajectory was not used in our study so far. The choice of the coordinates and hence the maximum field size is only limited by the outer frame size of the CIS and the stroke of the linear axis. A field size up to $15 \times 15 \text{ cm}^2$ is accessible which is sufficient for the most applications in radiobiological investigations. In this study, an in-house computer routine has been developed to simulate the motion-sequence of the CIS taking into account the technical specifications of the stepping motors.

With the aid of a dose distribution determined with EBT films during static irradiation at ELBE, the resulting distribution after the scanning movement of the sample can be calculated. For this, the stationary distribution is propagated numerically along the given coordinates and summarized. The resulting dose within the area of the cell sample and the duration of the irradiation process can be predicted.

Furthermore, the quality of the dose uniformity, expressed as the fraction of the standard deviation of the average dose in the region of interest $\sigma_{\bar{D}}$ and the average dose \bar{D} , can be optimized. This is done by varying the coordinates and, correspondingly, the gap between the lines and the line length. The total irradiation duration is controlled by the scan speed as well as the number of repetitions of the scanning program. It has to be practicable for radiobiological studies, and consequently a maximum dose rate per unit of area is desirable. Another important parameter is the dose fraction coming from background radiation onto the cell samples while they remain in the stack box. Apart from shielding, this fraction can only be minimized by reduction of the total irradiation duration. The dose delivered to the cell samples depends furthermore on the scan speed and on the fluctuations of the electron and, correspondingly, the photon beam intensity. These fluctuations can be compensated by an external feedback speed control signal. Therefore, the control unit of the irradiation system provides an interface for a voltage signal of ± 10 V. For calibration, the user adjusts a certain beam intensity and relates the corresponding feedback signal of an external detector to the initial scan speed as reference point for which further changes of the primary photon beam intensity are computer-controlled. Both feedback signal as well as velocity and position of the linear guides are logged with the PC for experimental control and further evaluation.

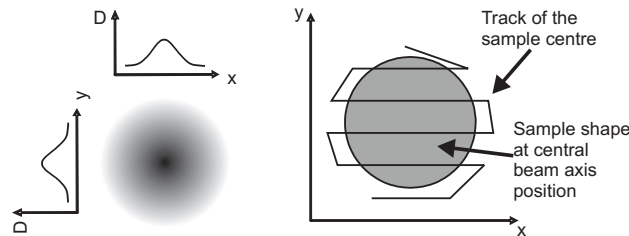


Figure 2.20: Schematic view of a dose beam profile and the meander-shaped track of the sample center for dose homogeneity over a circular sample.

Irradiation geometry

In radiobiological studies, mainly X-ray tubes are used for irradiation of biological objects. Attached cells are commonly irradiated in culture flasks or petri dishes with a vertical beam. Contrarily, *in vitro* cell experiments at the horizontal ELBE photon beam require a vertical position of the cell layer. Drying of the cell culture has to be prevented by placing the cells in a dish filled with culture medium. Moreover, sterility of the cell sample and the culture medium has to be assured during the whole process of irradiation and preparation until the final step of cell fixation. Another limiting condition comes from the energy range of the studied radiation field. In the case of low-energetic photons the cross section for photo effect increases strongly with decreasing photon energy. In order

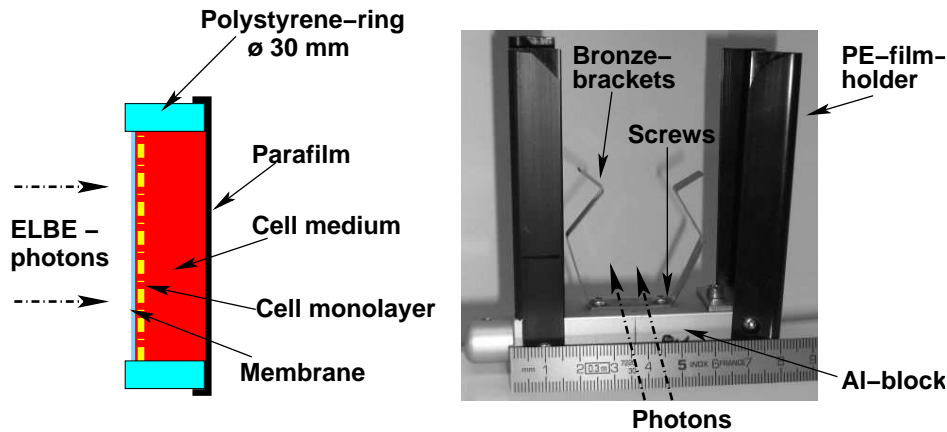


Figure 2.21: Schematic view of the cell culture vessel positioned for irradiation at the ELBE photon beam (left). Presentation of the sample holder components (right).

to minimize the attenuation of the primary photon flux, the amount of material in front of the irradiated cells should be reduced as far as possible. Additionally, Compton backscattering decreases the mean energy of the primary photon spectrum at the cell sample position. This demands a reduction of the material thickness behind the cell layer. In the contrary case of irradiation experiments with high-energetic photons, the dose build up effect in the material before the cell layer has to be taken into account. Furthermore, the influence of low-angle Compton scattering in the forward direction in the material surrounding the cells has to be considered.

In order to fulfill as far as possible all requirements, the following setup (Fig. 2.21, left) has been chosen for cell irradiations in first experiments [73]. The cells are cultivated on a 20 μm thick Biofolie membrane (Sartorius, Göttingen, Germany) fixed in a polystyrene ring (30 mm in diameter). Sealing is performed with Parafilm M (Merck, Darmstadt, Germany). The cell samples are mounted on sample holders, presented right in Figure 2.21, and can be reproducibly centered on the sample holder and thus on the beam axis by means of bronze brackets ($\rho = 8 - 9 \text{ g/cm}^3$) fixed with screws of stainless steel ($\rho = 7.5 - 8 \text{ g/cm}^3$) onto an aluminum block (96.5 % Al, $\rho = 2.7 \text{ g/cm}^3$). Film holders of polyethylene are additionally mounted on the sample holder for dose measurement purposes.

III. DOSE MEASUREMENT WITH RADIOCHROMIC FILMS

The core of the dosimetric system used in the presented study are GafChromic® EBT films (Prototype A, Lot number 35146-002AI). They have been chosen because of their appropriate sensitivity (dose range of 0.01 to 8 Gy), their low energy dependence of the dose response ($< 5 \%$ in the range from 30 keV to 18 MeV) [59] and because they allow simple readout with conventional flat-bed scanners [20, 21, 59]. Hence, EBT films have been recently introduced into experimental irradiation setups at radiotherapy machines [126].

At the radiation source ELBE, EBT films have been used to determine the absolute dose delivered to irradiated cell samples as well as for the development and verification of the dose homogenization procedure. The calibration of the EBT film dosimeter was performed according to the protocol de-

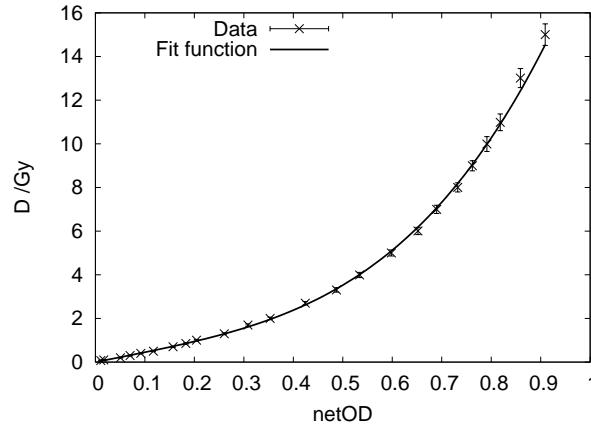


Figure 2.22: Fitted calibration data for GafChromic® EBT film using Microtek ScanMaker i900.

scribed in detail in [20, 21]. For radiation quality, a high-voltage X-ray unit Isovolt 320 HS (Pantak Seifert, Ahrensburg, Germany) with a tungsten anode, 7 mm Be inherent filtration and a 0.5 mm Cu filter was used. The device is situated in a laboratory near the radiation physics cave. The X-ray tube serves as reference radiation source in the frame of radiobiological studies [73, 74, 75] as well. Furthermore, with a special socket providing horizontal radiation direction, dosimetric systems and detectors as well as the radiation setup can be tested independently of ELBE operation.

The dosimetry for a 200 kV radiation field was performed by means of a Unidos dosimeter in combination with four ionization chambers (IC): two rigid stem and two Farmer ionization chambers (type M23332 and M30010, both PTW Freiburg, Germany). Different types were used in order to reduce the dose uncertainty, mainly influenced by the relative uncertainty of 2.2 % of the calibration factor for each IC. The calibration factors are specified by the manufacturer with a ^{60}Co source used for the calibration field. Averaging the dose signals of the used IC resulted in a relative over all dose uncertainty of < 2.7 %.

Similar to the proposed protocol [21] four film packets, each consisting of 25 film pieces, were prepared and irradiated with different dose values in the range of 0.072 to 15.0 Gy. Subsequently, the film samples were digitized with a flat-bed document scanner (Microtek ScanMaker i900), and the net optical density $netOD$ for each film sample was calculated. Following the approach proposed in [20], the calibration curve (Fig. 2.22) was obtained by fitting using the analytical form

$$(2) \quad D_{fit}(netOD) = p1 \cdot netOD + p2 \cdot netOD^{p3}$$

For the fixed parameter $p3 = 3.5$ the fitting parameters $p1 = 4.47 \pm 0.06$ and $p2 = 14.63 \pm 0.25$ were determined using the method of least-squares minimization, taking the dose errors as weights. A systematic error analysis has been performed where a total relative dose uncertainty of < 5 % has been obtained in the dose range of 0.5 to 15 Gy.

The stability of the calibration data has been investigated with films of the same lot 11 months after the first calibration. Therefore, 21 film samples have been exposed to 7 different dose values

in the range of 0.7 to 14.6 Gy using the 200 kV filtered X-ray source. Subsequently, the *netOD* values of the 3 samples with same dose have been averaged and inserted in Eq. 2. By comparing the calculated dose with the actually delivered dose, a relative deviation of $\lesssim 4\%$ has been determined. This is within the total relative dose uncertainty of 5% confirming the good stability of the EBT film over a long period of time.

Dosimetric procedure

An important technical prerequisite for irradiation experiments is the presetting of a certain dose value as precise as required. Direct measurement of the electron beam current is not efficiently sensitive. This is due to variations in the beam setting in conjunction with electron scattering and, correspondingly, with production of bremsstrahlung background radiation in parts of the beam line. For this reason, the photon flux has been measured directly using an ionization chamber positioned 2956 mm behind the target (see Fig. 2.18). A dose rate of 1 Gy/min is adjusted by variation of the electron beam current at the accelerator injector. By presetting a certain irradiation duration, several dose values are provided, whereas on/off-switching of the electron beam is realized with a precision of ± 2 s at the injector gate. Due to their poor spatial resolution, ionization chambers are not suitable for the determination of the spatial dose distribution at the cell position. This fact becomes even more important when the photon beam is not homogeneous. Also the influence of the sample geometry cannot be taken into account. Therefore, the EBT films have been introduced. The film samples were placed in special holders 5 mm in front of the cell samples (see right in Fig. 2.21). For the dose value of a certain cell sample, the film dose signal was averaged over the sample area. Subsequently, a correction of the obtained dose value is necessary which takes into account the beam induced interactions in the material surrounding the cell samples as well as the film itself, in accordance with the used photon energy range. Therefore, a piece of film is cut to fit in the Biofolie vessel. It is irradiated instead of the cell layer at exactly the same position. With the measured dose value in front of the sample D_{film} and the dose measured in the vessel $D_{Biofolie}$, a calibration factor k can be calculated by following expression

$$(3) \quad k = \frac{D_{Biofolie} - D_{bckg}}{D_{film} - D_{bckg}}.$$

The background dose D_{bckg} describes the dose fraction delivered to the cell samples in the stack box during the whole irradiation process (about 2 h). It is due to background radiation coming from photons as well as electrons mainly scattered in the region of the bending magnet and the beam dump (see Fig. 2.18). The background dose was measured using several film samples well distributed in the stack box. Vice versa, by applying Eq. 3, the corrected dose can be calculated as function of k , D_{film} and D_{bckg} . Due to temporal and spatial variations of the photon beam intensity and background radiation, the absolute dose was retrospectively measured with films for each single cell sample. It should also be mentioned, that according to the radiobiological objectives the dose fraction coming from background radiation has to be sufficiently small. For this reason an appropriate over all duration of the irradiation procedure needs to be chosen.

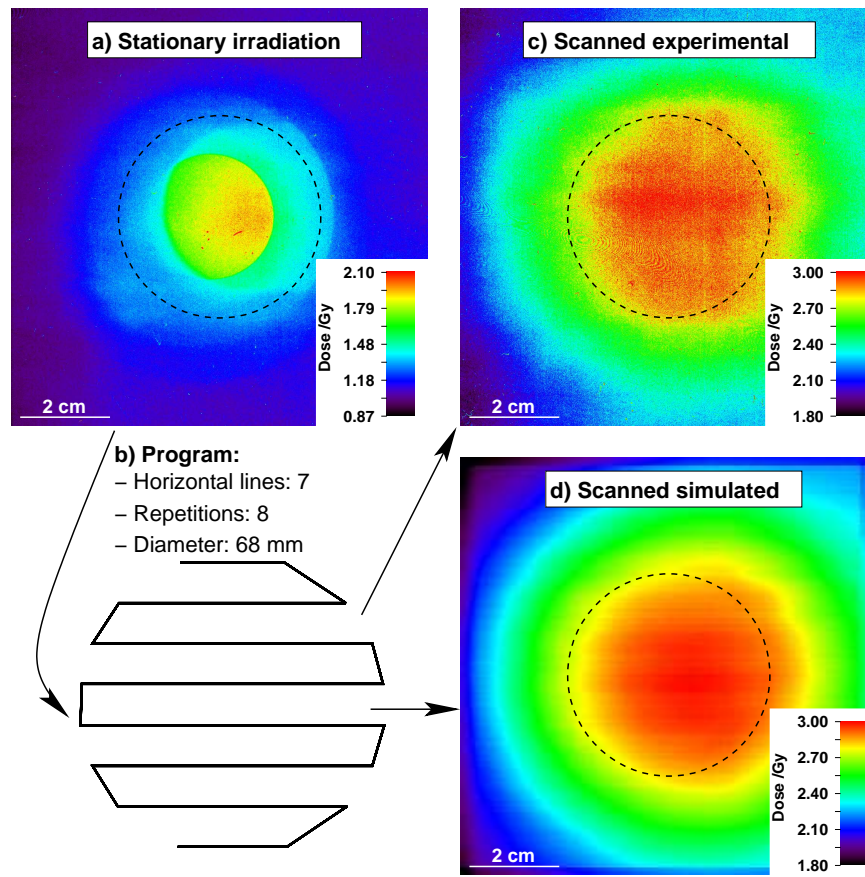


Figure 2.23: Dose homogenization with 34 MV bremsstrahlung in the area indicated by the dashed circles (petri dish); a) Measured dose distribution after stationary irradiation, b) Scanning program, c) Resulting dose distribution measured with a moved film sample and d) Predicted dose distribution.

IV. APPLICATION

Homogenization procedure in experiments

The feasibility of the developed dose homogenization method as well as the described dosimetry procedure have been demonstrated in independent experiments by reason of simplification. The verification of the dose homogenization procedure has been performed with 34 MV bremsstrahlung. Here, an aluminum foil of $18 \mu\text{m}$ thickness served as a production target. For experimental preparation, a stationary dose distribution measured on a previous experiment was taken to set up the scanning program. The program was optimized for homogeneously distributed dose within the area of a petri dish with a diameter of 45 mm. During the experiment, another stationary dose distribution has been determined to reconfirm simulated and measured distribution after the scanning process. As can be observed in Figure 2.23, the obtained distributions match very well. Since the beam spot is not symmetric in the stationary distribution (Fig. 2.23) the actually homogenized area is slightly displaced relative to its expected position (dashed circles). This effect has to be taken into account in following experiments, or better yet, the symmetry of the beam spot and the position of the dose maximum have to be online monitored.

Dose distribution	\bar{D} (Gy)	$\sigma_{\bar{D}}/\bar{D}$ (%)	\dot{D}_{eff} (mGy/min)
Stationary	1.53	14.1	365
Scanned experimental	2.87	3.5	280
Scanned simulated	2.91	2.3	—

Table 2.4: Comparison of the averaged effective dose rate \dot{D}_{eff} and the homogeneity of the different dose distributions $\sigma_{\bar{D}}/\bar{D}$ inside the region of the dashed circles in Fig. 2.23

For further illustration of the homogenization effect, the homogeneity parameter $\sigma_{\bar{D}}/\bar{D}$ of the different dose distributions is listed in Table 2.4. As can be seen, the inhomogeneity has been successfully reduced. The averaged effective dose rate \dot{D}_{eff} , where effective means after subtraction of the background dose fraction measured in the stack box, is listed in Table 2.4 as well. As expected, the sample movement leads to a reduction of \dot{D}_{eff} in comparison to the static irradiation which reveals another limitation. Since dose rate reduction correlates with an increase in irradiation duration, the dose delivered to the cell samples in the stack box due to isotropic and polychromatic background radiation is also augmented. Hence, the homogenization effect is decreased. In order to minimize the background dose, the film samples were removed from the irradiation site directly after two samples have been irradiated, with and without movement (14 min). But due to the large expenditure of time for opening and closing the radiation protection doors, this is not suitable in routine use. Therefore, in the following experiments the fraction of the background dose has been reduced by one order of magnitude with a 2.5 mm thick Pb foil for additional shielding of the stack box.

For simplification this experimental run was performed without the correction of the relative intensity fluctuations amounting only to 1 - 2 %. Contrarily, in the more time-consuming cell irradiation experiments (about 2 h), significant fluctuations (about 10 %) can occur which then have to be compensated.

RBE of 34 MV bremsstrahlung

The feasibility of the dosimetry method and the CIS has been demonstrated in the first cell irradiation series at ELBE. This study was aimed at the determination of the RBE of 34 MV bremsstrahlung relative to 200 kV X-rays. On four experiment days, cell monolayers in Biofolie vessels (about 40000 cells per sample) were irradiated. The 200 kV reference irradiation was performed with the mentioned Isovolt X-ray tube in petri dishes (about 50000 cells per sample). The used cell line 184A1 (purchased from ATCC, USA) consisted of the human mammary gland epithelial cells originating from mammaplasty tissue of a 21 year old woman showing no detectable breast epithelial cell pathology [120]. For the evaluation of radiation induced effects, the micronuclei (MN) induction was used [74, 75]. After irradiation, the cells were observed under a light microscope and the fraction of binucleated cells (BNC) with MN as an expression of the frequency of radiation damage was determined.

As mentioned the absolute dose delivered to the cell layer was measured with film dosimeters in front of each single cell sample. Since the beam spot on the film dosimeter was of the same size

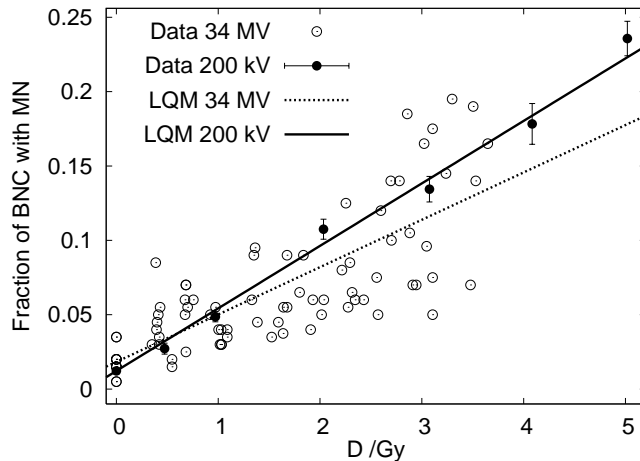


Figure 2.24: Dose response curves for 34 MV bremsstrahlung and 200 kV X-rays. The graph includes the corresponding fitting curves Eq. 7 as well.

as the cell samples, the film dose has been averaged over this area. In order to consider the dose build up effect of the front film sample and radiation scattering on parts of the sample holder, the calibration factor k (Eq. 3) was determined. In two different experiment runs, $k = 1.23 \pm 0.04$ has been calculated as an average over 12 single measurements. In the considered dose range from 0.5 to 4 Gy, a total relative error of 9 % for the measured dose values has been obtained. This dose error was mainly influenced by the uncertainty of the background dose fraction ΔD_{bckg} , which is not only due to the uncertainty of the film dose value but also due to variations in the experimental conditions such as tuning of the electron beam. The inhomogeneity (σ_D/D) of the area considered for the dose measurement amounted to 10 - 17 % mainly depending on the beam alignment, that underlines the necessity of the described homogenization procedure.

For illustration, the measured dose response curves meaning the fraction of BNC with MN as function of the dose are presented in Figure 2.24 for 34 MV bremsstrahlung and 200 kV reference radiation. For the reference irradiations, the delivered dose levels were provided by adjusting a certain irradiation duration where the dosimetry can have to be done in advance. Therefore, the biological effect of multiple experiments could be averaged for each dose level which leads to a high reproducibility. Contrarily, a significant spread of the determined data points for 34 MV due to the mentioned beam and variations of the background dose fraction can be observed. Particularly, the spread of the measured dose values points out the necessity of the dosimetry for each sample individually. Aside from the described dose uncertainties, this spread is also due to fluctuations in the biological effect. The harsh environment conditions in combination with longer and more differing stay of the samples at the ELBE irradiation site, in comparison to irradiation with the X-ray tube, cause larger variations of cell response. This can already be seen in an increased variation of the non-irradiation induced effect determined by unexposed control samples (cf. Fig. 2.24). The influence of the used culture vessel in comparison to more often used culture flasks has been found negligible [73].

However, a statistically significant radiobiological result has been obtained. The data was fitted by means of the linear-quadratic model

$$(4) \quad y(D) = c + \alpha D + \beta D^2,$$

with $y(D)$ as corresponding fraction of BNC with MN for dose values D . The parameter c stands for the background level given by non-irradiated control samples that were kept in the incubator in our laboratory. The fitting parameters α and β were obtained by applying the method of least-square minimization using the reciprocal standard deviations as weights. Finally, an RBE of 0.75 ± 0.05 was calculated as a fraction of the α -coefficients for 34 MV and 200 kV as reference. The given uncertainty represents exclusively the statistic accuracy. The relative dose error of 9 % has to be considered additionally.

In the literature no data is reported that can be directly compared to the here measured RBE of MV bremsstrahlung. In several experiments [48] monoenergetic ^{60}Co radiation is compared to X-rays in the range of 200 to 350 kV. The results show an RBE ranging from 0.25 to 1, strongly dependent on the applied high voltage and filtration of the used X-ray tube. Furthermore the RBE is strongly influenced by the used cell line and the investigated biological endpoint. The best matching RBE of 0.8 with an important uncertainty of 38 % has been determined for human lymphocytes using ^{60}Co radiation versus 350 kV X-rays filtered with 1.12 mm Cu and 1.02 mm Al for induction of micro-nuclei. However, the RBE obtained in our experiments is in good agreement with the systematics of the RBE values reported in [48].

It should also be mentioned that for the application of 34 MV bremsstrahlung the influence of photo nuclear particles, e.g., (γ, n) , (γ, p) created by high-energetic photons hitting parts of the beam line or the concrete wall of the cave has to be considered. Investigations of 50 MV bremsstrahlung compared with ^{60}Co radiation for several cell lines (V79-379A, GSH^{+/+} and U-1690) using clonogenic assay show an RBE in the range of 0.988 to 1.009 [96]. Thus, an influence of photo nuclear reactions is only marginal, if one accepts an error within a fraction of a per cent. In our experiments the neutron background dose rate was monitored by means of a neutron detector (purchased from Berthold, Bad Wildbad, Germany) consisting of a proportional counter filled with ^3He gas and embedded in a Bonner sphere of polyethylene with a diameter of 25 cm. It was situated in a distance of about 1 m to the stack box of the irradiation system. An equivalent dose rate in the range from 10 to 50 mSv/h has been measured. In comparison with the primary photon dose rate of ≈ 1 Gy/min, the influence of photo neutrons has been consequently found to be negligible.

V. CONCLUSION

In the present work, physical and technical prerequisites for *in vitro* cell irradiation experiments in the frame of radiobiological studies have been established and their feasibility has been successfully tested with 34 MV bremsstrahlung. Thereby, one major topic was the setup of the automatic cell irradiation system and its installation at the ELBE beam line for routine cell irradiation studies. An appropriate procedure to compensate spatial inhomogeneity of the dose distribution within the

beam spot has been demonstrated. The second essential part was the dosimetry with GafChromic® EBT film dosimeter. The films were calibrated with a 200 kV radiation field, where an accuracy of 5 % in the dose range of 0.5 to 15 Gy has been accomplished. Several specifications quoted by the manufacturer or determined in [21] have been reconfirmed. As practical, reliable and low-budget instruments, the EBT films were found to be highly suitable dosimetric instruments in experiments involving unconventional radiation sources. Based on the EBT film dosimeter, two dedicated methods have been separately developed. The film based measurement of the absolute dose delivered to the cell sample and the homogenization of the applied dose over the area of the cell samples. Both methods have already been introduced in extensive radiobiological studies to investigate the RBE of photon radiation as a function of the photon energy. Although a minor energy dependence of the dose response in the range from 30 keV up to 18 MeV has been quoted by the manufacturer [59] and validated in several works [12, 16, 102], further investigations according to the experimental requirements are of advantage. Especially for low-energetic photons (< 30 keV) the dose response has to be verified either by means of our X-ray tube in combination with a soft X-ray ionization chamber or in collaboration with the manufacturer.

The described methods can be easily transferred to experiments at ELBE with low-energetic CR or even with the primary electron beam after verification of the film calibration. Certainly, in the case of changed experimental conditions the contributions of dose build up effect and occurring scattering effects to the dose distribution have to be verified. For 34 MV bremsstrahlung, this has been exemplary demonstrated.

However, extensive radiobiological studies have been started. This includes RBE investigations for different cell lines and various endpoints, such as clonogenic cell survival, induction of micronuclei, chromosomal aberrations and DNA double strand break induction [6].

Acknowledgements

We are obliged to the ELBE crew for their interest and support of this work.

Author contributions

Study concept and design K.Z., E.B., J.P., W.W.; Experimental studies K.Z., E.B., J.P., E.L., W.W.; Data acquisition K.Z., E.L., E.B.; Literature research E.B., K.Z.; Data analysis K.Z., E.B.; Manuscript preparation K.Z.; Manuscript editing J.P., E.B., W.W., K.Z.; Guarantor of integrity of the entire study J.P.; Manuscript review was carried out by all authors.

Relative biological effectiveness of 25 and 10 kV X-rays for the induction of chromosomal aberrations in two human mammary epithelial cell lines

Elke Beyreuther^a, Wolfgang Dörr^b, Anna Lehnert^a, Elisabeth Lessmann^a and Jörg Pawelke^{c,a}

^a Forschungszentrum Dresden-Rossendorf, Dresden, Germany

^b Department of Radiotherapy and Radiation Oncology, Medical Faculty Carl Gustav Carus, Technische Universität Dresden, Dresden, Germany

^c OncoRay, Center for Radiation Research in Oncology, Technische Universität Dresden, Dresden, Germany

Corresponding author:

Elke Beyreuther

Institute of Radiation Physics

Forschungszentrum Dresden-Rossendorf

P.O. Box 510119

D-01314 Dresden, Germany

Fon: +49 351 260 3552

Fax: +49 351 260 3700

E-mail: E.Beyreuther@fzd.de

Radiation and Environmental Biophysics 48(3):333-40(2009)

DOI: 10.1007/s00411-009-0221-4

www.springerlink.com

ABSTRACT

Administration of ionizing radiation for diagnostic purposes can be associated with a risk for the induction of tumors. Therefore, particularly with regard to general screening programs, e.g., with mammography, cost-benefit considerations must be discussed including risk estimation depending upon the radiation quality administered. The present study was initiated to investigate the *in vitro* X-ray energy dependence for the induction of chromosomal aberrations in the two mammary epithelial cell lines, 184A1 and MCF-12A. The induced excess fragments, dicentric chromosomes and centric rings were analyzed and the relative biological effectiveness (RBE) was determined for 10 and 25 kV X-rays relative to 200 kV X-rays. The assumed energy dependence with higher values for 10 kV X-rays was confirmed for the excess fragments, with RBE_M values of 1.92 ± 0.26 and 1.40 ± 0.12 for 10 kV X-rays and 1.17 ± 0.12 and 0.97 ± 0.10 for 25 kV photons determined for cell lines 184A1 and MCF-12A, respectively. Meaningful results for the induction of dicentric chromosomes and centric rings were obtained only for higher doses with RBE values of 1.31 ± 0.21 and 1.70 ± 0.29 for 184A1 and 1.08 ± 0.08 and 1.43 ± 0.12 for MCF-12A irradiated with 25 and 10 kV X-rays, respectively.

I. INTRODUCTION

During the last years the relative biological effectiveness (RBE) of low-energy X-rays, particularly in the range below 50 keV, has been a topic of continuous discussions. One reason for this is a potential risk of radiation-induced cancer by mammography, especially in the light of the introduction of mammography screening programs in some countries, e.g., USA, The Netherlands and Germany [122]. Based on *in vitro* data [32, 40, 45, 68, 74, 75, 86, 108, 112, 113, 119], it must be assumed that X-rays in the low energy range are more effective per unit dose than X-rays of higher energy. In contrast, a weighting factor w_R of 1 is specified in the ICRP Recommendations [57], independent of the photon energy.

Radiobiological investigations focusing on the RBE of soft X-rays, using the induction of micronuclei as an endpoint, have been performed with human fibroblasts and keratinocytes [119] irradiated with 25 kV, and on human mammary epithelial cells irradiated with 25 kV [75] and 10 kV X-rays [74]. The maximum low-dose RBE values obtained for the number of micronuclei per binucleated cell and relative to photons from a 200 kV X-ray tube, range from 1.4 to 4.1 for 25 and 10 kV X-rays, respectively. Furthermore, enhanced RBE values have been found by experimental studies of neoplastic transformations of human hybrid cell line CGL1 irradiated with 29 kV X-rays compared to different reference radiation sources [32, 40, 45]. Frankenberg *et al.* [32] found an RBE of about 4 by using 200 kV X-rays filtered with 0.6 mm Cu as reference. Similar results have been obtained using 220 kV X-rays filtered with 4.05 mm Al and 0.5 mm Cu [40] as well as a ^{90}Sr - ^{90}Y electron source or a simulated atomic bomb spectrum [45].

Relative biological effectiveness values for the induction of chromosomal aberrations were determined depending upon the photon energy, especially for dicentric chromosomes in human lymphocytes [68, 108, 112, 113]. The photons applied were either generated by synchrotrons and were monoenergetic within an energy range of 1.83 - 40 keV. Or, they were produced by X-ray tubes with various filtrations and show a broad spectral distribution. Hill [48] reviewed these data and concluded an increasing RBE with decreasing photon energy to a maximum at 6.9 keV, followed by a decrease at lower energies. At the maximum of 6.9 keV Sasaki *et al.* [108] found an RBE of 4.6 ± 2.6 for monoenergetic synchrotron X-rays compared to photons from a 200 kV X-ray tube. Accordingly, a maximum RBE_M of 7.7 ± 3.0 was obtained for 6.9 keV monoenergetic synchrotron X-rays relative to ^{60}Co γ -rays [68].

Most of the experimental studies on the determination of RBE values for the induction of chromosomal aberrations have been performed on human lymphocytes and rarely on other human cell lines. However, mammary epithelial cells are of particular interest for the radiation induction of breast cancer. Therefore, two human mammary epithelial cell lines, MCF-12A and 184A1, were chosen in the present study to determine the relative biological effectiveness of soft X-rays for the induction of chromosomal aberrations, especially for excess fragments. The irradiations were performed with photons of 10 and 25 kV, and compared to 200 kV X-rays as reference.

II. MATERIAL AND METHODS

Cell culture

In the present experiments two human mammary gland epithelial cell lines, MCF-12A and 184A1 (both purchased from ATCC, USA), were applied.

The primary culture of 184A1 was established from the mammaplasty tissue of a 21-year-old woman and shows no detectable breast epithelial cell pathology. Applying the carcinogen benzo[a]pyren [120], a chemical transformation was induced resulting in the continuous cell line 184A1. This cell line is adherent and immortal, but not malignant, with a chromosome modal number of 45, which was determined in our laboratory using passage 7 cells. Monolayered 184A1 cells were maintained in serum-free mammary epithelial basal medium (MEBM, Cambrex, USA) supplemented with 5 $\mu\text{g}/\text{ml}$ human epidermal growth factor, 0.5 $\mu\text{g}/\text{ml}$ hydrocortisone, 5 $\mu\text{g}/\text{ml}$ insulin, 52 $\mu\text{g}/\text{ml}$ bovine pituitary extract, 5 $\mu\text{g}/\text{ml}$ gentamicin sulfate/amphotericin-B (all as MEGM SingleQuots®, Cambrex), 5 $\mu\text{g}/\text{ml}$ human apo-transferrin (Sigma-Aldrich, USA) and 50 $\mu\text{g}/\text{ml}$ prostaglandin E1 (Calbiochem, Germany). The medium and supplements were optimized for fast growing and high plating efficiencies of epithelial cell lines [42], whereas the addition of prostaglandin E1 resulted in a maximum plating efficiency of 35.2 ± 2.9 %.

Cell line MCF-12A, also originated from mammaplasty tissue, was derived by applying elevated temperatures to the primary culture [94]. However, the mammaplasty tissue exhibited a kind of benign breast disease (intraductal hyperplasia) and the derived cell line, although non-tumorigenic, possesses several consistent numerical and structural aberrations, correlated with a variable chromosome number between 65 and 71 [94]. A chromosome modal number of 64 was determined for the present experiments. For the culture of cell line MCF-12A, described more detailed in Lehnert *et al.* [75], a 1:1 mixture of DMEM and Ham's F12 medium was supplemented with 5 % horse serum (all from Biochrom, Germany), 0.5 $\mu\text{g}/\text{ml}$ hydrocortisone, 10 $\mu\text{g}/\text{ml}$ insulin (both from Sigma-Aldrich) and 20 ng/ml epidermal growth factor (Becton Dickinson, USA). The cholera toxin (100 ng/ml, Calbiochem, USA) originally added in the formula was substituted by 50 $\mu\text{g}/\text{ml}$ Prostaglandin E1, leading to a plating efficiency of 61.5 ± 4.7 %.

For detachment, a solution of 0.25 % trypsin and 0.03 % EDTA in PBS (all from Biochrom) was applied for 10 min at 37°C. Both cell lines were grown in 25 cm² culture flasks (Nunc or Greiner, Germany), with a seeding density of 6,000 cells per cm², and incubated at 37°C in humidified atmosphere containing 5 % CO₂. The media, normally 5 ml per flask, were exchanged every third day and subculturing was performed before reaching 70 % confluence.

In order to obtain synchronized cells, they were plated at densities between 6,000 and 12,000 cells per cm² and allowed to grow for 11 - 12 days to confluence arrest. Synchronization was verified by the BrdU staining (see below), and for 184A1 additionally a FACS analysis was performed. Using the BD FACSCalibur™ system (Becton Dickinson, USA) and cells stained with 50 $\mu\text{g}/\text{ml}$ propidium iodide, a fraction of 97 % of the cells was found in G0/G1-phase.

Chromosomal aberrations and differential chromatid labeling

For the determination of chromosomal aberrations (CA) and the number of cell cycles passed after

irradiation, we applied the method of Fluorescent plus Giemsa staining (FPG), as described by Perry and Wolff [95], optimized for the cell lines used in this study. After irradiation, the cells were subcultured at a density of 8,000 cells per cm^2 and incubated for 45 h (184A1) or 36 h (MCF-12A), respectively. In order to arrest mitotic cells in the first post irradiation division, colcemid (Biochrom) was added to the culture medium for the last 2 h at a final concentration of $0.74 \mu\text{g}/\text{ml}$ for 184A1 and for 3 h at $0.29 \mu\text{g}/\text{ml}$ for MCF-12A. After harvesting, a hypotonic treatment with a solution of 3 mg/ml trisodium citrate and 2.35 mg/ml potassium chloride (both from Merck, Germany) was performed for 15 min and finally, the cells were fixed in a 3:1 methanol/acetic acid fixative (both from VWR, Germany). The metaphase suspension was dropped onto grease-free, cold, wet slides and stained with 2.1 % Giemsa (Merck) in PBS after one week.

In order to determine the number of cell cycles passed after irradiation, cells from the control group as well as from the group irradiated with the highest dose of 5 Gy were incubated with 5-Bromo-2'-deoxyuridine (BrdU, Sigma-Aldrich) at final concentrations of $3 \mu\text{g}/\text{ml}$ for 184A1 and $5 \mu\text{g}/\text{ml}$ for MCF-12A, simultaneously to the probes where chromosomal aberrations were determined. The cells incubated with BrdU were harvested and the slides were stained for 10 min in a solution of 0.1 mg/ml Hoechst H33258 (Bisbenzimidazole, VWR) in Weise buffer ($25.1 \text{ mg}/\text{ml}$ disodium hydrogen-phosphate dodecahydrate, Merck and $9.1 \text{ mg}/\text{ml}$ potassium dihydrogen phosphate, Sigma-Aldrich). Subsequently, photolysis with 254 nm UV light was performed; the slides were incubated for 30 min at 61°C in a twofold SSC solution, made up of $13.2 \text{ mg}/\text{ml}$ sodium chloride and $2.2 \text{ mg}/\text{ml}$ trisodium citrate (both from Merck), and eventually stained with Giemsa as described above.

Irradiation and dosimetry

The irradiation setups, dosimetry and the determination of the spectral dose distribution were described previously in detail [74, 75]. In brief, the reference irradiation was performed with an Isovolt 320/20 X-ray tube (Roentgen Seifert, Germany) operated at 200 kV with a tungsten anode, 7 mm Be inherent filtration and a 0.5 mm Cu filter. The culture flasks were placed horizontally at a focus-to-cell distance of 45 cm and irradiated with a vertical X-ray beam through the top of the dish and the culture medium. Three flasks were irradiated simultaneously at a dose rate of 0.3 Gy/min for 0.5 Gy and 1.2 Gy/min for higher doses; those which were not currently irradiated were kept on ice. Dosimetry was performed with a Unidos dosimeter and an ionization chamber type 31003 (semi-flex tube chamber 0.3 cm^3 , both PTW, Germany).

Irradiations with soft X-rays were performed using a tungsten target Darpac 150-MC X-ray tube (Forward Raytech, UK) at 25 or 10 kV. The inherent filtration was 2 mm Be, the focus-to-cell distance 25 cm. Dose rates were measured with a small soft X-ray ionization chamber type 23342 (sensitive volume 0.02 cm^3) and a Unidos dosimeter (both from PTW). The application of a 0.3 mm Al filter resulted in a dose rate of 2 Gy/min for cell irradiations with 25 kV. For 10 kV no additional filtration was applied and the dose rate was 0.5 Gy/min. In order to minimize the beam attenuation through the medium in case of the soft X-rays, the culture flasks were placed upside down in a foamed polystyrene holder, and hence the cells were irradiated through the plastic bottom of the flasks. Irradiation times did not exceed 10 min and no consequences from medium depletion were

expected. The irradiations were performed at room temperature and the irradiated flasks were kept on ice until the experiment was finished. Afterwards all the flasks were treated simultaneously as described before.

Dose distribution and homogeneity within the irradiated field of both X-ray tubes were determined using GafChromic® EBT dosimetry films (ISP, USA), which are self-developing, consist of tissue equivalent materials and show high spatial resolution. The dose variation within the irradiated field was lower than 3.0 % for the 200 kV X-rays, 4.0 % for 25 kV X-rays and 2.5 % for 10 kV X-rays.

In order to calculate the correct dose at the position of the cells for the 10 kV irradiations, the thickness of the bottom was measured for all used culture flasks at five homogeneously distributed positions. A previously defined correlation between thickness and dose was applied to calculate the exact doses and their corresponding standard errors. In each experiment, two flasks per dose point were irradiated, and two additional flasks for the BrdU staining were irradiated with 5 Gy.

Data evaluation

Chromosomal analyses were performed with a Zeiss Axiostar microscope at a magnification of 1,000. Three independent experiments were analyzed for each dose point, except for the 25 kV irradiations of 184A1 with two successful experiments. Acentric fragments, dicentric chromosomes and centric

Dose (Gy)	Cells scored	Dic.	Rings	Excess fragments	Distribution of exfrag.				σ^2/λ	u value
					0	1	2	3		
<i>200 kV X-rays</i>										
0	1,235	0	0	30	1,205	30			0.98	-0.59
0.5	668	0	0	31	637	31			0.96	-0.84
1	554	1	0	44	510	44			0.92	-1.31
2	571	11	2	84	495	68	8		1.04	0.77
3	300	12	2	48	254	44	2		0.93	-0.91
5	300	15	12	86	226	63	10	1	1.02	0.23
<i>25 kV X-rays</i>										
0	1,120	0	0	22	1,098	22			0.98	-0.45
0.5	636	0	0	31	605	31			0.95	-0.86
1	450	4	0	41	410	39	1		0.96	-0.61
2	361	7	6	64	306	46	9		1.11	1.45
3	200	13	5	40	163	34	3		0.96	-0.46
5	200	19	11	63	143	51	6		0.88	-1.21
<i>10 kV X-rays</i>										
0	1,035	0	0	30	1,006	28	1		1.04	0.90
0.492 ± 0.002	762	1	0	48	717	42	3		1.06	1.25
0.980 ± 0.008	728	11	1	88	643	82	3		0.95	-0.99
1.966 ± 0.016	663	41	6	138	545	100	16	2	1.11	2.05
2.953 ± 0.021	278	23	11	78	214	52	10	2	1.13	1.58
4.922 ± 0.035	300	55	22	103	220	59	19	2	1.15	1.79

The dose values for 10 kV are the mean from all experiments ± SD

Table 2.5: Yields of excess fragments (exfrag.), dicentric chromosomes (dic.) and centric rings observed in metaphase cells of cell line 184A1 after irradiation with 200, 25 and 10 kV X-rays.

rings were determined in 300 - 1,200 metaphases per dose. One acentric fragment was related to each dicentric chromosome or centric ring; two of them were associated with the rare tricentric chromosomes, assessed as two dicentrics. Remaining acentric fragments were considered as “excess“ fragments. To fit the experimental data, the method of iteratively reweighted least-squares minimization was applied. For the excess fragments the reciprocal variances were used as weights and the data were fitted to the linear dose-response $y = c + \alpha D$, with y defined by the yield of induced excess fragments and c by the background values found in the controls. The combined yields (y) of dicentric chromosomes and centric rings were fitted to the quadratic equation $y = \beta D^2$, whereas no background value c was defined and weighting was not indicated due to the absence of exchange aberrations in the low dose region. RBE_M and RBE values were calculated on the basis of obtained dose dependencies, their corresponding errors by error propagation using the uncertainties of the fitted parameters. Statistical significance was proven by Student’s t test.

III. RESULTS

In order to avoid the distortion of the primary damage by subsequent divisions, cells in the first metaphase are required. Therefore, the number of cell cycles passed was determined with the BrdU staining. For cell line 184A1 we found that 45 h after irradiation 91 % of the cells from the control group and 100 % of the 5 Gy irradiated ones underwent exactly one division. A similar result was

Dose (Gy)	Cells scored	Dic.	Rings	Excess fragments	Distribution of exfrag.				σ^2/λ	u value
					0	1	2	3		
<i>200 kV X-rays</i>										
0	600	0	0	30	570	30			0.95	-0.85
0.5	600	0	0	53	547	53			0.91	-1.52
1	600	7	0	57	543	57			0.91	-1.63
2	300	15	2	35	266	33	1		0.94	-0.70
3	300	22	8	46	256	42	2		0.94	-0.78
5	300	53	12	60	241	58	1		0.84	-2.02
<i>25 kV X-rays</i>										
0	600	0	0	41	561	37	2		1.03	0.54
0.5	600	1	0	40	560	40			0.93	-1.14
1	600	4	1	61	541	57	2		0.97	-0.60
2	350	19	2	57	298	48	3	1	1.05	0.68
3	662	41	7	137	534	120	7	1	0.94	-1.09
5	300	62	20	66	240	54	6		0.96	-0.43
<i>10 kV X-rays</i>										
0	600	0	0	35	565	35			0.94	-1.00
0.507 ± 0.003	600	3	1	48	552	48			0.92	-1.37
1.007 ± 0.007	600	14	3	61	539	61			0.90	-1.75
2.023 ± 0.015	347	27	4	58	293	50	4		0.97	-0.35
3.032 ± 0.022	300	39	9	64	239	58	3		0.88	-1.44
5.061 ± 0.039	200	77	18	60	146	49	4	1	0.94	-0.62

The dose values for 10 kV are the mean from all experiments \pm SD

Table 2.6: Determined chromosomal aberrations and the distribution of excess fragments found in metaphase cells of MCF-12A irradiated with 200, 25 and 10 kV photons.

obtained for MCF-12A 36 h post irradiation, with 95 % for the controls and 100 % for the irradiated cells. In addition, the mitotic indices were determined depending upon the dose and energy applied. For 184A1 the fraction of mitotic cells was reduced from 3.0 ± 0.4 % in the control groups to 0.26 ± 0.08 % in cell samples irradiated with the highest dose of 5 Gy. A reduction from 7.7 ± 1.5 % for the controls to 4.0 ± 0.3 % for the 5 Gy irradiations was obtained for MCF-12A cell line.

The chromosomal aberrations depending upon X-ray energy and dose are presented in Tables 2.5 and 2.6, with pooled data from two to three independent experiments for each energy and dose point. For the 10 kV irradiations the calculated dose values are given as the mean from all pooled data for the same dose point together with their corresponding standard deviations.

To verify, whether the excess fragments and dicentric chromosomes were Poisson distributed, the relative variance (σ^2/λ) and the unit normal deviate (u) were calculated as test quantities. If the relative variance approximated unity, the intercellular distributions of these aberrations followed a Poisson distribution, and if the absolute value of the test quantity u did not exceed 1.96, no significant over- or under-dispersion was present at the 5 % level of significance [25]. The attained relative variances were about one in all instances. Moreover, no systematic change with dose or energy was found for the test quantity u , and, for the excess fragments, a significant over- or under-dispersion occurred only at one of ten doses of 10 and 200 kV X-rays, respectively. Additionally, by analyzing the distribution of dicentric chromosomes (data not shown), significant over- or under-dispersion was found only for one dose of 25 kV and two doses of 10 kV photons. Hence, the induced excess fragments and dicentric chromosomes follow an underlying Poisson distribution. The derived distributions of excess fragments for the cell lines 184A1 and MCF-12A are also included in Tables 2.5 and 2.6, together with their corresponding test quantities.

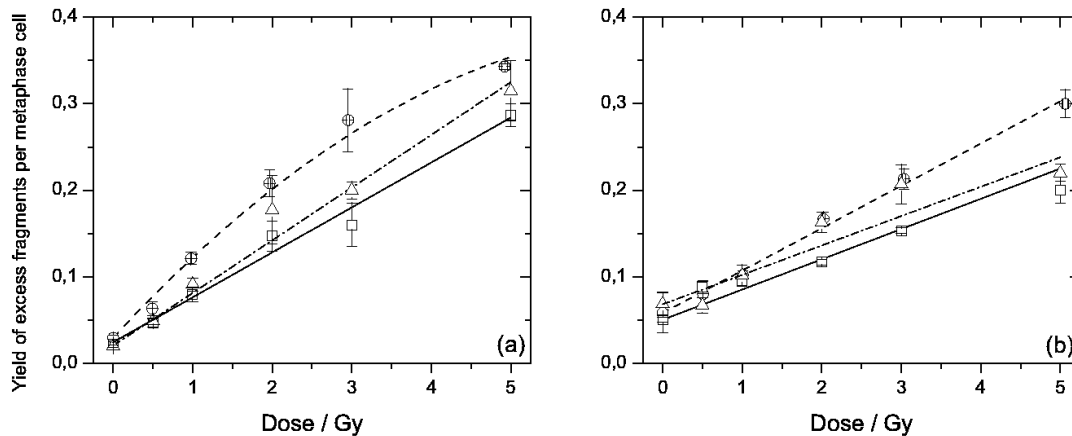


Figure 2.25: Yields of excess fragments per metaphase cell (\pm SEM) induced in cell lines 184A1 (a) and MCF-12A (b) by 200 kV (box, solid line), 25 kV (triangle, dashed-dotted line) and 10 kV (circle, dashed line) X-rays in dependence on dose.

Both types of chromosomal aberrations, excess fragments and exchange aberrations, represented by dicentric and centric ring chromosomes, were analyzed with regard to their underlying dose dependencies. In the case of excess fragments, no significant β -values were obtained by the fit, so that

linear dependencies were used to describe the dose-responses for 184A1 and MCF-12A. An exception was the 10 kV dose response of 184A1, where a negative β -coefficient indicates a saturation effect for higher doses. The induced excess fragments, normalized to aberrations per metaphase cell and in dependence on dose, are displayed in Figure 2.25, together with their corresponding dose-response curves. Table 2.7 summarizes the obtained fit parameters, their standard errors (SE), the coefficients of determination R^2 and the resultant RBE_M . These were calculated as ratio of the α -coefficients of the linear dose responses, whereas the RBE_M was generally defined as ratio of the α -coefficients of linear-quadratic dependencies.

Regarding the dose response of dicentric chromosomes and centric rings, no significant α -values were allocable for 184A1 and MCF-12A, in addition to the absence of background levels. As a consequence of this, a pure quadratic function was used for the fit procedure and RBE values were calculated as the square root of the ratio of β -coefficients (Table 2.8). The corresponding dose response curves as well as the yields of dicentric chromosomes and centric rings, normalized to aberrations per metaphase cell, are shown for both cell lines in Figure 2.26.

IV. DISCUSSION

Up to now, most of the *in vitro* experiments on the determination of RBE values for the induction of chromosomal aberrations have been performed on human lymphocytes. In contrast, in the present

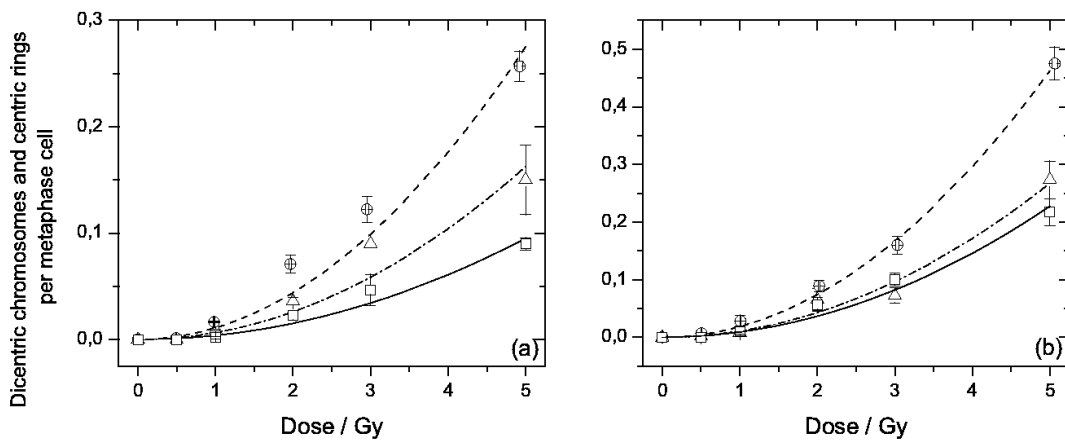


Figure 2.26: The yields of dicentric chromosomes and centric rings per metaphase cell ($\pm SEM$) of cell line 184A1 (a) and MCF-12A (b), respectively, in dependence on dose for 200 kV (box, solid line), 25 kV (triangle, dashed-dotted line) and 10 kV (circle, dashed line) X-rays.

study, two human mammary epithelial cell lines, 184A1 and MCF-12A, were chosen to investigate the RBE of soft X-rays for the particular endpoint. Both cell lines were different in their intrinsic radiosensitivity, expressed by differences in the incidence of chromosomal aberrations, with a two- to threefold higher number of radiation induced dicentrics per metaphase cell for MCF-12A. Despite these differences, comparable RBE values ($p < 0.05$) were determined for both cell lines. Based on linear relationships, RBE_M of 1.17 ± 0.12 and 0.97 ± 0.10 were obtained for the induction of excess fragments by 25 kV X-rays in 184A1 and MCF-12A, respectively. Additionally, the 10 kV

Radiation quality	$c \pm SE$	$(\alpha \pm SE)/Gy^{-1}$	$(\beta \pm SE)/Gy^{-2}$	R^2	$RBE_M \pm SE$
<i>184A1</i>					
200 kV	0.024 ± 0.004	0.052 ± 0.004	0^a	0.994	
25 kV	0.020 ± 0.004	0.061 ± 0.004	0^a	0.995	1.17 ± 0.12
10 kV	0.029 ± 0.005	0.100 ± 0.011	-0.007 ± 0.002	0.999	1.92 ± 0.26
<i>MCF-12A</i>					
200 kV	0.050 ± 0.009	0.035 ± 0.002	0^a	0.945	
25 kV	0.068 ± 0.011	0.034 ± 0.003	0^a	0.894	0.97 ± 0.10
10 kV	0.058 ± 0.010	0.049 ± 0.003	0^a	0.985	1.40 ± 0.12

Coefficient c was given by the corresponding background of excess fragments.

^a The β -coefficient was set to zero

Table 2.7: Regression coefficients and the derived low-dose RBE obtained for the linear dose-effect relationships of excess fragments induced in 184A1 and MCF-12A by 200, 25 and 10 kV X-rays.

irradiations of 184A1 and MCF-12A revealed RBE_M of 1.92 ± 0.26 and 1.40 ± 0.12 . Similar results of 1.4 ± 0.2 and 1.4 ± 0.3 were determined in human lymphocytes for the same endpoint by applying 29 kV (filtered with $30 \mu\text{m Mo}$) [113] and 10 kV X-rays (0.02 mm Cr, 5.4 keV mean energy) [105], in comparison to 220 kV photons (0.5 mm Cu). And in good accordance with the present results, RBE values of 1.13 ± 0.03 [75] and 1.21 ± 0.03 [74] were achieved in our laboratory for the clonogenic survival using cell line MCF-12A and the same 25 and 10 kV X-ray tubes.

Despite these consensuses, the RBE_M calculated here for excess fragments are based on linear relationships instead of linear-quadratic relations generally assumed for that endpoint (e.g., [107]). The existence of composite fragments generated by exchange processes of two single primary fragments cannot be excluded, especially for higher doses. These composite fragments, which are not distinguishable by Giemsa staining, lead to an underestimation of the real amount of excess fragments, and therefore, contribute to saturation effects, as observed in the present work for the 10 kV dose response of 184A1. Boei *et al.* [9] partly solved this problem by applying fluorescence in situ hybridization in combination with telomeric DNA. In addition, the amount of detected chromosomal aberrations may be influenced by the sampling time. Again, Boei *et al.* [10] investigated this phenomenon for human lymphocytes and found increasing amounts of dicentric and acentric fragments for later sampling times within the same post irradiation mitosis. Regarding the epithelial cells in the present work, the sampling time was optimized for harvesting a maximum number of cells in the first post irradiation mitosis. By accident, the chosen incubation times seem to be ideal for lower doses whereas for higher doses the cell cycle delay lead to reduced amounts of excess fragments. Additionally, as indicated by the mitotic indices, a remarkable number of cells were not able to meet the first mitosis after irradiation with the highest dose of 5 Gy.

Systematic investigations on the dependence of the RBE on photon energy have been performed by several groups [68, 108, 112, 113] for the induction of dicentric chromosomes in human lymphocytes by applying monoenergetic X-rays in the energy range of 1.83 - 40 keV as well as X-ray tubes with various filtrations and a broad spectral distribution. The results were reviewed by Hill [48], who concluded increasing RBE values with decreasing energy in the range of about 1.2 MeV to some keV

Radiation quality	$(\alpha \pm SE)/Gy^{-1}$	$(\beta \pm SE)/Gy^{-2}$	R^2	$RBE \pm SE$
<i>184A1</i>				
200 kV	0 ^a	0.0038 ± 0.0003	0.963	
25 kV	0 ^a	0.0065 ± 0.0006	0.932	1.31 ± 0.21
10 kV	0 ^a	0.0110 ± 0.0007	0.967	1.70 ± 0.29
<i>MCF-12A</i>				
200 kV	0 ^a	0.0091 ± 0.0005	0.976	
25 kV	0 ^a	0.0107 ± 0.0005	0.984	1.08 ± 0.10
10 kV	0 ^a	0.0185 ± 0.0003	0.998	1.43 ± 0.12

The resulting RBE ($\pm SE$) were calculated on the basis of β -ratios.

^a The α -coefficient was set to zero

Table 2.8: Parameters ($\pm SE$) describing the dose-responses of dicentric chromosomes and centric rings induced in cell lines 184A1 and MCF-12A.

and a maximum at 6.9 keV for dicentric chromosomes induced in human lymphocytes. Regarding the acentrics, a constant increasing slope and no defined maximum were present for the linear coefficients, and therefore, for the RBE_M in the considered energy range [48]. This energy dependence was confirmed in the present work for the induced excess fragments in both mammary epithelial cell lines. Similar to the results obtained for monoenergetic photons [68, 112], an increase in the linear coefficient (Table 3) of the dose-response, associated with increasing RBE_M , was achieved by reducing the photon energy from 200 to 10 kV.

Comparable to this finding were the results achieved by analyzing the dose responses of dicentric chromosomes and centric rings. RBE values of 1.31 ± 0.21 and 1.08 ± 0.08 were determined for cell lines 184A1 and MCF-12A irradiated with 25 kV X-rays, whereas a reduction of the photon energy to 10 kV resulted in RBE values of 1.72 ± 0.29 and 1.43 ± 0.12 , respectively. Similar results of 1.6 ± 0.3 and 1.9 ± 0.3 were obtained by others for the induction of dicentric chromosomes in human lymphocytes by 29 kV [113] and 10 kV X-rays [105], relative to weakly filtered 220 kV photons (0.5 mm Cu filter). Moreover, a comparable RBE value of 1.73 ± 0.59 was achieved for the dose-dependent induction of dicentric chromosomes in peripheral blood samples comparing 30 kV mammographic X-rays (0.8 mm Al) with 120 kV photons (1.3 mm Al and 0.3 mm Cu) [86]. Despite these similarities, the underlying dose response curves are not in accordance with the generally assumed linear-quadratic dose response [105, 107, 113]. In contrast, quadratic dependencies were obtained here for both cell lines and all energies, likely caused by an insufficient number of dicentrics and centric rings found in the low dose region. Therefore, RBE values calculated on basis of these dependencies can only estimate the real RBE for higher doses and further experiments in the low dose region are required.

Regarding the RBE_M of mammographic X-rays (29 kV), values not significantly higher than one were obtained in the present work for the induction of excess fragments in both epithelial cell lines. Additionally, RBE values between 1 and 2 have been found for dicentric chromosomes [86, 113], the clonogenic survival [75] and the induction of micronuclei [75, 119]. In clear contradiction to these data are the high RBE values of about 4 reported for neoplastic transformations of human

CGL1-hybrid cells irradiated with 29 kV X-rays, compared to higher energy photons of a 200 kV (0.6 mm Cu) [32] or 220 kV (0.5 mm Cu) [40] X-ray tube. These results clarify that the assessment of the biological effectiveness cannot be performed on the basis of one individual biological endpoint and cell type. Cell line and type-specific differences in the radiosensitivity and repair capability should be noted for a realistic estimation of the radiation risk. Considering the two human mammary epithelial cell lines used in the present study, a higher radiosensitivity, expressed by a higher frequency of dicentrics, was obtained for MCF-12A. Inherent genomic disorders of this cell line [94] and their influence on the repair capability are reasonable explanations.

Author contributions

Study concept and design A.L., E.L., J.P., E.B.; Literature research E.B., A.L.; Experimental studies E.L., A.L.; Data acquisition E.L.; Data analysis and Manuscript preparation E.B.; Manuscript editing A.L., J.P., W.D., E.B.; Guarantors of integrity of the entire study J.P., W.D.; Manuscript review was carried out by all authors.

DNA double-strand break signaling: X-ray energy dependence of residual co-localized foci of γ -H2AX and 53BP1

Elke Beyreuther^a, Elisabeth Lessmann^a, Jörg Pawelke^{b,a} and Stefan Pieck^b

^a Institute of Radiation Physics, Forschungszentrum Dresden-Rossendorf, Dresden, Germany

^b OncoRay, Center for Radiation Research in Oncology, Medical Faculty Carl Gustav Carus, University of Technology Dresden, Dresden, Germany

Running header: X-ray energy dependent DNA double-strand break signaling

Corresponding author:

Elke Beyreuther

Institute of Radiation Physics

Forschungszentrum Dresden-Rossendorf

P.O. Box 510119

D-01314 Dresden, Germany

Fon: +49 351 260 3552

Fax: +49 351 260 3700

E-mail: E.Beyreuther@fzd.de

International Journal of Radiation Biology 85(11):1042-50(2009)

DOI: 10.1080/09553000903232884

www.informahealthcare.com/rab

ABSTRACT

Purpose: The application of ionizing radiation for medical purposes requires the investigation of induced and persistent DNA damages, especially for soft X-rays that are assumed to be more effective than higher energy photons. Therefore, we examine the energy dependent time and dose response of residual DNA damage foci for soft X-rays in comparison to 200 kV photons.

Materials and methods: DNA damage present in cell line 184A1 within 48 h after irradiations with 10 kV, 25 kV and 200 kV photons was analyzed by immunochemical detection of co-localized γ -H2AX (phosphorylated histone H2AX) and 53BP1 (tumor protein 53 binding protein) foci.

Results: The dose dependencies of the co-located foci revealed significant energy dependent differences with increasing amounts of residual foci at decreasing X-ray energy independent on post irradiation time. Dose dependent RBE (relative biological effectiveness) values ranging from 4 to 7 were determined for 10 kV relative to 200 kV X-rays based on the 24 hour dose responses. For 25 kV photons, ratios considerably higher than one were obtained only for doses above 2 Gy.

Conclusions: The expected energy dependence with increasing DNA damage at decreasing photon energy was confirmed for the residual co-localized foci measured at different time points after irradiation.

Keywords: γ -H2AX, 53BP1, 184A1, soft X-ray, DNA DSB

I. INTRODUCTION

DNA double-strand breaks (DSB) represent one of the most dangerous lesions induced by ionizing radiation. Unrepaired DSB can lead to reduced clonogenic survival, while incorrect repair can result in chromosomal damages, genetic instabilities and transformations. Several methods have been established to detect DSB, whereas one of the most sensitive ones is based on intracellular DNA DSB signaling pathways that are switched on rapidly after the induction of radiation damage. As an early step, the histone H2AX is phosphorylated at the sites of DNA DSB [104]. Subsequently, the phosphorylated histone (γ -H2AX) is accumulated by distinct nuclear foci that are detectable with appropriate antibodies. Due to its rapid appearance and good correlation to the number of DSB, the determination of γ -H2AX foci have been used as a sensitive method to detect DSB at a broad dose range, starting with doses of some cGy [80, 106]. However, the cell cycle dependent expression of γ -H2AX with high amounts at late S- and G2/M-phase could reduce the detection sensitivity [53, 79]. Confluent non-proliferating cells are then typically used for such experiments to avoid the cycle-dependent influence. Another alternative is the detection of a second signaling molecule downstream of the pathway in overlapping with the γ -H2AX signal.

The tumor protein 53 binding protein 1 (TP53BP1/53BP1) has been proposed as a good candidate for double staining experiments by Rappold *et al.* [99]. This group demonstrated rapid radiation-induced relocation of 53BP1 from a homogeneous distribution to nuclear foci that were stable and co-localized with γ -H2AX foci for long times. Additionally, a clear dose dependence of 53BP1 foci formation was apparent, but no clear dependence on cell cycle stage [2, 85, 127]. Accordingly, co-localized 53BP1 and γ -H2AX foci have been used to detect DNA double-strand breaks.

Medical application of ionizing radiation requires the quantification of induced and even more persistent DNA damages to estimate the risk of late effects. In this context, photon energies below 50 keV are of particular interest, due to their wide usage for therapeutic and diagnostic purposes and their assumed enhanced relative biological effectiveness (RBE). Continuous discussions arise especially with the introduction of mammography screening programs and the potential risk of radiation-induced breast cancer in consequence of repeated screening (e.g., [37, 39]). Taking into account these considerations, human mammary gland epithelial cells have been chosen by our group to investigate the RBE of soft X-rays [6, 74, 75].

Nevertheless, systematic investigations on the photon energy dependence of the RBE have only been performed for the induction of chromosomal aberrations in human lymphocytes. Summarizing these studies, Hill [48] concluded an increasing RBE with decreasing photon energy and a maximum at 6.9 keV. At this particular energy, RBE values of 4.6 ± 2.6 and 7.7 ± 3.0 were obtained comparing 6.9 keV monochromatic synchrotron X-rays and 200 kV photons [108] or ^{60}Co γ -rays [68], respectively.

In the present work, the amount of co-localized γ -H2AX and 53BP1 foci was determined in the human mammary gland epithelial cell line 184A1 with respect to post irradiation time and radiation energy. Photons of 25 kV and 200 kV were applied to measure the kinetics within 48 hours. Dose responses were examined 2 hours, 24 hours and 48 hours after irradiation using both X-ray tubes as well as 10 kV photons. RBE values were calculated on basis of the 24 hour dose responses.

II. MATERIAL AND METHODS

Cell line

The human mammary gland epithelial cell line 184A1, described more detailed in Beyreuther *et al.* [6], was derived by applying the carcinogen benzo[a]pyren to epithelial cells established from the mammaplasty tissue of a 21-year-old healthy woman [120]. The cells are adherent and immortal, but not malignant, and show low genomic instability and the absence of estrogen receptors [121]. The cells were obtained from the American Type Culture Collection (ATCC, LGC Promochem, Wesel, Germany) and maintained in serum-free mammary epithelial basal medium (MEBM, Lonza, Verriers, Belgium) supplemented with 5 $\mu\text{g}/\text{ml}$ human epidermal growth factor, 0.5 $\mu\text{g}/\text{ml}$ hydrocortisone, 5 $\mu\text{g}/\text{ml}$ insulin, 52 $\mu\text{g}/\text{ml}$ bovine pituitary extract, 5 $\mu\text{g}/\text{ml}$ gentamicin sulfate/amphotericin-B (all as MEGM SingleQuots®, Lonza), 5 $\mu\text{g}/\text{ml}$ human apo-transferrin (Sigma-Aldrich, Taufkirchen, Germany) and 50 $\mu\text{g}/\text{ml}$ prostaglandin E1 (VWR, Darmstadt, Germany). Cells were grown in 25 cm^2 culture flasks (Nunc, Wiesbaden or Greiner, Frickenhausen, Germany) and incubated at 37°C in a humidified atmosphere containing 5 % CO_2 . The growth medium (5 ml per flask) was exchanged every third day and subculturing was performed before reaching 70 % confluence. For detachment, a solution of 0.25 % trypsin and 0.03 % ethylenediaminetetraacetic acid (EDTA) in phosphate buffered saline (PBS) (all from Biochrom, Berlin, Germany) was applied for 10 min at 37°C.

To assure adherence, proliferating cells were plated in 8-well-chamber slides one day prior the irradiation experiment. Two different slide materials, soda-lime glass (VWR) and PermanoxTM plastic (VWR), were utilized to assess the kinetics and the X-ray energy dependence, respectively. Chamber slides enclosed with Parafilm (Brand, Wertheim, Germany) were positioned upside down in the irradiation field of the X-ray tubes. The experiment and the storage of probes that were not currently treated take place at room temperature. Afterwards, the cells were transferred back to the incubator as soon as possible.

Irradiation and dosimetry

Irradiations with 10 kV and 25 kV soft X-rays were performed with a tungsten target Darpac 150-MC X-Ray tube (Forward Raytech, Swindon, UK) possessing an inherent filtration of 2 mm Be. Due to beam attenuation, the chamber slides were placed upside down in a specially designed foamed polystyrene holder with a resulting focus-to-cell distance of about 25 cm. Considering the beam attenuation, the dose rate was measured with a small soft X-ray ionization chamber (Type 23342) with a sensitive volume of 0.02 cm^3 and a Unidos dosimeter (both from PTW, Freiburg, Germany). The measured dose rate at the cell monolayer position for 25 kV X-rays (0.3 mm Al filter) was 2 Gy/min for the plastic and 0.25 Gy/min for the glass slides. For 10 kV X-rays (no additional filtration) a dose rate of 0.65 Gy/min was attained for plastic slides. Due to their strong attenuation, the glass slides were not used for this X-ray energy.

The reference irradiations were performed with two 200 kV X-ray tubes (Yxlon International A/S, Taastrup, Denmark or Isovolt 320/20, Roentgen Seifert, Ahrensburg, Germany), both equipped with a tungsten anode and filtered with 0.5 mm Cu. They were however differing in inherent filtration

with 7 mm Be for the Isovolt 320/20 and 3 mm Be + 3 mm Al for the Yxlon tube, respectively. To achieve comparable conditions the chamber slides were also placed upside down with a focus-to-cell distance of 44 cm. The dose rates, measured with a Unidos dosimeter and two Farmer ionization chambers (Type 30010, 0.6 cm³ sensitive volume, PTW) were 1.34 Gy/min and 1.24 Gy/min for the PermanoxTM (Yxlon) and glass (Isovolt) slides, respectively. A current reduction from 20 mA to 5 mA, necessary for the 0.25 Gy irradiations, resulted in a dose rate of 0.27 Gy/min (on glass). Dose distributions and homogeneities within the irradiation fields were measured with GafChromic® EBT films (ISP Corp., Wayne, NJ, USA), which consist of tissue equivalent materials, are self-developing and show high spatial resolution. The determined dose variation within the fields of 10, 25 and 200 kV X-rays was better than 4.0 %. Because of this high homogeneity, chamber slides that were assembled for the same radiation dose but analyzed after different periods of time were irradiated simultaneously for each experiment.

Influence of the different slide materials on the photon spectra

Since the densities of the different slide materials varied between 2.5 g/cm³ for glass and 1.19 g/cm³ for plastic, the material influence on the primary photon spectra have to be considered carefully. Spectra of the three radiation qualities applied were provided by Lehnert *et al.* [74, 75]. Together with the simulation tool GEANT4 (version 8.1 [35]) these spectra were utilized to simulate the transition of the original photon spectra through glass or plastic. Moreover, the number and energy of secondary electrons generated in the slide material and escaping into the cell monolayer have been determined by approximating the cell monolayer with a 10 micrometer thick water layer in the GEANT4 simulation.

Immunofluorescence staining of γ -H2AX and 53BP1

The applied method of immunofluorescence staining of the two DSB signaling molecules (γ -H2AX and 53BP1) was adopted from Eke *et al.* [27] and customized for our cell line. Following irradiation, the cells were incubated at 37°C for times between 5 minutes and 48 hours. Subsequently, they were fixed in 1 % formaldehyde/PBS (5 min, Sigma-Aldrich/Biochrom), washed two times in PBS/glycine (VWR), permeabilized for 10 min in ice cold 0.25 % Triton X/PBS (VWR), and washed in PBGT, which is a solution of 0.5 % Gelatine (neolab, Heidelberg, Germany) and 0.05 % Tween 20 (Sigma-Aldrich) in PBS. Cells were then incubated with an anti-phospho-Histone H2AX monoclonal antibody (1:1000, 1 h, Chemicon via Millipore, Schwalbach, Germany), Alexa Fluor 594 goat anti-mouse secondary antibody (1:400, 30 min, Invitrogen, Karlsruhe, Germany), 53BP1 rabbit polyclonal antibody cocktail (1:3000, 1 h, Acris, Hiddenhausen, Germany), and Alexa Fluor 488 goat anti-mouse secondary antibody (1:1000, 30 min, Invitrogen). The antibodies and fluorescent dyes were diluted in PBGT, which is also used for washing between the antibody incubations in a wet chamber at 37°C. Lastly, the samples were washed two times in PBS and mounted under coverslips with 4 μ l 4'-6-Diamidino-2-phenylindole (DAPI)/Vectashield (1200) mounting medium (Axxora, Lörrach, Germany) per well. Kinetic investigations were performed with longer incubation times of 90 minutes for the primary and 45 minutes for the secondary antibodies.

The co-localized foci of γ -H2AX and 53BP1 (Fig. 2.27) were counted by eye under a Zeiss Axiovert fluorescence microscope (1000 \times magnification) (Carl Zeiss, Jena, Germany) using the “HC Triple-band - Filterset DAPI/FITC/TxRed“ (4'-6-Diamidino-2-phenylindole/Fluorescein-5-isothiocyana/Texas Red) (AHF Analysentechnik, Tübingen, Germany).

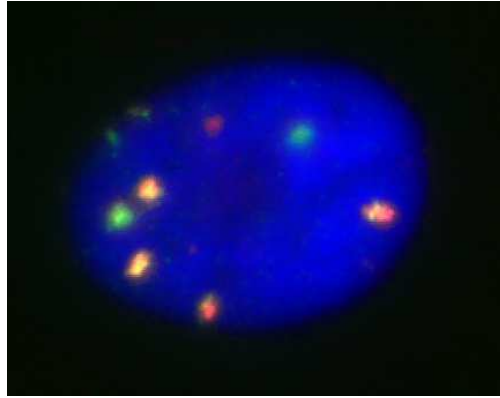


Figure 2.27: Co-localized foci of γ -H2AX and 53BP1 (yellow/orange) detected in cell line 184A1 48 hours post irradiation with 6 Gy of 10 kV X-rays. The dominant green fluorescence was caused by different fluorescence intensities and a color preference of our microscope camera. Foci, that were not localized in the regarded sectional plane appear either in pink (γ -H2AX) or green (53BP1).

Data evaluation and statistics

For each experiment 300 - 400 randomly chosen cells were analyzed, not only in one sectional plane under the microscope, but also scanning through the whole thickness of the cell. The co-localization of γ -H2AX and 53BP1 was checked for non-irradiated and irradiated samples before the experiment, and the received one-to-one correlation was applied but not controlled during the analysis. The resulting numbers of foci per cell were obtained by two independent experiments and given as mean values \pm standard error of mean (*SEM*).

Dose response curves were determined for the co-localized foci remaining 24 hours after irradiation with 10, 25 and 200 kV X-rays. For this, the method of iteratively reweighted least-squares minimization was applied to fit the data, using the linear-quadratic model $y(D) = c + \alpha D + \beta D^2$ and, except for the 10 kV X-rays, the reciprocal variances as weights. The yield $y(D)$ was given by the number of foci per cell; c was defined by the background values. Ratios of the 24 hour dose responses of the soft X-rays (10 and 25 kV) and the 200 kV reference source were determined in order to evaluate the biological effectiveness of the different radiation qualities. Corresponding errors were calculated by error propagation, using the uncertainties of the fit parameters α and β , and their covariance. Statistical significance was proven by Student's t -test.

III. RESULTS

The transmitted photon spectra

Information on the mean photon energies and relative intensities of the 10, 25 and 200 kV photon spectra after transmission through 1 mm glass or plastic were provided by GEANT4 simulations (Table 2.9). The dose rates, also displayed in Table 2.9, reflect the changes in photon intensity

and energy, taking into account the corresponding photon energy dependence of the mass energy-absorption coefficients [51].

Regarding the 200 kV reference source, only small changes of the mean photon energy, beam intensity and dose rates of the transmitted photon spectra were achieved for the different slide materials. By contrast, the usage of glass slides result in clearly shifted mean photon energies and considerably reduced intensities for the 25 and 10 kV photons. Moreover, no dose signal was detectable after attenuation of the 10 kV X-rays by 1 mm soda-lime glass. Slightly shifted mean photon energies and reduced photon intensities and dose rates were also obtained for both soft X-rays passing through a 1 mm plastic slide. The reduced dose rates were compensated by longer irradiation times but not

Influence on the spectra	Mean photon energy /keV	Relative photon intensity	No. of sec. electrons per 10^6 photons	Mean energy of sec. electrons /keV	Dose rate /Gy/min
<i>200 kV photons</i>					
Undisturbed ²	89.78	1	-	-	1.36 ¹ /1.30 ²
Plastic ²	89.76	0.990	50	21.4	1.34 ¹
Glass ²	90.29	0.962	207	43.7	1.24 ²
<i>25 kV photons</i>					
Undisturbed	15.42	1	-	-	2.24
Plastic	15.74	0.909	81	7.0	2.04
Glass	19.26	0.180	148	10.3	0.25
<i>10 kV photons</i>					
Undisturbed	6.93	1	-	-	1.47
Plastic	7.46	0.490	99	3.7	0.65
Glass	9.15	1e-05	0	-	not detectable

200 kV X-ray tubes: ¹Yxlon International A/S; ²Isovolt 320/20, Roentgen Seifert

Table 2.9: Parameters of the applied photon spectra transmitted through 1 mm soda-lime glass or Permanox® plastic. Mean photon energies of the undisturbed spectra were provided by Lehnert *et al.* [74, 75]. The mean energies and relative intensities of the transmitted photons as well as the fraction and mean energy of secondary (sec.) electrons produced in the slides and escaping into the cell monolayer were simulated by GEANT4. For the 200 kV reference source the parameters were simulated on basis of the spectrum of the Isovolt tube, whereas only small deviations were expected for the Yxlon tube. Dose rates were measured in consideration of the irradiation geometry.

exceeding 10 minutes to avoid effects of medium depletion. Furthermore, the 10 kV X-ray tube was not applied for cell irradiations on glass slides.

Concerning the production of secondary electrons, additional simulations were performed to ascertain the spectra and number of those electrons that were transferred from the slides to the cell monolayer. For the glass slides, both the number and the mean energy of the produced secondary electrons were increased with X-ray energy. Consequently, the electron range and with it the probability that these electrons penetrate the cell nucleus and contribute to DNA damage was increased. By comparison, fewer secondary electrons with a lower mean energy and range were produced in the plastic slides, associated with a lower probability of penetrating the cell nucleus.

Kinetics

In a first series of experiments, the time course of foci appearance and loss was studied after 25 kV and 200 kV X-ray irradiations of the human mammary epithelial cell line 184A1. Despite the higher yields obtained for 25 kV photons, similar biphasic and energy independent kinetics were found (Fig. 2.28). Additionally, a constant maximum was attained 0.5 and 2 hours after irradiation with 0.25 and 2 Gy, respectively. The repair, or better loss, half times measured for the higher dose were 4.5 h and approximately 15 h for the steep and the flat sloping curve progression, respectively. A dose reduction to 0.25 Gy lead to a change in foci loss half times to 3.5 h and 25 h for the faster and slower decreasing slopes.

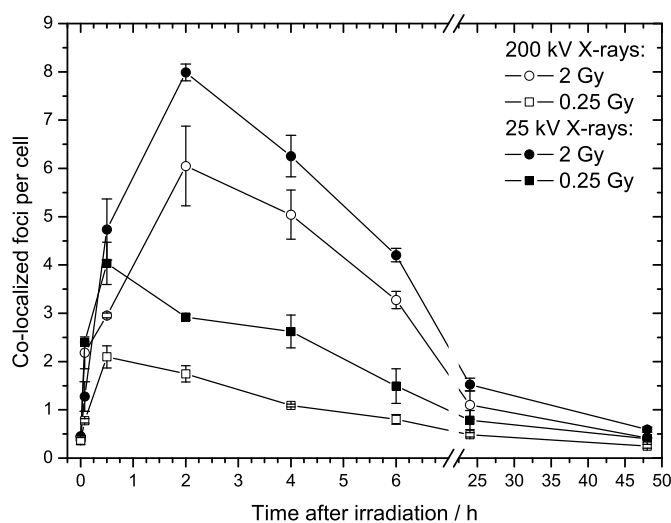


Figure 2.28: Time courses of co-localized foci measured between 5 minutes and up to 48 hours post irradiation. Cells were irradiated with doses of 0.25 Gy (squares) and 2 Gy (circles) of 25 kV (black) or 200 kV (open) X-rays. All values are displayed as average \pm SEM based on two independent experiments.

X-ray energy and dose dependence of the number of co-localized foci of γ -H2AX and 53BP1

In addition to the kinetic considerations, the X-ray energy dependence and dose-effects for low and higher energy X-rays were ascertained in more detail. For this, visible co-localized foci were analyzed at three different times following irradiation with doses of up to 6 Gy (Table 2.10). The earliest time (2 h) was chosen because of the maximum obtained at 2 Gy; remaining foci were determined at 24 and 48 hours following irradiation.

In order to evaluate the possible influence of the slide material on the induction of γ -H2AX and 53BP1 foci, the results obtained at 2, 24 and 48 hours after irradiations with 25 kV and 200 kV photons were compared (not shown). No significant differences ($p \leq 0.05$) were found between the number of foci determined on glass or plastic slides for both X-ray energies. For this, it was concluded that dose rate compensation was done quite well and that the shifted mean energy and produced secondary electrons have in this case no great influence on DNA damage. The dose responses (Table 2.10) measured 2 hours after irradiation revealed a significant increase in the number

Dose/Gy	Average number of foci per cell		
	2 h	24 h	48 h
<i>200 kV X-rays</i>			
0	0.40 ± 0.05	0.31 ± 0.04	0.31 ± 0.01
0.49 ± 0.02	1.03 ± 0.09	0.43 ± 0.01	0.26 ± 0.03
1.01 ± 0.02	2.72 ± 0.25	0.50 ± 0.03	0.28 ± 0.01
2.01 ± 0.02	4.84 ± 0.21	0.87 ± 0.06	0.37 ± 0.06
4.00 ± 0.03	8.42 ± 0.04	1.51 ± 0.01	0.60 ± 0.06
6.01 ± 0.03	-	3.75 ± 0.18	0.94 ± 0.06
<i>25 kV X-rays</i>			
0	0.27 ± 0.02	0.29 ± 0.09	0.26 ± 0.04
0.51 ± 0.04	2.84 ± 0.22	0.62 ± 0.03	0.31 ± 0.04
1.00 ± 0.04	6.02 ± 0.03	0.75 ± 0.14	0.39 ± 0.10
2.00 ± 0.04	8.26 ± 0.02	0.98 ± 0.02	0.51 ± 0.12
3.99 ± 0.04	11.39 ± 0.02	3.01 ± 0.12	1.29 ± 0.05
6.01 ± 0.05	-	5.87 ± 0.12	2.22 ± 0.12
<i>10 kV X-rays</i>			
0	0.40 ± 0.03	0.32 ± 0.09	0.26 ± 0.03
0.50 ± 0.02	5.57 ± 0.08	1.72 ± 0.04	0.66 ± 0.08
1.00 ± 0.03	7.59 ± 0.06	2.07 ± 0.04	0.95 ± 0.03
2.00 ± 0.05	12.30 ± 0.36	3.59 ± 0.29	1.22 ± 0.15
4.00 ± 0.08	17.22 ± 0.76	4.13 ± 0.02	1.47 ± 0.08
6.00 ± 0.12	-	6.40 ± 0.08	2.70 ± 0.38

Table 2.10: Dose response of cell line 184A1, measured on PermanoxTM at different time points after irradiation with 10 kV, 25 kV and 200 kV X-rays. The dose of 6 Gy was excluded at the first time (2 h) due to analytical limits. Yields of two independent experiments were pooled ($\pm SEM$) and the dose values were given with their uncertainties.

of foci with decreasing X-ray energy. These X-ray energy dependent differences partly disappeared later on with no significant different results ($p \leq 0.05$) for doses up to 2 Gy of 200 and 25 kV X-rays (Fig. 2.29, Table 2.10). Nevertheless, the yields measured for 10 kV X-rays remained elevated and comparable results were obtained for higher doses (4 Gy and more) and both soft X-ray energies 24 and 48 hours post irradiation. The number of co-localized foci per cell, determined 24 hours after irradiation, was used to calculate the dose response curves displayed in Figure 2.29 for the three X-ray energies investigated. Table 2.11 summarizes the corresponding regression parameters, their standard errors and covariances as well as the coefficients of determination (R^2). A negative β -coefficient was obtained for 10 kV X-rays likely caused by foci overlap or an occlusion effect [98] at higher doses. The biological effectiveness of the soft X-rays was assessed regarding their 24 hour dose responses in relation to the 200 kV reference source. The results (Table 2.12) reveal a ratio or relative biological effectiveness (RBE) of about one considering doses of up to 2 Gy of 25 and 200 kV X-rays. Significantly enhanced values ($p \leq 0.05$) were obtained for all doses of 10 kV relative to 200 kV photons, whereas comparable results were ascertained for both soft X-rays and doses above 3 Gy. For the data achieved at 48 hours, although elevated for 10 kV X-rays, regression was not realized as the cell cycle duration is generally 30 hours.

Radiation quality	$(\alpha \pm SE)/\text{Gy}^{-1}$	$(\beta \pm SE)/\text{Gy}^{-2}$	Covariance $cov(\alpha, \beta)$	R^2
200 kV	0.211 ± 0.014	0.023 ± 0.004	-1.04×10^{-5}	0.989
25 kV	0.110 ± 0.025	0.134 ± 0.074	-1.60×10^{-4}	0.963
10 kV	1.596 ± 0.315	-0.106 ± 0.060	-0.046	0.931

Table 2.11: Parameters returned from the fit procedure of the dose responses measured 24 hours after irradiation with 10, 25 and 200 kV X-rays. The parameters ($\pm SE$) were obtained by application of the linear-quadratic model.

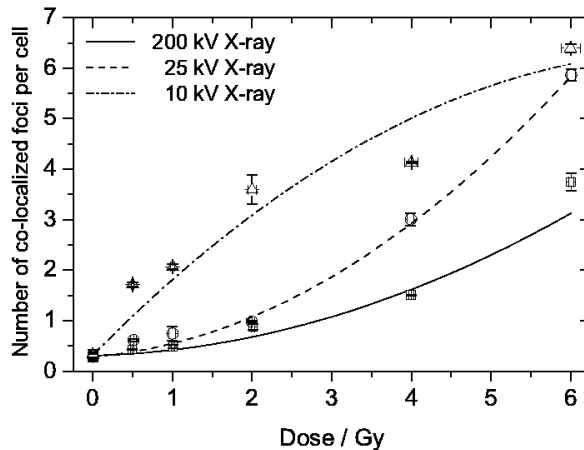


Figure 2.29: Dose-effect curves derived from the average number of co-localized foci per cell ($\pm SEM$) measured in 184A1 cells in dependence on X-ray energy versus dose 24 hours after irradiation. The measured values and fitted curves are given for 10 kV (triangle), 25 kV (circle) and 200 kV (square) X-rays, respectively.

IV. DISCUSSION

The primary aim of this study was the investigation of energy dependent differences for remaining co-localized foci of γ -H2AX and 53BP1 as a marker of DNA double-strand breaks. Regarding the photon energy range of 25 kV to 660 keV (^{137}Cs), similar kinetics as detected for co-localized foci in cell line 184A1 in the present study were found for γ -H2AX foci induced in human fibroblasts [61], V79 lung and different tumor cells [80]. Complemented by the 10 kV data of this study and the kinetics found for ^{60}Co [70], these data show that the kinetics of foci removal were resistant to doses up to 50 Gy [79] as well as photon energies up to 1.33 MeV (^{60}Co). In this context, it should be stated that the group of MacPhail *et al.* [79, 80] has used flow cytometry instead of microscopy to analyze the radiation induced formation of γ -H2AX. How far the statement of resistant kinetics of foci removal holds true for the underlying kinetics of DSB repair has to be considered carefully. For instance, Kinner *et al.* [62] receive considerable differences between the kinetics of radiation induced DSB measured by pulsed-field gel electrophoresis and the associated γ -H2AX foci, and they draw the conclusion that the DSB signaling machinery seems to persist longer than the original DSB, possibly representing a DSB-related modification of the chromatin.

Keeping the possible discrepancy between DSB repair and foci removal in mind, dose effects were

Dose/Gy	$RBE(D)_{25\text{kV vs. }200\text{kV}}$	$RBE(D)_{10\text{kV vs. }200\text{kV}}$
0.5	0.80 ± 0.20	6.94 ± 1.11
1	1.04 ± 0.33	6.37 ± 0.53
2	1.47 ± 0.58	5.39 ± 1.02
4	2.13 ± 0.97	3.87 ± 1.51
6	2.62 ± 1.27	2.75 ± 1.63

Table 2.12: Dose (D)-dependent RBE values determined by comparing the 24 hour dose responses of the soft X-rays (10 and 25 kV) and the 200 kV reference radiation source. Displayed errors are calculated by error propagation using the standard errors and covariances provided by the fit procedure.

ascertained at different time points after irradiations with 10, 25 and 200 kV X-rays (Table 2.10). The expected energy dependence with increasing amounts of residual co-localized foci of γ -H2AX and 53BP1 at decreasing X-ray energies was confirmed to be independent on post irradiation time. This dependency was also observed for dicentric chromosomes [6, 68, 108], micronuclei and the clonogenic survival [74, 75]. Hill [48] summarized the different data sets in the literature and concluded that biological effectiveness was increased by reducing the photon energy from ^{60}Co to 6.9 keV, whereas the latter was associated with the maximum efficiency. Conversely, Kegel *et al.* [61] assessed the kinetics of γ -H2AX foci induced by 25 kV, 120 kV and 660 keV photons and found 120 kV X-rays most effective. This unexpected result was likely caused by secondary electrons generated in glass slides by 120 kV photons and contributing to a considerable increase of dose and damage [61]. By contrast, no significant differences ($p \leq 0.05$) were found in the present work comparing the results obtained on plastic and glass. Potential explanations are the applied X-ray energies and filtrations as well as the slide materials with varying composition for borosilicate [61] versus soda-lime glass. The ratio of the 24 hour dose responses (Table 2.12) of the soft X-rays and the 200 kV reference source were considered as a measure of the relative biological effectiveness, keeping in mind the possible discrepancy between DNA DSB and co-localized foci [62]. For the mammographic X-rays RBE values higher than one were achieved only for doses higher than 2. Using the same 25 kV X-ray tube, similar results in the range of 0.97 to 1.60 were observed at the 10 % survival level, the induction of micronuclei [75] and excess fragments [6] induced in human mammary epithelial cells. Schmid *et al.* [113] found a similar result of 1.6 ± 0.3 for dicentric chromosomes induced in human lymphocytes by 29 kV X-rays relative to 220 kV photons (0.5 mm Cu filter). Considering doses below 2 Gy, the high uncertainties obtained for the ratio of the co-localized foci of γ -H2AX and 53BP1 avoid clear conclusions. For 10 kV X-rays RBE values of about 3 - 7 were achieved for the remaining co-localized foci. The decrease towards higher doses can be explained by an overlap of foci regions [80] or the detection limit resulted from foci scoring by eye. With increasing dose the probability of foci overlap and of the presence of two DSB within one visible focus rises up [98], leading to an underestimation of the real amount of damage. To overcome this limit, automatic foci evaluation, the detection of fluorescence intensity or the analyses of DSB with another method can be deployed.

Comparing the RBE values achieved here for 10 kV photons with those of other biological endpoints,

no consistent conclusion can be drawn. Irradiating the epithelial cells with the same 10 kV X-ray tube values of 1.21 ± 0.03 and in the range of 1.4 - 1.9 were obtained at the 10 % survival level [74] and for the induction of chromosomal aberrations [6], respectively. By contrast, the application of this tube and cell type results in an RBE of 4.1 ± 1.0 analyzing the number of micronuclei per binucleated cell. Both findings were affirmed by 1.40 ± 0.34 and 4.6 ± 2.6 for dicentric chromosomes induced in human lymphocytes by 10 kV photons (0.02 mm Cr filter) [105] or 6.9 keV monoenergetic synchrotron X-rays [108], respectively.

This result can be ascribed to the selected biological endpoint, varying radiosensitivities of the cell lines and the delivered photon spectra. It is quite evident that for 6.9 keV, the energy associated with the maximum biological effectiveness, monoenergetic photons [108] are more effective than polychromatic photons delivered by X-ray tubes. In addition, utilized filters and slide materials also affect the photon spectra and the RBE. Beside this physical contribution the choice of biological endpoint and with it the cellular processes that take place within the time range after irradiation are crucial. For instance, Blöcher [8] investigated the number of DNA double-strand breaks occurring in Ehrlich ascites tumor cells after irradiations with 3.4 MeV α -particles (^{241}Am) and 140 kV X-rays. As result, increasing RBE values with post irradiation time were obtained for DNA DSB analyzed 24 hours and shortly after irradiation [8]. In the present work, this finding was confirmed just for the dose responses obtained 2 and 24 hours post irradiation. Longer incubation times that exceed the cell cycle duration of 30 hours result in stable or reduced RBE values (not shown). And, despite different initial yields and repair rates, this result is accompanied by comparable numbers of residual co-localized foci of γ -H2AX and 53BP1 for doses up to 2 Gy of 25 and 200 kV X-rays ($p \leq 0.05$) (Fig. 2.28) and doses above 2 Gy of 25 kV and 10 kV X-rays ($p \leq 0.01/0.05$ for 4/6 Gy) (Table 2.10), respectively. The elevated levels, found for doses above 2 Gy and for the whole dose range delivered by 10 kV photons, can be interpreted as unrepaired DSB persisting in cells maintained in cell cycle arrest. Otherwise, Löbrich and Jeggo [69] have pointed out that cells with DSB levels below a certain G2/M checkpoint threshold were released from checkpoint and can enter mitosis. In the following the reproductive capacity might be reduced by unstable chromosomal exchange aberrations that disrupt mitosis or stable chromosomal rearrangements like translocations that lead to genetic instabilities [69].

It is an open question as to how far the *in vitro* data presented here for human mammary epithelial cells as well as those of other cell lines might contribute to the cost-benefit discussion of mammography screening. Unquestionably, these investigations provide useful hints about the biological effectiveness of mammographic X-rays and reveal the underlying photon energy dependence of the RBE. But, for realistic estimations and a possible implementation in radiation risk calculations, biological objects, endpoints and doses more closely to real clinical conditions should be chosen. Moreover, radiobiological differences that arise from differing spectra of clinically applied mammographic X-ray tubes should be verified using the hints derived from investigations of lower energy X-rays, like the 10 kV photons in the present work. Taking into account all these considerations the concerns pertaining to repeated mammography screening and the potential accumulated radiation damage were neither approved nor dispelled with the present results.

V. CONCLUSION

The expected energy dependence with increasing amounts of damage for decreasing X-ray energy was confirmed for residual co-localized γ -H2AX and 53BP1 foci. Accordingly, RBE values calculated on the basis of the 24 hour dose effects reveal that soft X-rays induce more DSB than higher energy photons. For 25 kV this was only proven for doses above 2 Gy.

Acknowledgements

The authors are grateful to Dr. N. Cordes for providing protocols and fruitful discussions, K. Storch for her introduction to the work, and F. Leonhard for her assistance during the experiments. We also thank Dr. L. Karsch for the performance of the GEANT4 simulations. The work was supported by the BMBF, Grant No. 03ZIK042.

Author contributions

Study concept and design E.B., E.L., J.P., S.P; Experimental studies E.L., E.B.; Data acquisition E.L.; Literature research and Data analysis E.B.; Manuscript preparation E.B., S.P.; Manuscript editing J.P., S.P., E.B.; Guarantor of integrity of the entire study J.P.; Manuscript review was carried out by all authors.

3 *In vitro* cell irradiation experiments with laser-accelerated electrons at JETI

3.1 Background

Over the last two decades, the laser technology has rapidly progressed and high intensity lasers are now available enabling the laser-based acceleration of charged particles. Ultrashort laser pulses (fs ... ps) can be focused to intensities of more than 10^{19} W/cm² being equivalent to the intensity achieved by focusing the whole sunlight arriving on earth on the tip of a pencil. The high-intensity laser pulses are focused in a gaseous or solid state target leading to charge separation and consequently to the formation of plasma. Subsequently, the interaction of the intensive laser light and the plasma results in electric fields in the order of 100 GV/m [29] or even 1 TV/m [43, 117] exceeding those achieved in conventional particle accelerators (some tens of MV/m) by several orders of magnitude. Hence, electrons [29, 36, 84], protons [97, 117] and ions [43] can be accelerated within distances of a few mm or cm to the high energies required, for example for physical or radiobiological experimentation, and the construction of more compact particle accelerators becomes conceivable. Moreover, the perspective of compact and potentially more cost-effective particle accelerators gives rise to the expectation that medical application, especially for radiotherapy, might become feasible in the upcoming decade.

Today, the majority of tumors treated in radiotherapy are irradiated with high-energy photons and electrons (≤ 20 MeV). These particles are delivered by medical linear electron accelerators (LINAC), that fit well in a hospital treatment room and are sophisticated with respect to dose delivery, quality assurance and treatment planning. By contrast, the radiotherapeutic application of protons and ions is provided in just a fistful therapy centers worldwide. Reasons are the investment costs for a proton and ion accelerator facility, i.e., accelerator, beam line, hospital etc., being more than one order of magnitude higher than for a conventional LINAC, and the huge dimension of the corresponding accelerator technique (synchrotron, cyclotron) as well as of the auxiliary “equipment“, that prevent the implementation in an existing hospital.

Disregarding the costs, the application of protons and ions offers several advantages for the radiotherapy of specific tumors: their inverse dose profile (Fig. 3.1) and, in the case of ions, a higher RBE value in the dose maximum (Bragg peak) at the end of their trajectory. For electrons and photons, the maximum dose deposition is achieved shortly beneath the entrance surface, for example the patient skin, followed by a successive fall off. By contrast, for protons, and likewise for ions, where the dose deposition is maximized in the so-called Bragg-peak, accompanied with a steep fall off behind. This characteristic in combination with a low lateral scattering enables the treatment of deep-seated tumors in the vicinity of organs at risk under sparing of the surrounding tissue. Considering the RBE, those for ions follow in principle the dose distribution, that is the RBE maximum is also obtained in a finite range, whereas almost constant RBE values are found along the whole

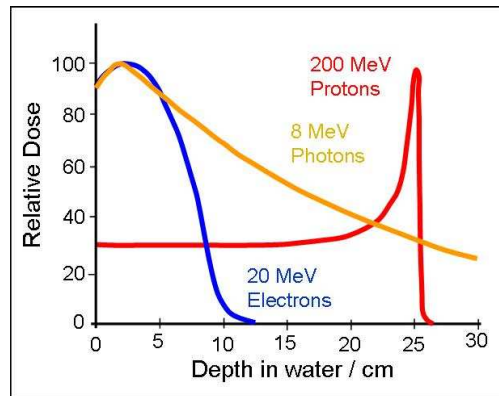


Figure 3.1: Comparison of the depth dose profiles of 200 MeV protons, 8 MeV photons and 20 MeV electrons in water.

proton trajectory. Both, finite particle range and inverse depth dose deposition were successfully applied, for example for the treatment of brain tumors next to the visual nerve or brain stem [116]. Although radiotherapy with protons or ions will be advantageous for a part of the cancer patients the high costs involved prevent their broad distribution. In this context, the new technology of laser-based acceleration of charged particles has the potential to provide a more cost-effective alternative. However, the medical application of these unconventional accelerators requires further technological improvements of the currently available systems as well as their dosimetric and radiobiological characterization. The former includes the need for monoenergetic particles instead of broad energy spectra and for sufficient energy and intensity (cf. section 3.4.1) in order to guarantee appropriate penetration depths and irradiation times of just a few minutes, respectively. The laser systems have also to be improved with respect to the reproducibility and reliability of the emitted particle beam. At present, the parameters of the particle beams vary from shot to shot, whereas stable and reliable particle beams are demanded for radiobiological experiments and even more for radiotherapy. Beyond the technical improvement and physical characterization, radiobiological experiments and clinical trials have to be performed in order to ascertain the consequences arising from the differing time structure or pulse regime. Assuming that equal doses can be administered for radiotherapy, the pulse structure of laser-accelerated particles, which is coupled to the laser frequency of some Hertz and the laser pulse length of some 100 fs, will result in ultrahigh pulse dose rates of up to about 10^{11} Gy/min exceeding those of conventional accelerators by several orders of magnitude (Table 3.1). Comprehensive radiobiological studies are necessary to investigate the relative biological effectiveness of laser-accelerated particles starting with *in vitro* cell experiments and end up with animal studies and clinical trials. Moreover, these studies also involve an appropriate and precise response of the necessary dosimetry system, which has to be guaranteed for medical application.

The joined project **onCOOPtics** was initiated in 2007 with the objective to develop a laser-based particle accelerator for radiotherapy. This includes the improvement of the present and the development of new laser technology and, in parallel, the physical, dosimetric and radiobiological characterization of the generated particle beams. Therefore, the competences of two research cen-

Electrons	Therapy LINAC	Laser accelerator
Frequency	3 GHz	10 Hz
Pulse duration	30 ps	50 fs
Charge per pulse	0.1 - 1 fC	0.1 - 1 nC
Relative pulse dose rate	1	10^9
Protons	Cyclotron	Laser accelerator
Frequency	100 MHz	0.1 Hz
Pulse duration	1 ns	120 fs
Particles per pulse	100	10^9
Relative pulse dose rate	1	10^{11}

Table 3.1: Comparison of the parameters presently achieved by conventional and laser-based electron and proton accelerators.

ters are combined: **OncoRay** in Dresden and **ultra optics** in Jena. Whereas, **ultra optics** is responsible for the development of the laser technology and **OncoRay** for the physical and radiobiological characterization of the particle beams with regard to clinical application.

Within the scope of onCOOPtics the research of the present work focused on the realization of *in vitro* cell experiments with laser-accelerated electrons produced by the Jena Titanium:Sapphire laser system (JETI). The radiobiological requirements listed afore have to be fulfilled, that is the laser system JETI was optimized with regard to radiobiological requirements, and a dose and beam monitoring system was implemented that allowed for the worldwide first and systematic *in vitro* cell irradiation experiments with laser-accelerated electrons (sections 3.4.1, 3.4.2). In this context, the present dissertation represents an important step on the long way from basic radiobiological *in vitro* studies to the point of clinical application.

3.2 Laser wake field acceleration of electrons (LWFA)

Primarily proposed by Tajima and Dawson in 1979 [124], the concept of laser wake field acceleration was advanced, e.g., by means of self-modulation, now providing the possibility to generate high-energy laser-driven electron beams. The concept of laser wake field acceleration consists of two steps: The generation of a moving space charge region (a plasma wave) and the acceleration of electrons with this moving electric potential barrier. This concept was realized at the JETI laser system producing electron beams with maximum energies of several ten MeV. A schematic drawing of the processes that occur during the laser wake field acceleration is shown in Figure 3.2. The initial point is a ultrashort laser pulse (red) focused to high intensity into a gas jet. Within the focus, the gas, e.g., helium at JETI, is almost completely ionized, generating a plasma or rather a plasma channel in the course of the laser pulse propagation (Fig. 3.2a). Electrons from this plasma are deflected in forward direction by the radiation pressure (ponderomotive force) of the laser pulse (Fig. 3.2b). The electrons in front of the laser pulse are attracted by the atomic nuclei behind and experience a coulomb force in backward direction. When the laser pulse has passed the region, electrons will swing back to the nuclei. By that, a periodic charge separation is excited which is just a plasma wave (green, wavelength λ_P), co-propagating with the laser pulse. This is comparable to the wake

of a moving boat. In principle, the plasma wave describes the electron density distribution behind the laser pulse and propagates in the same direction but under a small phase shift (Fig. 3.2b). In the second step, electrons that oscillate in phase and being fast enough are trapped in the wave and start to “surf” on the plasma wave (Fig. 3.2c) running with the laser pulse. These electrons surf down the wave, gain velocity and thereby energy from the potential gradient formed by the plasma wave (Fig. 3.2d). With ongoing propagation of both the laser pulse and the plasma wave, the electrons are accelerated in accordance to their gradient position, where the broad distribution of occupied positions causes a broadband electron spectrum. Maximum energies of several tens MeV can be achieved during this process along less than 1 mm of acceleration length, since ultrahigh electric fields arise from the charge separation in wake of the high intensity laser pulse.

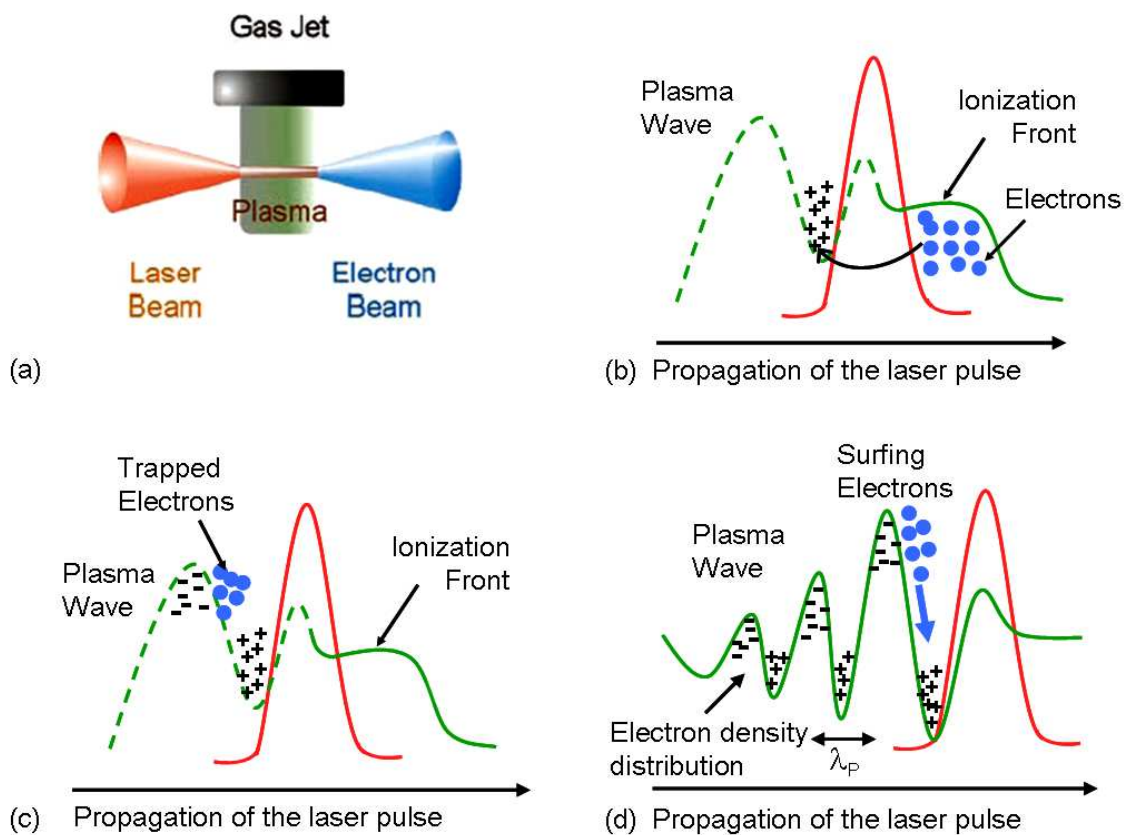


Figure 3.2: a) Schematic diagram of the incident laser, the plasma channel and the emitted electron beam [83]. b-d) Illustration of the process of laser wake field acceleration of electrons by means of a high intensity laser (modified after [14]). The laser pulse is represented by a red curve, electrons are given in blue, the green curve describes the electron density.

3.3 Dosimetric and radiobiological characterization

Usually the JETI laser system is applied for physical experiments, where a few single electron shots with poor reproducibility are sufficient for further evaluation. Contrary, a stable and reliable beam delivery is required for *in vitro* cell irradiations and even more for future radiotherapeutic appli-

cation. Therefore, in a first step, the parameters of the JETI laser system were adjusted to meet radiobiological requirements and to allow for cell irradiation experiments (section 3.4.1).

Based on the dosimetric experiences gained at the ELBE accelerator various types of dosimeters were implemented at the JETI system in order to characterize the laser-accelerated electrons with regard to their general beam parameters and dosimetric properties. External beam parameters, like beam spot size and dose homogeneity over the irradiated field, were determined by means of GafChromic® EBT films (section 2.3.4), which were also used for the retrospective determination of the absolute dose administered to the cell samples during irradiation. Comparable with the experiments at ELBE, the pulse to pulse fluctuations of the JETI electron beam parameters enforce the implementation of an online dose and beam monitoring system. However, the Farmer ionization chamber (cf. section 2.3.2) used at ELBE is calibrated in accordance to the measurement of photons and not suitable for electron dosimetry. In consequence, a Roos ionization chamber, developed and calibrated for the dose measurement of therapeutic MeV electron beams, was introduced providing online dose information during the experiment. Moreover, a Faraday cup was implemented in the JETI setup also allowing for the online control of beam parameters, especially the charge delivery for each single pulse. The general functioning of a Faraday cup and the specification applied in the present work are described in sections 3.3.1 and 3.4.1, respectively. The experimental set-up at JETI inclusive EBT films, Roos electron chamber and Faraday cup as well as the practical limits arising from the set-up and the spectral energy distribution of the laser-accelerated electrons are discussed in section 3.4.1.

For the radiobiological characterization of laser-accelerated electrons both human normal (fibroblasts, mammary epithelium) and human tumor (squamous carcinoma) cell lines were deployed analyzing the influence on the cellular survival and the number of residual DNA DSB (cf. section 2.4.4) following irradiation.

Dosimetry with the Faraday Cup

In principle, a Faraday cup is deployed to measure the current of a charged particle beam, e.g., electrons, protons or heavier ions. It consists of a solid metallic body, heavy and long enough to stop the particles under investigation, at which an electric potential is applied. Incoming charged particles lead to a potential change, that is discharged by a resistor or amplifier. The resultant current (I) is being processed by means of an electrometer or oscilloscope and can be used to estimate the number of charged particles:

$$(5) \quad I = \frac{N \cdot e^-}{t}$$

with N the number of electrons e^- (elementary charge), either incident or needed to compensate a positive charge, detected in a time t .

The Faraday cup used in the present work (section 3.4.1) consists of a 20 cm long aluminum cylinder and was constructed in accordance to the measurement of electron bunches with energies of up to 50 MeV. Moreover, the bunch (i.e., pulse) charge was readout as voltage per bunch, because the

ultrashort pulse duration of ≈ 5 ps prevented the readout of currents. The voltage, recorded for every single pulse, allowed for the recalculation of the number of electrons per bunch by means of a known conversion factor. In order to apply the Faraday cup for absolute charge measurement it has to be operated in vacuum. This requirement cannot be met for the experimentation with living cell samples, for which reason the Faraday cup has to be operated on air in the present work. Therefore, it was used for pulse monitoring during the experiment, whereas the absolute doses administered to the cell samples were determined retrospectively by means of EBT films (section 2.3.4).

First systematic radiobiological experiments

Two biological endpoints were analyzed in order to determine the biological effectiveness of laser-accelerated electrons relative to conventional 200 kV X-rays. The analysis of residual DNA double-strand breaks (cf. section 2.4.4), was chosen for practical reasons, e.g., a short handling time after irradiation. As a second method, the influence of laser-accelerated electrons on the cellular survival was investigated by means of the clonogenic survival assay, representing the “gold standard“ in radiotherapy related research. The measured variable of this method is the reproduction capability, which is inherent in normal tissue stem cells and tumor stem cells, but also in immortalized cell lines of originally non dividing tissues, like the mammary gland epithelium. Moreover, the reproduction capability is of great importance for such tumor cells, that tend to recover and repopulate after radiotherapy. In consequence, new radiation qualities have to be characterized with respect to their influence on the clonogenic survival, especially of tumor cells but also of normal tissue cell lines. Following irradiation, three cellular mechanisms are known that lead to the reduction of the reproduction capability of a cell line [44]:

- Most frequently in human normal and tumor cells is the **mitotic death**, describing the accumulation of DNA damages by subsequent cell divisions up to a certain degree. Beyond this limit the cell is not capable of completing the cell cycle or cell division.
- The **interphase death** affect those cells that die before entering mitosis, for instance by apoptosis.
- The **differentiation** of clonogenic cells will result in specialized cells, for example skin cells, neurons, etc., without cell dividing capability.

In order to quantify the clonogenic survival of irradiated cells, their colony forming ability is determined and compared to those of non-irradiated controls. Therefore, cell solutions with defined concentrations are prepared enabling for the plating of a defined number of cells (Fig. 3.3). Subsequently, the cells are incubated under normal growth conditions, long enough to allow for the formation of colonies, fixed and stained. For analysis, the number of colonies, consisting of at least 50 cells, are counted and the plating efficiencies (PE) and surviving fractions (SF) are calculated. The former, the PE , is achieved by dividing the number of plated cells and colonies received:

$$(6) \quad PE = \frac{\text{Number of colonies}}{\text{Number of plated cells}}$$

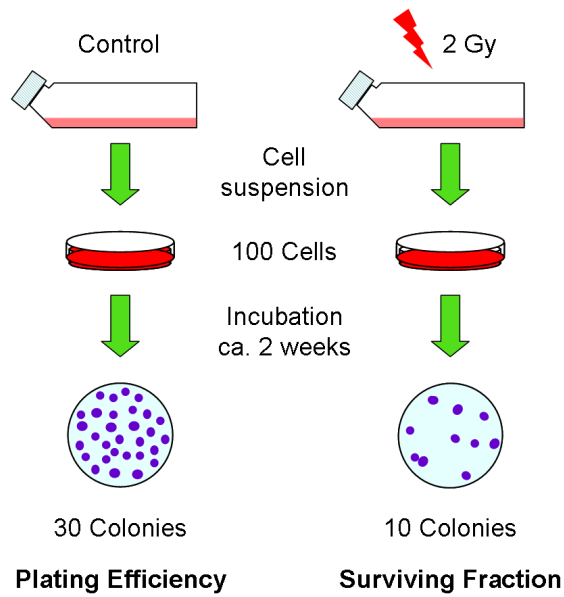


Figure 3.3: Schematic illustration of the colony formation assay. The determination of the plating efficiency of unirradiated controls is depicted on the left, those of the surviving fraction of irradiated samples on the right side.

Regarding the unirradiated controls, the plating efficiency expresses the colony forming ability of a certain cell line under normal growth conditions. A comparison of the PE of the irradiated cells and the controls reveals the cellular surviving fraction after irradiation.

$$(7) \quad SF = \frac{PE_{\text{irradiated}}}{PE_{\text{control}}}$$

For a given radiation quality, the cellular survival is considered in dependence on dose, whereas the resultant survival curves can be used to compare different radiation qualities, e.g., unconventional laser-accelerated electrons and the 200 kV X-ray reference (section 3.4.2).

3.4 Application and first results

1. Establishment of technical prerequisites for cell irradiation experiments with laser-accelerated electrons
2. Laser particle acceleration for radiotherapy: A first radiobiological characterization of laser-accelerated electrons

**Establishment of technical prerequisites for cell irradiation experiments with
laser-accelerated electrons**

Elke Beyreuther^a, Wolfgang Enghardt^{b,a}, Malte Kaluza^c, Leonhard Karsch^b, Lydia Laschinsky^b,
Elisabeth Lessmann^a, Maria Nicolai^c, Jörg Pawelke^{b,a}, Christian Richter^{b,a}, Roland Sauerbrey^a,
Hans-Peter Schlenvoigt^c, Michael Baumann^b

^a Forschungszentrum Dresden-Rossendorf, Bautzner Landstraße 400, 01314 Dresden, Germany

^b OncoRay, Center for Radiation Research in Oncology, Technische Universität Dresden, Fetscher-
str. 74, 01307 Dresden, Germany

^c Institut für Optik und Quantenelektronik, Friedrich-Schiller-Universität Jena, Max-Wien-Platz 1,
07743 Jena, Germany

Short running title: Laser accelerated electrons for cell irradiation experiments.

Corresponding author:

Elke Beyreuther

Institute of Radiation Physics

Forschungszentrum Dresden-Rossendorf

P.O. Box 510119

D-01314 Dresden, Germany

Fon: +49 351 260 3552

Fax: +49 351 260 3700

E-mail: E.Beyreuther@fzd.de

Medical Physics 37(4):1392-1400(2010)

DOI: 10.1118/1.3301598

www.medphys.org

ABSTRACT

Purpose: In recent years, laser-based acceleration of charged particles has rapidly progressed and medical applications, e.g., in radiotherapy, might become feasible in the coming decade. Requirements are monoenergetic particle beams with long-term stable and reproducible properties as well as sufficient particle intensities and a controlled delivery of prescribed doses at the treatment site. Although conventional and laser-based particle accelerators will administer the same dose to the patient, their different time structures could result in different radiobiological properties. Therefore, the biological response to the ultrashort pulse durations and the resulting high peak dose rates of these particle beams have to be investigated. The technical prerequisites, i.e., a suitable cell irradiation setup and the precise dosimetric characterization of a laser-based particle accelerator, have to be realized in order to prepare systematic cell irradiation experiments.

Methods: The Jena Titanium:Sapphire laser system (JETI) was customized in preparation for cell irradiation experiments with laser-accelerated electrons. The delivered electron beam was optimized with regard to its spectrum, diameter, dose rate and dose homogeneity. A custom-designed beam and dose monitoring system, consisting of a Roos ionization chamber, a Faraday cup and EBT-1 dosimetry films, enables real-time monitoring of irradiation experiments and precise determination of the dose delivered to the cells. Finally, as proof-of-principle experiment cell samples were irradiated using this setup.

Results: Laser-accelerated electron beams, appropriate for *in vitro* radiobiological experiments, were generated with a laser shot frequency of 2.5 Hz and a pulse length of 80 fs. After laser-acceleration in the helium gas jet, the electrons were filtered by a magnet, released from the vacuum target chamber and propagated in air for a distance of 220 mm. Within this distance a lead collimator (aperture 35 mm) was introduced leading, along with the optimized setup, to a beam diameter of 35 mm, sufficient for the irradiation of common cell culture vessels. The corresponding maximum dose inhomogeneity over the beam spot was less than 10 % for all irradiated samples. At cell position, the electrons possess a mean kinetic energy of 13.6 MeV, a bunch length of about 5 ps (FWHM) and a mean pulse dose of 1.6 mGy per bunch. Cross correlations show clear linear dependencies for the online recorded accumulated bunch charges, pulse doses and pulse numbers on absolute doses determined with EBT-1 films. Hence, the established monitoring system is suitable for beam control and a dedicated dose delivery. Additionally, reasonable day-to-day stable and reproducible properties of the electron beam were achieved.

Conclusions: Basic technical prerequisites for future cell irradiation experiments with ultrashort, pulsed laser-accelerated electrons were established at the JETI laser system. The implemented online control system is suitable to compensate beam intensity fluctuations and the achieved accuracy of dose delivery to the cells is sufficient for radiobiological cell experiments. Hence, systematic *in vitro* cell irradiation experiments can be performed, being the first step towards clinical application of laser-accelerated particles. Further steps, including the transfer of the established methods to experiments on higher biological systems or to other laser-based particle accelerators, will be prepared.

Key words: laser electron acceleration (SM-LWFA), laser radiotherapy, cell irradiations

I. INTRODUCTION

Starting with the invention of the technique of chirped pulse amplification (CPA) [81], a tremendous progress in high-power laser technology was made over the past two decades. The associated increase in peak power and intensity available with such systems together with substantial reductions in system size has enabled the realization of table-top laser-based particle accelerators easily fitting into a university-scale laboratory. Furthermore, a careful control of the experimental parameters allowed for the first time the observation of electron [29, 36, 84], proton [97, 117] and ion pulses [43]. Narrow or even quasi-monoenergetic spectra of the accelerated particles make such laser systems candidates for next generation particle accelerators. During the interaction of the laser pulse with the plasma, electric fields in the order of 100 GV/m [29] or even 1 TV/m [43, 117] can be achieved, exceeding the field strengths available in conventional electromagnetic accelerators [109] by more than four orders of magnitude. This makes the laser-technology attractive for the realization of compact particle accelerators. Another important property of laser-driven particle pulses is the ultrashort pulse duration, which initially can be as short as the laser pulse length itself, i.e., of the order of 100 fs. The perspective of compact and potentially more cost-effective accelerators initiated discussions on their application in radiotherapy [31, 71]. Therefore, the particle beams have to meet several requirements. The particle spectra should be monoenergetic with energies of $\lesssim 50$ MeV for electrons, $\lesssim 230$ MeV for protons and $\lesssim 430$ MeV/amu for carbon ions. Intensities should amount up to $\approx 10^{10}$ particles per second. Additionally, stable and long time reproducible properties of the beams as well as a homogeneous exposure of the irradiation field are needed [109]. The delivered dose rates should be high enough to guarantee treatment times of a few minutes [109]. Further demands on electron and proton acceleration and required dose properties were discussed in several feasibility studies [15, 28, 31, 60, 78, 83].

Regarding the electrons, energies of ≤ 1 GeV [72] and maximum intensities of $\leq 3 \times 10^9$ electrons per bunch [29, 36] were achieved by laser-based particle acceleration. However, these parameters were measured in single shot experiments, and the available repetition rates are currently not sufficient to obtain the intensities and dose rates required for therapy. For protons and ions, both the energies and the intensities presently achieved are insufficient for radiotherapy.

In addition to technological requirements, the radiobiological characteristics of these new quality of particle beams have to be investigated. Compared to conventional radiotherapy, the ultrashort pulse duration of laser-accelerated particles lead to $10^9 - 10^{11}$ times higher peak dose rates and peak currents of some thousand amperes [36]. Although conventional and laser-based accelerators will administer the same dose to the patient, the different time structures and peak currents could result in different radiobiological properties. Therefore, the biological effectiveness of laser-accelerated particles has to be characterized in appropriate experiments. Previous studies have been performed with ultrashort pulsed electron [18, 87, 115] and soft X-ray [49, 118, 125] beams delivered with maximum pulse dose rates of 10^9 Gy/s [87] for electrons and 10^{13} Gy/s [118] for photons, respectively. In all of these studies the cellular survival was investigated revealing either no influence [18, 87, 125] or a reduction [49, 115, 118] of the cytotoxicity by means of the ultrahigh dose rate.

So far, no systematic radiobiological studies are published for laser-accelerated particles. The first at-

tempts in this context were recently made for protons by Yogo *et al.* [131], those for laser-accelerated electrons in the present work. Several requirements, depending on each other, have to be fulfilled including the improvement of the laser particle acceleration technology for potential radiotherapeutic application and, simultaneously, their biological characterization starting with *in vitro* cell irradiation experiments. An important step will be the transition from basic physical experiments, where few single shots with poor reproducibility are considered for further evaluation, to routine particle beam delivery with long-term stable and reliable properties. Moreover, these properties have to be controlled to such an extent, that prescribed doses can be applied to any biological object under observation.

The aim of the present work was the establishment of the technical prerequisites for cell irradiation experiments at the Jena Titanium:Sapphire laser system (JETI) [110]. This includes the optimization of the laser system and the electron beam in accordance with radiobiological requirements, like the transition to stable and reproducible irradiation of biological samples. A custom-designed beam and dose monitoring system was implemented that enables a real-time monitoring of the irradiation and a controlled dose delivery to biological samples. Moreover, a first test of cell irradiation experiment was performed demonstrating the feasibility of radiobiological studies at the JETI accelerator.

II. MATERIAL AND METHODS

The Jena Titanium:Sapphire laser system

The electron pulses were generated in a vacuum chamber, hereafter referred to as target chamber, using the 10 TW laser system JETI. Pulses of 80 fs pulse duration (FWHM) [97, 117], containing 800 mJ of energy at a central wave length of 800 nm, were delivered with a maximum repetition frequency of 10 Hz. Every fourth pulse was focused to an intensity of 5×10^{18} W/cm² into a pulsed subsonic helium gas jet which was generated by a cylindrical nozzle of 1 mm diameter. The gas density profile was approximately Gaussian, and the peak gas density could be varied in the range of $0.5 - 3 \times 10^{19}$ molecules/cm³ by changing the backing pressure of the gas jet. In this regime, the laser pulse undergoes relativistic self-focusing and self-modulation and produces pulses of highly relativistic electrons by self-modulated laser wake field acceleration (SM-LWFA) [47, 110]. The need of a sufficient high average dose, i.e., electron number, per shot made it necessary to tune the acceleration conditions by carefully changing the gas jet parameters and its position. The electron beam propagates over a length of about 400 mm in vacuum and was released from the target chamber through a 1 mm thick aluminum vacuum window. Subsequently, the electron beam and adjacent components have to be optimized to enable radiobiological experiments.

Cell irradiation geometry

With regard to radiotherapy, the dose response of both, normal tissue and tumor cells, has to be investigated for several biological endpoints, e.g., the number of DNA double-strand breaks and the cellular survival, to get a comprehensive picture of the biological effectiveness of laser-accelerated electrons. For this purpose, the whole setup has to be customized in such a way that the irradiation of adherent cell monolayers in standard cell culture vessels becomes feasible. Moreover, an online

dose monitoring system has to be chosen suitable for the usage of different sample geometries. In the present work, the electron beam diameter and homogeneity as well as the experimental setup were adjusted to the application of standard petri dishes (Greiner, Frickenhausen, Germany) and 8-well-chamber slides (VWR, Darmstadt, Germany). The former exhibit an inner diameter of 32 mm, whereas the latter ones consist of $9 \times 9 \text{ mm}^2$ plastic wells arranged in two lines on a plastic slide. Single wells are separated by 1 mm plastic and a little gap of air. Both, the petri dishes and the 8-well-chamber slides, possess an 1 mm plastic bottom, where the cell monolayers are grown. In general, petri dishes are applied to investigate the cellular survival [75], whereas the 8-well-chamber slides are used for the analysis of DNA double-strand breaks [7].

For *in vitro* cell experiments, the irradiation time and culture medium supply have to be considered carefully in order to avoid effects of medium depletion to the cells. At JETI, the delivery of an horizontal electron beam demand for the upright positioning of the cell samples and for the enclosing of medium filled culture vessels with Parafilm M (Merck, Darmstadt, Germany). For practical reasons, e.g., handling procedure and the risk of medium loss, half-filled vessels were used for short irradiation times ($\leq 10 \text{ min}$), whereas longer irradiations were performed with completely filled vessels. In consequence, the upright positioning of the cell samples resulted in a 10 mm thick medium layer of differing filling height and limited by the plastic bottom and the height of the culture vessel enclosed with Parafilm. During irradiation the plastic bottoms of the culture vessels were turned in beam direction minimizing the material in front of the cell monolayer.

Beam monitoring and dosimetry system

Because the electron beam delivered by the JETI system fluctuates in both, beam intensity and dose rate, the control of dose delivery during irradiation and a precise determination of dose for each individual cell sample are required.

Absolute dosimetry was realized with GafChromic® EBT-1 dosimetry films (ISP Corp., Wayne, NJ, USA), which are self-developing after irradiation, offer a high spatial resolution and feature a low thickness of $234 \mu\text{m}$. However, their main advantages are an almost dose rate [33] and, for the relevant energy range (MeV), energy [101] independent dose response. Irradiated films were digitized with an Epson Perfection V750 flat-bed document scanner (Seiko Epson Corp., Nagano, Japan) and their optical density (film darkness) was converted to dose within an IDL code (Interactive Data Language, ITT Visual Information Solutions, Boulder, CO, USA). The EBT-1 dosimetry films were calibrated in accordance to a previously described protocol [132], that was adopted from Devic *et al.* [21]. For this purpose, electrons of 6 MeV as delivered by a clinical electron accelerator and characterized by in-house dosimetry in compliance to DIN6800-2 [1] were applied.

For cell irradiation experiments, two EBT-1 films have been positioned both in front and behind of each cell sample. The front film was applied for precise retrospective dosimetry and the rear one for additional control. By preliminary tests with both standard cell culture vessels chosen, a dose correction factor, defined as the ratio of the dose at the cell location to the dose in front of the cell vessel, of 1.03 ± 0.05 has been determined considering the dose build up effect in the culture vessel bottom. Hence, the dose delivered to the cell monolayer inside the culture vessel can be deduced

from the dose measured by EBT-1 film in front of the sample. EBT-1 films were also utilized to monitor the beam diameter and dose homogeneity during the optimization process.

Owing to the above mentioned beam fluctuations, a standard Roos ionization chamber (type 34001, PTW, Freiburg, Germany) was applied to control the irradiation experiments and for real-time observation of the integral dose of the electron beam. Ionization chamber readout was performed with an Unidos electrometer (PTW). The Roos chamber possesses a vented sensitive volume of 0.35 cm^3 (15 mm in diameter) and is calibrated by the manufacturer using a ^{60}Co γ -source. Accordingly, the chamber provides the absorbed dose in water within an energy range of 2 - 45 MeV by using the appropriate energy dependent beam quality correction factors (k_Q). Commonly accepted as standard for absolute dosimetry of high-energy electrons in radiotherapy, in the present work the Roos chamber was just employed for relative online dosimetry. The main reason for this decision was the experiment geometry, i.e., the positioning of the Roos chamber ≈ 45 mm behind the cell sample, and the associated beam scattering in the culture vessel. Additional arguments were possible saturation effects due to the high pulse doses and potential variations of beam quality and field size that conflict with the specification of correction factors.

A custom-made Faraday cup (length: 20 cm, material: aluminum) was used to monitor the delivered bunch charge. The cup was operated in single shot mode providing output signals of 25 mV/pC. Digital oscilloscope readouts displayed the mean voltage per pulse, which is converted to a total voltage (U_{tot}) by multiplication with the number of laser pulses counted with a fast photodiode for the corresponding irradiation. Moreover, the individual bunch charges, i.e., the voltage per pulse, were logged allowing for the retrospective statistical analysis with respect to inevitable shot-to-shot fluctuations. Typically, 80 % of the pulses possessed bunch charges that were within the range of ± 40 % of the mean.

Dose evaluation and error consideration

Radiobiological experiments demand a correct and precise determination of the dose administered to the cell sample. Hence, possible influences on the beam monitoring and dosimetry system, established for cell irradiations at the JETI facility, have to be discussed.

EBT-1 dosimetry films were applied for both beam monitoring (beam spot size and dose homogeneity) and absolute dose determination. Different doses up to 5.2 Gy were delivered to the cells, and the dose errors were calculated on the basis of dose variations within the analyzed area and the uncertainties of the calibration curve [132].

For the usage of the Roos electron chamber, uncertainties arise from statistical errors, shot-to-shot fluctuations of the field size, and homogeneity as well as of the electron spectrum, which prevent the specification of correct beam quality correction factors. In addition, pulse-to-pulse variations of the beam intensity might lead to saturation effects of the Roos chamber. However, since the experiment geometry (cf. Fig. 3.4) avoids precise absolute dosimetry with the Roos chamber, detailed error considerations and quantifications were not indicated. The Faraday cup provides the bunch charge as mean voltage per pulse that is multiplied by the recorded pulse numbers resulting in a total voltage. The statistical error of this total voltage was calculated by error propagation with contributions of

the standard deviation of the average voltage per pulse and an intrinsic statistical uncertainty of 0.1 % of the cup. Additionally, a systematic error of 10 mV was assumed for the conversion of the total voltage in applied electron bunch charge, due to a possible offset of the measurement system. The number of laser pulses (≤ 3000) was accurately counted with a fast photodiode. Only reading errors (± 1 pulse) by the operator might contribute to an uncertainty. All errors given in the figures and the text were calculated on the basis of the afore described statistical uncertainties. Systematic errors were not included in calculations and fit procedures.

Proof-of-principle test irradiation

Subsequent to beam optimization and setup adjustment, a test cell irradiation experiment was performed to evaluate the practical procedure and cell handling at JETI. Mimicking the measurement of dose response curves, 47 cell samples were prepared in 8-well-chamber slides and irradiated with doses between 0.3 and 5.2 Gy. The experiment was performed at two consecutive days, which also allows to test the long-term stability and day-to-day reproducibility of the laser system and the electron beam, respectively. Moreover, with this test experiment the interplay of all components, which means the tuning and operation of the laser system, the electron beam delivery, the dose monitoring system and the cell irradiation, was investigated.

Besides practical evaluation, the test cell irradiation experiment was also used to evaluate how far the JETI system met basic requirements for radiobiological experimentation. Therefore, the electron beam should be well defined with respect to its spectral intensity distribution and to the character and spectral intensity distribution of the associated secondary radiation. The beam cross-sectional area should cover at least 0.5 cm^2 , whereas the dose deviation within this area should be less than 10 %. Furthermore, the irradiation of living cells demand for a quantifiable dose delivery within an uncertainty of typically less than 10 % and irradiation times of a few minutes, that is, the dose rate or beam intensity should be high enough.

III. RESULTS

Optimized setup for radiobiological experiments

The final experimental setup for cell irradiations at the JETI facility (Fig. 3.4) was the result of an iterative optimization process. The setup was adjusted according to radiobiological requirements, like an appropriate beam spot size, and to minimize the number of necessary setup components. Moreover, low-energy electrons ($\leq 2 \text{ MeV}$) have to be separated from the beam since only energies above this limit are used for radiotherapy and because of the energy dependence of the biological effectiveness [52]. For this, a pair of permanent dipole magnets [material: Neodymium Iron Boron, NdFeB] with opposing polarity and a magnetic flux density of 0.04 T were used for energy filtration. Each magnet consisted of eight smaller ones ($40 \times 20 \times 2 \text{ mm}^3$) and the two dipole magnets of the energy filter were separated by 145 mm along the electron beam trajectory (see Fig. 3.4). The electrons were forced on a S-shaped trajectory, and those with energies below 2 MeV were deflected from the beam and could not pass the lead collimator. Subsequently, the slowest electrons were decelerated down to approximately 1 MeV at cell position by 1 mm aluminum (vacuum window),

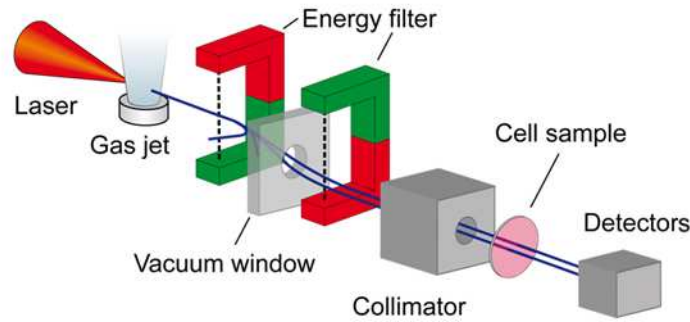


Figure 3.4: Schematic drawing of the experimental setup at the JETI system including the electron beam generation, the beam line and the online beam monitoring system (not to scale). The electrons propagate in air at a distance of about 220 mm.

220 mm air and 1 mm plastic (culture vessel bottom). This energy limit is high enough to minimize possible interference to the examined radiobiological effect.

The lead collimator ($10 \times 10 \times 10 \text{ cm}^3$, aperture of 35 mm) was introduced in order to protect the cell samples from deflected electrons and inevitably emitted secondary radiation. As shown by an irradiation with one dipole magnet deflecting all electrons, the measured dose contribution of bremsstrahlung, produced by wake field acceleration (betatron radiation) and deflection, was negligible. Moreover, the aperture of the lead collimator and the optimized distance between vacuum chamber and cell sample (220 mm) resulted in a beam diameter of 35 mm, sufficient to irradiate a petri dish or the four middle chambers ($21 \times 21 \text{ mm}^2$) of the 8-well-chamber slides. Special sample holders were designed enabling a practical and fast alignment of one petri dish or one chamber slide with the electron beam axis. At the end of the beam line (cf. Fig. 3.4), the Roos electron chamber and the Faraday cup were installed in a distance of 45 mm from the cell sample. Due to practical reasons, the smaller Roos chamber was mounted at the entrance of the Faraday cup (diameter of the sensitive volume: $\approx 10 \text{ cm}$), minimizing disturbances of the Faraday cup signal. Adjusting the Roos chamber centric to the electron beam, the entire sensitive volume of the chamber (0.35 cm^3) was irradiated.

Characterization of the electron beam

Since both cell irradiation experiments and future radiotherapeutic application require irradiation times of a few minutes [109], the mean dose rate of the electron beam had to be maximized. For this the beam pulse intensity, i.e., electron yield, was increased gradually with laser power. Moreover, the repetition rate of the laser-accelerated electron pulses was maximized by improving the vacuum in the target chamber and therefore allowing an high helium gas flow per time. The actual achieved parameters of the laser system and a summary of the electron beam parameters at cell position are shown in Table 3.2. According to the propagation of the electron beam in the vacuum window and in air, the electron beam was broadened to a bunch length of 5 ps (FWHM) as estimated by GEANT4 simulations (version 8.1 [35]). Moreover, the corresponding electron spectrum

Laser peak power (on gas jet target)	(9.0 ± 0.1) TW
Laser pulse length	80 fs
Laser pulse repetition rate	2.5 Hz
Mean kinetic energy of accelerated electrons	13.6 MeV
Electron bunch length (FWHM)	5 ps
Mean charge per electron bunch	8.3 pC
Mean pulse dose	1.6 mGy
Mean pulse dose rate*	0.3×10^9 Gy/s

*Mean pulse dose related to the electron bunch length of 5 ps

Table 3.2: Actual parameters of the laser system and the electron beam at cell position.

was simulated by GEANT4 on the basis of depth dose distributions measured with EBT-1 films in a $50 \times 50 \times 20$ mm³ stack [10 × 1 mm water (RW3), 2 × 1 mm aluminum, 16 EBT-1 films in front of and 12 EBT-1 films between the plates] at cell position. As a result, an exponential electron spectrum with a mean kinetic energy of 13.6 MeV, a low-energy cutoff of 1 MeV, and a maximum energy of 50 MeV was estimated. The laser peak power and electron bunch charge were calculated on the basis of the average laser power of 720 mJ recorded for the experiments and the measured dose-to-pulse relation (see below), respectively.

Besides adequate beam diameter and dose rate, a homogeneous exposure of the cell sample is also required for radiobiological experiments. For the present work, the dose homogeneity was examined by means of EBT-1 films positioned in front of the cell samples. Dose deviations within the cell covered area of an 8-well-chamber slide (four middle chambers, 21×21 mm²) were analyzed (Fig. 3.5). For the applied setup at JETI, a maximum dose inhomogeneity of less than 10 % was achieved for all doses. This inhomogeneity is acceptable for cell irradiation experiments.

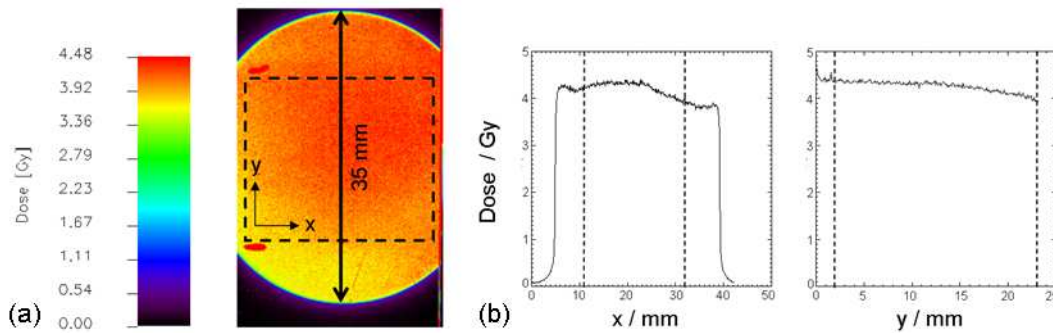


Figure 3.5: a) Exemplary dose distribution measured with a radiochromic EBT-1 film over the whole 35 mm beam diameter and the cell covered area (black dashed square) irradiated with a dose of 4.1 ± 0.3 Gy (2000 pulses). The corresponding color scale is also shown. b) Dose distribution determined for two lateral sections vertical and horizontal across the center of the sample area, delimited by the dashed lines. The cross-sectional directions were also displayed in the left picture.

Monitoring, stability and reproducibility of irradiation experiments

Due to biological heterogeneity and dose dependency of biological effects, numerous samples in

several independent repetitions have to be investigated in radiobiological experiments. Therefore, a stable beam with long-term reproducible properties as well as a beam monitoring system that ensures a controlled dose delivery to the sample is required. To meet these demands, the stability and reproducibility of the laser-accelerated electron beam were determined and the custom-designed beam and dose monitoring system was tested at two experimental days.

At the beginning of each day, the system was tuned to a stable dose-to-pulse relation of about 2 mGy/pulse. Subsequently, this dose-to-pulse relation was used to estimate the number of laser pulses necessary to deliver the prescribed doses, whereas the actual absolute doses were determined retrospectively by means of EBT-1 films. Correlating the absolute doses and the number of laser pulses (Fig. 3.6) the preset dose-to-pulse relation was confirmed by 1.90 ± 0.04 mGy/pulse for the second day. For the first day, the linear fit of the data reveals a dose-to-pulse relation of 1.30 ± 0.02 mGy/pulse. The two outliers (Fig. 3.6, black arrows) were caused by a 90 min interruption of the experiment at day one. During this interruption, the vacuum pumps cooled down, which resulted in an increased pumping rate and hence a higher electron yield correlated with an increased dose per pulse. The effect vanished 45 min after the break. In response to these outliers, which were also detected by the online monitoring system, the vacuum and temperature of the JETI system were carefully controlled at the second day in order to ensure constant dose-to-pulse relations.

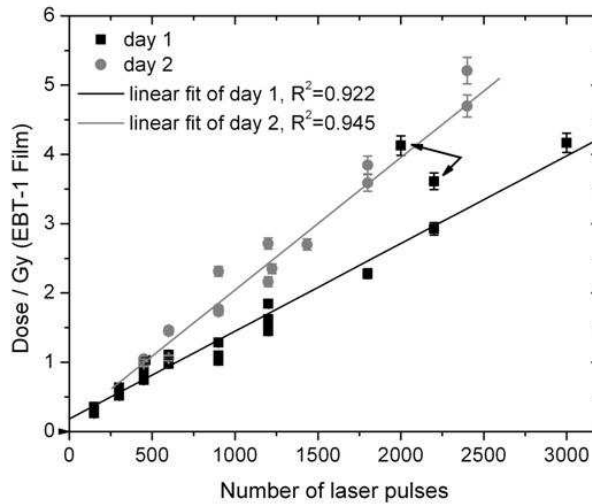


Figure 3.6: Actual doses at cell position compared to the number of applied laser pulses individually for both experimental days. The arrows mark two outliers due to different pumping rates and corresponding vacuum conditions. Dose errors were calculated by error propagation; fit parameters are given in the text.

In addition to the number of laser pulses, the relative accumulated dose and the bunch charge measured with the Roos electron chamber and the Faraday cup were correlated to the EBT-1 film-measured absolute dose in order to reveal the beam stability and their capability for online dose monitoring. For the Roos electron chamber, this comparison (Fig. 3.7a) results in a linear dose-to-dose dependence of 1.61 ± 0.03 Gy_{EBT}/Gy_{Roos} for the film-measured relative to the chamber-measured dose at both days. Furthermore, a clear linear correlation with a slope or sensitivity of 0.010 ± 0.001 Gy_{EBT}/V (Fig. 3.7b) was obtained for the total voltage (U_{tot}) provided by the Faraday

cup. In consequence, the pulse voltage, which is a measure of the delivered bunch charge, can be applied to estimate the number of laser pulses required to deliver a particular dose. The apparent wider distribution of accumulated doses (Roos chamber) and total voltages (Faraday cup) at higher film-measured doses is explainable with the filling level of the cell samples. As mentioned before, the samples were completely filled with medium if the irradiation time exceeds 10 minutes in order to avoid effects of medium depletion. Hence, volume deviations and small air bubbles in the medium might lead to differences in beam scattering and electron stopping-power, resulting in measurable effects. In contrast, samples irradiated with lower doses (≤ 2 Gy) were filled with an accurately pipetted volume providing constant conditions for electron beam transmission.

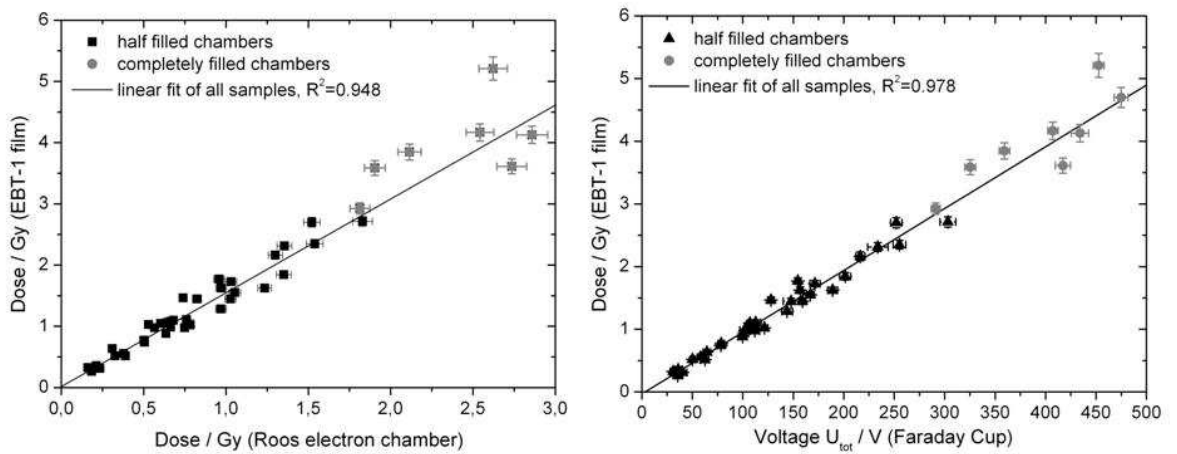


Figure 3.7: Accumulated relative dose (a) and total voltage (b) measured during the irradiation and compared to the absolute doses determined retrospectively by means of EBT-1 dosimetry films. Completely (grey) and half-filled samples (black) were distinguished in the graph, whereas the linear fits were performed with all data. Displayed errors are statistical errors, calculated by error propagation.

The good linearity of the relative dose measurements (Roos chamber and Faraday cup) over the whole dose range also indicates a negligible contribution of low-energy electrons (≤ 2 MeV) to the electron dose delivered to the cells. For longer irradiation times, a 1 cm thick medium layer was necessary. Furthermore, the electron stopping-power in water is ≈ 2 MeV/cm [51]. Hence, low-energy electrons would contribute to the dose measured with EBT-1 films in front of the sample, but not to the relative dose detected behind with the Roos electron chamber or Faraday cup. As a consequence, a deviation from the linear fit curve, especially in the high dose region, would be observable, if electrons below 1 MeV would significantly contribute to the dose.

To sum up, the observed parameters (number of laser pulses, accumulated dose measured with the Roos electron chamber and pulse voltage obtained with the Faraday cup) can be applied to monitor the electron beam and to provide relative dose information during cell irradiation. Moreover, the good linear correlations between the film-measured absolute doses and these parameters indicate a stable beam with reproducible properties during the whole experiment. Overall, the precision and stability achieved during these irradiations as well as the dosimetry and beam monitoring system are sufficient for radiobiological cell irradiation experiments.

IV. DISCUSSION

To date, the application of laser-based particle acceleration for radiotherapy has been described only theoretically (e.g., [15, 28, 31, 60, 78, 83]). The proposed properties and parameters of such beams are currently not experimentally validated. A first step in this direction are the experiments reported in this work, demonstrating the technological improvement of the JETI laser system and its feasibility for cell irradiation experiments with laser-accelerated electrons. Although not yet fulfilling the requirements needed for radiotherapeutic applications with respect to beam energy and stability, field size and dose rate, the parameters achieved at JETI are sufficient for radiobiological cell experiments.

For clinical radiotherapy, particle beams have to be monoenergetic with sufficient charge and negligible fluctuations of the physical parameters [109]. By contrast, only a configuration of the JETI laser accelerator producing broad exponential electron spectra led to beams with sufficient charge and reproducibility. However, this broad spectrum can be accepted for cell irradiation experiments because the underlying setting allows for a constant beam delivery. Moreover, the energy was high enough to achieve the required penetration depth. Low-energy electrons of ≤ 2 MeV are separated from the beam due to their elevated linear energy transfer that could influence the radiation induced effect in the cell sample. The remaining electrons were released from the target chamber in an intensity of up to 3×10^8 electrons/bunch that is sufficient for the necessary dose delivery in cell irradiation experiments. For radiotherapy, one order of magnitude more electrons is required to achieve the desired $\approx 10^{10}$ particles per second and the typical dose rates of some Gy/min [109], respectively. Nevertheless, the beam diameter of 35 mm and a dose homogeneity better than 90 % allow for a homogeneous exposure of the whole cell sample.

In parallel to the adjustment of JETI, a dose and beam monitoring system, consisting of EBT-1 dosimetry films, a Roos electron chamber and a Faraday cup, was implemented at the experimental setup. Initially applied for the optimization and fine-tuning of the beam, the devices were deployed later on for monitoring the dose and beam delivery during the experiment. The EBT-1 films were used for retrospective determination of the absolute dose delivered to the cells. A comparison of the doses determined by EBT-1 films and measured online with the Roos electron chamber revealed a correlation factor of 1.61 ± 0.03 Gy_{EBT}/Gy_{Roos}. Thus, the Roos electron chamber underestimates the actual applied doses, whereas the relative dose information is sufficient to monitor the beam and control the irradiation experiment. The beam scattering in the ≈ 1 cm thick cell sample and the distance of ≈ 4.5 cm between the sample and the Roos electron chamber are most likely responsible for the dose deviation. A clear linear dependence was also found for the comparison of the Faraday cup signal and the dose delivered to the cells determined by EBT-1 films.

In spite of these encouraging results for dose monitoring, more detailed considerations on the influence of the ultrahigh dose rates on the measured signal are desirable if the Roos electron chamber should be applied for absolute dosimetry. A strong pulse dose dependency of the dose measurement was found by Di Martino *et al.* [22] for pulse doses above 1 cGy. Regarding the mean pulse dose of 2 mGy achieved in the present work, a dose correction factor of 1.03 has to be applied in order to correct the displayed dose for the induced saturation effect [22]. However, since the Roos chamber

was deployed for relative and not for absolute dosimetry, this factor is of little importance. In addition, the application of the Roos chamber for absolute dosimetry would also demand a constant electron spectrum allowing for the specification of a correct beam quality correction factor k_Q .

Future cell irradiation experiments will require a stable particle beam with reproducible properties. For the experiments presented here, these requirements were investigated by comparing the number of laser pulses, the accumulated dose and the bunch charge with the actual dose delivered to the cells during two experimental days. A stable dose-to-pulse relation was obtained within each day, but there were differences of approximately 45 % between both days. However, these day-to-day fluctuations of the dose rate can be corrected with the information from the online beam monitoring system. Already, an improvement was achieved by carefully controlling the vacuum conditions and the temperature of the JETI system. Further developments and advancements of the laser acceleration technology and the auxiliary equipment are expected to lead to more stable and reproducible particle beams in future.

Although various outstanding improvements were identified, the main goal of the present work was achieved. The transition from experiments with single electron shots of poor reproducibility to relative stable and repeatable irradiations was accomplished and a test cell irradiation experiment was performed demonstrating that the JETI system meets key requirements for radiobiological *in vitro* experimentation. The achieved electron energy and intensity were high enough for the irradiation of living cells; the beam diameter of 35 mm and a dose homogeneity better than 90 % over the corresponding cross-sectional area guaranteed the homogeneous exposure of cell monolayers in different sample geometries. Moreover, the setup and handling procedure were found to be practical for comprehensive radiobiological studies, the dose delivery to the cells was controllable and quantifiable with sufficient accuracy, and the emitted secondary radiation were quantified and found to be negligible at the cell position. For these reasons, the JETI laser system fulfills basic radiobiological requirements and was successfully prepared for systematic *in vitro* cell irradiation studies.

IV. CONCLUSION

The aim of the presented work was the advancement of the laser-driven accelerator technology in order to establish the basic technical prerequisites for future *in vitro* cell irradiation experiments with ultrashort pulsed laser-accelerated particles as one step toward radiotherapeutic application. Therefore, the JETI laser system was optimized now allowing for the delivery of stable electron beams sufficient for radiobiological experiments, instead of single shots with low reproducibility. Moreover, an online control system was implemented that enables the compensation of beam and dose fluctuations and the delivery of prescribed doses with sufficient accuracy for radiobiological cell experiments. For this reason, systematic *in vitro* cell irradiation experiments are prepared, being a step further toward clinical application of laser-accelerated particles. The performance of such systematic cell experiments will result in information on the biological effectiveness of laser-accelerated particle beams. With this work, major technological progress has been achieved on the way towards establishing a laser-particle accelerator for radiotherapeutic application. In further steps, the transferability of the established methods to experiments on higher biological systems (e.g., tissue or animals) or other laser-based particle accelerators has to be proven.

Acknowledgments

This work has been supported by the German Federal Ministry of Education and Research (BMBF) under contract 03ZIK445.

Author contributions

Study concept and design E.B., J.P., L.K., E.L., H.-P.S.; Experimental studies E.B., L.K., E.L., J.P., H.-P.S., L.L., C.R., M.N.; Data acquisition E.L., L.K., E.B., H.-P.S., L.L., C.R.; Literature research E.B., L.K.; Data analysis E.B., L.K., C.R.; Definition of intellectual content J.P., M.B., W.E., R.S.; Manuscript preparation E.B., H.-P.S.; Manuscript editing R.S., M.K., H.-P.S., W.E., L.K., J.P., M.B., C.R., L.L.; Guarantors of integrity of the entire study J.P., M.B., W.E., M.K., R.S.; Manuscript review was carried out by all authors.

Laser particle acceleration for radiotherapy: A first radiobiological characterization of laser accelerated electrons

Jörg Pawelke^{a,b}, Elke Beyreuther^b, Wolfgang Enghardt^{a,b}, Malte Kaluza^c, Leonhard Karsch^a, Lydia Laschinsky^a, Elisabeth Lessmann^b, Doreen Naumburger^a, Maria Nicolai^c, Christian Richter^{a,b}, Roland Sauerbrey^b, Hans-Peter Schlenvoigt^c, Michael Baumann^a

^a OncoRay - Center for Radiation Research in Oncology, Technische Universität Dresden, Medical Faculty, Dresden, Germany

^b Forschungszentrum Dresden-Rossendorf, Institute of Radiation Physics, Dresden, Germany

^c Friedrich-Schiller-Universität Jena, Institute of Optics and Quantumelectronics, Jena, Germany

Corresponding author:

Jörg Pawelke

OncoRay-Center for Radiation Research in Oncology

Medical Faculty Carl Gustav Carus

Technische Universität Dresden

Fetscherstraße 74

D-01307 Dresden, Germany

Fon: +49 351 458 7430

Fax: +49 351 458 7311

E-mail: Joerg.Pawelke@oncoray.de

O. Dössel and W.C. Schlegel (Eds.): WC 2009, IFMBE Proceedings 25/III, pp. 502-04, 2009.

www.springerlink.com

ABSTRACT

In recent years, the technology of laser-based particle acceleration has developed at such a rate that compact and potentially more cost-effective accelerators are promised for medical application, e.g., for high precision hadron radiotherapy. Necessary requirements are the supply of stable and reliable particle beams with reproducible properties, sufficient particle intensities and monoenergetic spectra. Additionally, a precise dose delivery in an appropriate time and the exposure of a desired irradiation field are needed. Beside these physical demands, the consequences on detection and dosimetry as well as the radiobiological effect on living cells have to be investigated for the ultrashort pulsed laser-based particle beams.

As a first step, the laser accelerator facility at the Jena Titanium:Sapphire system was customized for *in vitro* cell irradiation experiments and the delivered electron beam was improved with regard to its spectrum, diameter, dose rate and dose homogeneity. Furthermore, a custom-designed beam and dose monitoring system was established that enables real-time monitoring of the irradiation experiments and a precise determination of the dose delivered to the cells. Moreover, stable and reproducible beam properties were achieved during the whole three month experiment campaign.

Dose-effect-curves were obtained for four cell lines and two endpoints, generally displaying a lower biological effectiveness for short-pulsed laser-accelerated electrons relative to the continuous 200 kV X-ray reference irradiation. Possible reasons will be discussed.

Keywords: laser-based particle acceleration, radiotherapy, *in vitro* cell experiments, biological effectiveness

I. INTRODUCTION

Over the past years, the technological progress in high-power laser technology results in increasing peak powers and intensities associated with substantial reductions in system size, which enables the realization of table-top laser-based particle accelerators. This novel technology of particle acceleration promises accelerators of compact size and reasonable costs that may contribute to a widespread use of high precision hadron radiotherapy.

Some basic properties of laser-acceleration are reasonably well known from theory, simulations and fundamental physical experiments [29, 36, 43, 84, 117], but considering medical application several further requirements have to be fulfilled. The particle beam should be stable and reliable with reproducible properties; the intensity and with it the dose rate should be high enough to guarantee appropriate irradiation times. Likewise, a precise and controlled dose delivery and the exposure of a desired irradiation field are required.

In addition to the physical demands, the radiobiological properties of these particle beams have to be characterized. Compared to conventional electromagnetic accelerators, the ultrashort pulse durations (in the order of 100 fs) of laser-accelerated particle beams result in $10^9 - 10^{11}$ times higher peak dose rates and peak currents of some thousand Ampere [29]. These differences in time structure and dose delivery could lead to different radiobiological effects, although both kinds of accelerators will administer the same dose to the patient. Consequently, the biological effectiveness of laser-accelerated particle beams have to be investigated starting from human cells and end up with clinical studies.

As a first step in this chain, laser-accelerated electrons were applied for *in vitro* cell irradiations in order to investigate the dose dependent induction of radiation damage. For that reason, the experimental setup at the Jena Titanium:Sapphire (JETI) laser system [110] as well as the generated electron beam were customized with regard to radiobiological requirements. In addition, a custom-designed beam and dose monitoring system was established. Subsequently, dose-effect-curves for four cell lines and two endpoints were obtained and compared to the results of a conventional 200 kV X-ray tube.

II. MATERIAL AND METHODS

The Jena Titanium:Sapphire laser system (JETI)

Electron pulses were generated using the 10 TW laser system JETI that delivers 80 fs pulses (800 mJ energy, 800 nm central wave length) [110] at a repetition rate of 2.5 Hz. Focused into a subsonic helium gas jet the laser pulses produce plasma and accelerate electrons in the forward direction. The generated electron beam left the vacuum system through a 1 mm thin aluminum window and propagated in air by reason of the living cell samples that demand for atmospheric pressure. In the following, the laser system, the beamline and the electron beam itself had to be optimized in order to perform radiobiological experiments.

Setup of the beam monitoring and dosimetry system

A beam monitoring and dosimetry system, consisting of a Faraday cup, a Roos ionization cham-

ber (sensitive volume of 0.35 cm², PTW, Germany) and GafChromic® EBT dosimetry films (ISP, USA) were established at the JETI system. Firstly used for beam optimization, the system was employed later on for a careful control of the cell irradiation experiments. Here, the Faraday cup and the ionization chamber provide an online dose information, whereas the radiochromic films were applied for retrospective precise dosimetry.

Cell irradiation experiments

Samples of two squamous cell carcinoma (FaDu, SKX) and two normal tissue (mammary gland epithelial cells 184A1, human skin fibroblasts HSF2) cell lines were irradiated with prescribed doses in the range of 0.3 to 10 Gy at several experiment days over a period of three months. During irradiation each sample was equipped with two EBT radiochromic films, one in front of and one behind the cell monolayer, providing a retrospective precise dose determination.

Following irradiation the dose dependent cellular survival was measured using the clonogenic survival assay. Additionally, the immunochemical detection of co-localized γ -H2AX and 53BP1 molecules [27] was applied to analyze DNA double-strand breaks which remain in the cells 24 hours post irradiation. Parallel to the experiments at the JETI electron accelerator reference irradiations were performed with a conventional 200 kV X-ray tube.

III. RESULTS

Adjusted setup for radiobiological experiments

The measured exponential energy spectrum of the JETI electron beam was limited to a minimum energy of 2 MeV using a pair of permanent magnets for energetic filtration. Additionally, the beam spot size was adjusted by means of a lead collimator ($10 \times 10 \times 10$ cm³) with an aperture of 35 mm. As a result, a MeV electron beam of 35 mm diameter was achieved sufficient to irradiate common cell sample vessels like petri dishes (32 mm inner diameter). The dose homogeneity was improved resulting in less than 10 % inhomogeneity over the cell sample as proven by radiochromic films.

The electron yield and with it the mean dose rate of the pulsed electron beam was increased gradually with laser power using the Faraday cup to monitor the delivered bunch charge. In the end, a mean dose rate of 0.36 Gy/min or 2.4 mGy per pulse was achieved for cell irradiation.

Beam monitoring, stability and reproducibility

Basic requirements for radiobiological experiments are a stable beam with reproducible properties as well as a beam monitoring system that ensures a controlled dose delivery to the cells. The beam stability and reproducibility were checked by comparing the actual dose, determined retrospectively with EBT radiochromic films, to the parameters monitored during the experimental period of ten weeks. As result, clear linear dependencies were achieved for all three parameters - the number of laser pulses, the accumulated dose (Roos ionization chamber) and the bunch charge (Faraday cup) - recorded. Hence, the beam properties were stable and reproducible over the time and the parameters can be deployed to control the dose delivery to the cells. Exemplary, the correlation of the doses measured with the Roos ionization chamber and the EBT radiochromic films were displayed

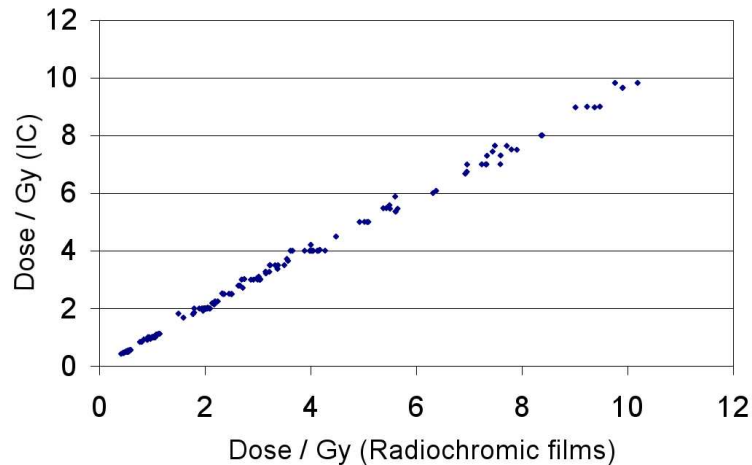


Figure 3.8: The accumulated dose measured online with the Roos ionization chamber compared to the dose determined retrospectively by EBT dosimetry films for the irradiation of 163 cell samples.

in Figure 3.8. Regarding the beam intensity, variations of up to 40 % or 130 % were observed taken into account one day or all days of the experiment, respectively. These variations were compensated by means of the established online dose monitoring system.

The biological effectiveness of laser-accelerated electrons

The dose-effect-curves obtained for both endpoints and all cell lines investigated show in general a lower biological effectiveness for the ultrashort pulsed laser-accelerated electron beams relative to continuous 200 kV X-ray irradiation. Possible reasons are differences in time structure, mean dose rate and energy spectrum of both radiation qualities. The results of current investigations dealing with this topic will be discussed.

IV. CONCLUSION

The successful realization of the presented *in vitro* cell experiments demonstrates that the application of prescribed doses, a controlled dose delivery and accurate dosimetric measurements are feasible at laser-based electron accelerators. All technical requirements were established and all components and methods have proven their stability and reliability in systematic radiobiological cell studies over months. Obtained differences in the biological effectiveness of laser-accelerated electrons and conventional 200 kV X-rays can be explained by means of physical properties of radiation.

In a second step, experiments are prepared at a 100 terawatt laser system, which will provide laser-accelerated proton beams for radiobiological cell irradiation studies.

Acknowledgment

This work has been supported by the German Federal Ministry of Education and Research (BMBF) under contract 03ZIK445.

Author contributions

Study concept and design J.P., L.L., L.K., C.R., E.L., H.-P.S., E.B.; Experimental studies L.L., E.L., L.K., C.R., J.P., H.-P.S., M.N., E.B., D.N.; Data acquisition E.L., L.L., L.K., C.R.; Literature research E.B., Data analysis L.L., D.N., C.R., L.K.; Manuscript preparation E.B., J.P.; Manuscript editing J.P., M.B., E.B.; Guarantors of integrity of the entire study J.P., M.K., R.S., W.E., M.B.; Manuscript review was carried out by all authors.

4 Discussion

The overarching issue of the present dissertation was the realization of *in vitro* cell irradiation experiments at conventional and unconventional radiation sources, bearing in mind the potential application of their emitted radiation for medical purposes. Two specific topics were addressed within this general context - the photon energy dependence of the relative biological effectiveness of X-rays and the performance of first *in vitro* cell experiments at a laser-driven electron accelerator. Therefore, several consecutive requirements, like the establishment of appropriate radiation sources and their dosimetric and biological characterization, have to be fulfilled independent on the applied radiation quality.

The first issue was motivated by the ongoing cost-benefit discussion that begun in 2002 with the introduction of a nationwide mammography screening program in Germany and the simultaneous publication of an alarming high RBE value for mammographic X-rays by Frankenberg *et al.* [32]. Accordingly, several *in vitro* studies were initiated aiming on the photon energy dependence of the RBE [40, 41, 45, 68, 105, 111, 112, 113], especially in the energy range below 50 keV. Likewise in our laboratory, where the biological response to low-energy X-rays was reviewed for human mammary gland epithelial cells. Previous experiments performed with cell line MCF-12A [74, 75] were not only pursued in the present work, but also extended by the establishment and examination of a second human mammary epithelial cell line (184A1). Moreover, two additional endpoints, the investigation of chromosomal aberrations and the detection of DNA double-strand breaks, were established and successfully applied (sections 2.4.3 and 2.4.4) to analyze the relative biological effectiveness of 25 kV and 10 kV X-rays (Table 4.1). Regarding the resulting RBE values (Table 4.1), the biological

Biological endpoint	RBE \pm Δ RBE	
	Cell line 184A1	Cell line MCF-12A
<i>10 kV X-rays</i>		
Excess fragments: Dicentric chromosomes and centric rings:	1.92 \pm 0.26	1.40 \pm 0.10
Residual DNA DSB (24 hours post irradiation):	2.8 – 6.9*	-
<i>25 kV X-rays</i>		
Excess fragments: Dicentric chromosomes and centric rings:	1.17 \pm 0.12	0.97 \pm 0.10
Residual DNA DSB (24 hours post irradiation):	0.8 – 2.6*	-
<i>34 MV bremsstrahlung</i>		
MN pro BNC	0.75 \pm 0.05	-

* Dose dependent RBE values

Table 4.1: RBE values determined in the framework of the present dissertation on basis of dose-effect-curves for various biological endpoints and photon energies using conventional 200 kV X-rays as reference.

effectiveness of 25 kV mammographic X-rays seems to be equal or just slightly enhanced compared

to the 200 kV reference. By contrast, a significant increase was found for 10 kV X-rays. Both, the determined tendency of photon energy dependence as well as the RBE values itself, are in good agreement with those published in the literature for the same endpoints and similar photon energies but differing cell systems [41, 68, 105, 108, 112, 113, 119]. In addition, comparable RBE values were determined by previous studies of our laboratory using cell line MCF-12A and the same X-ray tubes to analyze the cellular survival and the induction of micronuclei [74, 75].

Although the results achieved for these particular energies are quite reasonable, no detailed conclusions can be drawn for the underlying photon energy dependence of the RBE because of the spectral energy distribution of X-ray tube photons. Therefore, more detailed investigations were planned using quasi-monochromatic channeling X-rays provided at the radiation source ELBE, which are tunable in the range of 10 to 100 keV. These photons were well characterized with regard to their general physical properties, like the available energy range and intensities [3, 73, 129], but not assessed for radiobiological *in vitro* experiments. Beside low-energy X-rays the present work focused also on the RBE of high-energy photons (≤ 40 MV) generated as bremsstrahlung at ELBE. Photons of these high energies are better focusable to narrow pencil beams than those photons with a maximum energy of up to 20 MeV, which are nowadays applied in radiotherapy. In consequence, high-energy photons are proposed for application in radiotherapy [123], possibly improving the tumor conformity and sparing of the normal tissue during the treatment [96, 123].

Nevertheless, the dosimetric characterization and, furthermore, the realization of *in vitro* cell irradiations at the channeling X-ray source and for high-energy bremsstrahlung at ELBE turned out to be more ambitious than for conventional X-ray tubes. There, stable radiation properties enable the application of predetermined dose rates and the replacement of cell samples is allowed at any time. By contrast, the radiation protection regulations at ELBE inhibit the fast access to the cell samples and practical beam deviations in intensity and positioning of the secondary radiation avoid the employment of predetermined irradiation times, respectively. The first point was circumvented with the development of a remote-controlled cell irradiation system (section 2.5.2); the second one demanded for the implementation of an adequate dosimetry system at ELBE that allow for the online dose control during irradiation, for the analysis of dose distributions over the cell sample and for the precise determination of the absolute dose administered to the cells. Differing types of detectors were evaluated for the varying requirements. Due to their pin point geometry, that prevent the dose measurement over the whole cell covered area, standard ionization chambers (section 2.3.2) were chosen for the online dose control of the irradiation experiment. Therefore, one ionization chamber was positioned on beam axis behind the cell sample, providing the relative dose delivered to the cells, and a second one was placed next to the cell sample container measuring the radiation background exposure. For absolute dosimetry and the determination of spatial dose distributions two types of detectors, based on thermally stimulated exoelectron emission (section 2.3.3) and radiochromic films (section 2.3.4), were evaluated. Whereas both types of detectors are suitable for absolute dosimetry, the TSEE detectors offer the particular advantage of a nanometer thick sensitive layer enabling the measurement of dose gradients in a 10 μm thick cell monolayer. For comparison, the sensitive volume of the EBT films used in the present dissertation is $\approx 40 \mu\text{m}$

thick. However, the TSEE detectors were found to be not practicable for routine cell irradiations, since their mechanical stability and dose response reproducibility under real experiment conditions were inadequate. Consequently, radiochromic EBT films were deployed for the retrospective determination of the absolute dose administered to the cell sample, of dose inhomogeneities over the cell covered area and of deviations of the electron beam positioning. Moreover, the implementation of EBT films in front of each sample allows for the retrospective analysis of beam deviations for individual cell samples and, hence, for the tracking of beam deviations during the experiment.

Based on the observation of the radiation background the channeling X-ray source was found to be not applicable for radiobiological experiments in the framework of the present dissertation, by reason that the background dose contribution is as high as the planned dose delivery to the cells. The main part of the background radiation is produced by electrons, that were scattered in the diamond crystal, loss some energy and are subsequently not fully deflected to the beam dump (cf. section 2.5.2, e.g., Fig. 2.18, for setup). In the following, these electrons might hit the beam line components and generate bremsstrahlung. Moreover, a significant contribution to the radiation background arise from bremsstrahlung produced during the electron stopping in the beam dump. A minor, but unavoidable, source of radiation background are non-channeling electrons that produce bremsstrahlung directly in the diamond crystal. Although, this bremsstrahlung is also emitted in forward direction, like the quasi-monochromatic channeling X-rays, their contribution to the entire background is very small. Practicable solutions for background reduction are a better shielding of the beam line and the beam dump or the guidance of channeling X-rays in the adjacent experimental hall using the lead-containing concrete wall as additional shielding. However, this is connected with high investment costs and new extensive practical regulations in order to fulfill the radiation protection directives.

Contrary to the channeling source, applicable beam parameters and an acceptable radiation background level were obtained for the high-energy bremsstrahlung source (section 2.5.2). Following dosimetric characterization, first *in vitro* cell irradiation experiments were performed aiming on the analysis of micronuclei induced by 34 MV bremsstrahlung in cell line 184A1. The resulting RBE value, relative to the 200 kV X-ray reference, is shown in Table 4.1. Presently, very few data on the RBE of high-energy photons can be found in the literature; indeed their exist no possibility of direct comparison for the RBE value of 34 MV bremsstrahlung obtained in the present dissertation. Similar RBE values of about 1 were revealed by Persson *et al.* [96], which investigated the clonogenic survival of 50 MV bremsstrahlung relative to those after ^{60}Co γ -radiation. Furthermore, RBE values ranging from 0.25 to 1 were ascertained comparing the biological effectiveness of several reference radiation sources, like ^{60}Co γ -rays and 200 - 350 kV X-rays [48]. Summarizing these data, the RBE value obtained in the present work is quite reasonable demonstrating that radiobiological experimentation under the harsh conditions at ELBE is possible. However, taken into account the medical application of high-energy photons (≥ 20 MeV), neutrons arising from high-energy bremsstrahlung via photo nuclear reactions with parts of the beam line have to be considered. At ELBE the neutron background dose rate was monitored by means of a neutron detector (section 2.5.2), whereas Persson *et al.* [96], who obtained a similar RBE, have identified just a marginal neutron

influence on the relative biological effectiveness of 50 MV photons.

Regarding the RBE values obtained in the present work an inverse relationship between the photon energy and the RBE becomes evident, independent on the examined biological effect. This tendency reconfirms previously published studies [48, 52], which also reveal increasing RBE values for decreasing photon energies starting in the MeV range and end up with a maximum RBE at 6.9 keV [48]. A reasonable explanation for these findings is given by the physical model of the “**Linear Energy Transfer (LET)**“, which is in its most general form defined for ionizing charged particles as “the average energy (dE) lost by the particle due to electronic interactions per unit length (dl) of its trajectory“ [17]:

$$(8) \quad LET = \frac{dE}{dl}.$$

The LET is expressed as keV/ μm and depends on the mass, charge and velocity, i.e., the probability of interaction, of the incident charged particle. Different radiation qualities are classified either as low or high LET radiation depending on whether their LET is lower or higher than 3.5 keV/ μm [65]. Non-ionizing particles, like photons or neutrons, are characterized by means of their secondary particles. In dependence on their energy photons are assigned either to low or high LET radiation, whereas neutrons, which generate protons and heavier atomic nuclei with a higher probability of interaction, belong in general to the high LET radiation. The biological consequences that arise from the different LET, especially for the target molecule DNA, are displayed in Figure 4.1.

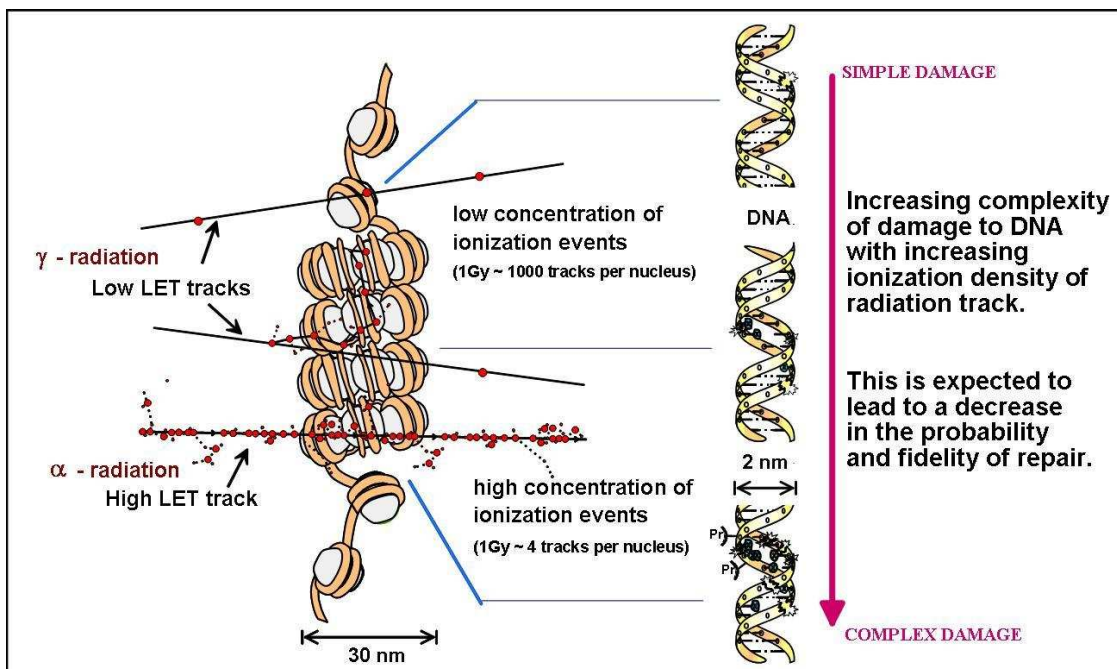


Figure 4.1: Schematic representation of the linear energy transfer and the resultant biological consequences, exemplary for low LET γ -radiation and high LET α -particles (Kindly provided by Marc Hill, MRC Radiation and Genome Stability Unit, Harwell, Oxfordshire, UK).

Considering the photon energy dependence of the RBE, the range and accompanied LET distribution of the generated secondary electrons are the most likely explanation for the obtained tendencies. For high-energy photons or γ -rays the secondary electrons released in matter are of high-energy and long ranging. Consequently, their probability of interaction and therefore the linear energy transfer are quite low, e.g., $0.22 \text{ keV}/\mu\text{m}$ [55] for ^{60}Co γ -rays. With decreasing photon energy both energy and range of the secondary electrons also decrease resulting in an increasing probability of interaction and in LET values reaching those of high-LET radiation. Moreover, the range of the secondary electrons arrives at distances that are comparable and even lower than the size of a cell ($\approx 30 \mu\text{m}$). Exemplary for 6.9 keV, the LET amounts to $4.1 \text{ keV}/\mu\text{m}$ and the maximum range of the secondary electrons is in the order of $1.2 \mu\text{m}$ [4] associated with a higher probability of consecutive interactions within the same cell, i.e., with a higher risk of DNA DSB induction. Even higher LET values might be proposed for photon energies below the maximum at 6.9 keV, but the range of their secondary electrons (down to nm) is too short to induce complex DNA damages, like DSB. In addition, the very low range of these secondary electrons is contrary to the LET model, where the energy distribution is regarded on a trajectory.

Although the underlying photon energy dependence of the RBE is commonly accepted and explainable with the LET model, no revision or energy dependent specification of the radiation weighting factor for photons was realized within the radiation protection directives of the ICRP [57]. The results obtained by the various *in vitro* studies were of course discussed with respect to the underestimation of the radiation risk, especially for low-energy photons (e.g., [11, 37, 57]), but there are several reasonable arguments against an adjustment. The absolute numbers and energy dependent variations of the RBE values achieved for photons are quite low compared to those found for other radiation qualities, like heavy ions or neutrons. For example, RBE values ranging from 16.6 (36 keV) to 23.4 (385 keV) have been determined for the neutron based induction of dicentric chromosomes in human lymphocytes using 220 kV X-rays as reference [114]. In this context, the twofold to sixfold higher biological effectiveness of low-energy X-rays ($\leq 50 \text{ keV}$) relative to ^{60}Co γ -rays and 200 kV X-rays as reference do not justify an energy dependent radiation weighting factor, respectively. Even more, if one considers the modification of the photon energy spectra by the transition from flat cell samples to large human bodies. Low-energy photons will be absorbed in the outer skin layers, whereas high-energy photons will interact with tissue atoms and produce secondary electrons that might contribute to the organ doses. However, the maximum photon energy difference and with it the RBE variations averaged over the whole human body will be much smaller than for cell culture samples used in radiobiological experiments [23].

Another important aspects are the absence of significant epidemiological data and the question, to what extent *in vitro* data can be applied to estimate the radiation risk for large and complex human bodies. So far, the high RBE values revealed by *in vitro* cell experiments are not supported by animal studies or epidemiological surveys [52, 58], due to the fact that the existing epidemiological data cannot be analyzed with respect to particular energies [52] or that the underlying statistic is insufficient [58]. Moreover, the revision of the weighting factor has to be considered carefully, since it will have practical consequences on radiation protection regulations [23]. Taking into account these

arguments and the absence of more comprehensive epidemiological studies, the ICRP still specifies a radiation weighting factor of 1 for all photon energies in their 2007 recommendations [58].

An analogue line of arguments has to be regarded to judge the *in vitro* results determined for mammographic X-rays. The most important question in this context is again the validity or adaptability of *in vitro* data for the radiation risk estimation for healthy women which attend the mammography screening program. Less relevant for these considerations is the cellular survival following irradiation, because the average glandular dose administered to the female breast lies in the range of 4.5 to 21.4 mGy per screening [46]. By contrast, doses of ≥ 500 mGy are typically required for radiobiological examination in order to detect any effect on the cellular survival with reasonable statistic. In consequence, the induction of radiation late effects, especially the induction of cancer, whereto the analysis of micronuclei [74, 75, 119], chromosomal aberrations [6, 41, 68, 112, 113] or remaining DNA double-strand breaks [7] may provide useful hints, is more relevant to estimate the risk of mammography. In doing so, RBE values between 1 and 2, not confirming the alarming RBE of about 4 published by Frankenberg *et al.* [32], were obtained by several groups comparing mammographic X-rays to higher energy photons. These results, including the new data obtained within this dissertation, were presented on the 2007 Retreat of the German Commission on Radiological Protection (SSK) [38]. There and in other committees, the different *in vitro* results were discussed, since RBE values higher than one still indicate an additional risk for woman that participate on a nationwide mammography screening program. Again, the validity of the *in vitro* data, even though consistent for the varying groups, remains unclear for the risk estimation of mammography screening. Controversial points are the complexity of the human body, the time frame of cancer induction (≈ 20 a), which is incompatible with the methodology of *in vitro* investigations, and the absence of significant epidemiological or clinical studies [46, 52]. Although the need of more detailed and target-oriented research was identified, reasonable precautions were taken anyway. Mammography screening is just indicated for women between 50 and 69 years by reason of the mean cancer incidence time, which would be an additional risk for younger women. The examination of younger or familial predisposed women is considered carefully [46] taken into account their higher risk for tumor induction. Moreover, the SSK recommends the independent evaluation of the German mammography screening program with respect to quality-assurance and risk-benefit analysis [39].

To sum up, the experiments and investigations realized within this particular issue of the present dissertation are a valuable contribution to the ongoing cost-benefit discussion on the mammography screening program. Our analysis of DSB related biological endpoints result in photon energy dependent RBE values that were similar to those published for other cell lines and to known RBE trends. For this reason, the *in vitro* data base is extended by an additional cell system, being more relevant for mammography; whereas the collected data provide useful hints on the underlying mechanism that lead to reduced survival or the incidence of cancer. Beside these meaningful results, necessary and important knowledge and experiences were acquired in the course of the realization of *in vitro* cell experiments at unconventional secondary radiation sources. The established dosimetric methods, sample setups and handling procedures can be transferred to other (unconventional) radiation qualities allowing for an efficient radiobiological characterization.

Exactly these experiences were required for the second issue of the present dissertation - the realization of radiobiological *in vitro* cell experiments with laser-accelerated electrons. These experiments were carried out at the Jena Titanium:Sapphire laser system representing so far an unconventional class of particle accelerators that are considered to replace the huge and cost-intensive proton and ion acceleration technique nowadays applied in radiotherapy. In general, these unconventional particle accelerators are based on high intensity lasers that allow for the acceleration of charged particles (electrons, protons, ions) in a very short distance, i.e., by means of ultrahigh acceleration gradients (section 3.2). The generated particle beams are delivered in the same time regime as the laser pulse (≈ 100 fs), a feature that result in ultrashort particle beam pulses with ultrahigh dose rates during the pulse exceeding those of conventional particle accelerators by several orders of magnitude. In consequence, one or just a couple of bunches (i.e. pulses) will be sufficient to deliver the therapeutic dose of about 2 Gy to the patient. Before such a new type of particle accelerator can be applied for medical purposes, the radiobiological consequences that arise from the unusual irradiation regime have to be investigated and compared to those of a continuous reference radiation. Therefore, the laser technology has to be adapted for radiobiological requirements, e.g., for the delivery of stable particle beams. Furthermore, the dosimetric properties have to be characterized very precisely in order to allow for radiobiological *in vitro* studies that aim on the determination of the RBE of laser-accelerated particles.

Worldwide first experiments in this direction were performed with JETI electrons already available with sufficient intensity and energy for cell irradiation, whereas available laser-driven proton [97, 117] and ion [43, 82] beams are still insufficient on both parameters. The electron beam was characterized and optimized with respect to radiobiological properties using the dosimetric methods implemented at ELBE and an in-house made Faraday cup. That is, the electron energy spectrum was limited by a low-energy cutoff (≈ 3 MeV) and the beam spot as well as the beam intensity were adjusted to sample size and the performance of cell irradiations in a reasonable time, respectively. However, the intensity and vice versa the pulse dose rate used for the cell experiments are not maximized, since the JETI system was not capable of providing single electron pulses with maximum intensity and a controlled pulse dose at the same time. In regard to patient treatment, especially the last point will be hazardous and consequently the pulse dose rate was adjusted to $\approx 10^9$ Gy/s anyhow exceeding those of conventional electron accelerators by several orders of magnitude.

Beside electron beam characterization, the readouts of the established beam and dose monitoring system were found to be linear correlated to the absolute dose administered at cell position. Hence, the system was applicable for a careful online control of the irradiation and enables the delivery of prescribed doses to the cells, a feature so far unique for laser-based particle accelerators. Furthermore, the linear dose correlations were confirmed for repeated experiment days indicating long-term stable and reproducible beam properties as demanded for radiobiological studies and being stringent for radiotherapy. Accordingly, the performance of systematic *in vitro* cell irradiations was feasible and a substantial progress from physical single-shot experiments with poor reproducibility towards medical application was achieved. Further advancements of the laser technology and the auxiliary equipment are expected to lead to even more stable and reproducible particle beams, necessary for

patient irradiation in future.

In parallel to the technological improvement, a test cell irradiation was performed at the JETI laser system followed by the worldwide first systematic radiobiological *in vitro* cell experiments with laser-accelerated electrons. The results obtained at the JETI system reveal a reduced biological effectiveness for laser-accelerated and therefore ultrashort pulsed electron beams in comparison to continuous 200 kV X-ray irradiation. This finding was consistent for the examined human tumor and human normal cell lines and for both analyzed biological effects, that is the cellular survival and the residual DNA double-strand breaks. Some decades afore similar experiments were accomplished addressing the influence of high pulse dose rates on the RBE of electrons [18, 87, 115]. For this purpose, conventional electron sources were adjusted to shorter electron pulses with maximum dose rates of up to 10^9 Gy/s during the pulse delivering the required dose to the cells in one single or a few electron pulses. As result, a comparable or even higher survival was achieved by comparing the pulsed radiation quality with a continuous reference source. Similarly, laser-driven bremsstrahlung possessing a maximum dose rate of 10^{13} Gy/s [49, 118] result also in a comparable or reduced biological effectiveness.

One hypothesis that might explain these findings is the influence of the ultrahigh pulse dose rate on the oxygen effect, which generally describes the influence of the oxygen content and supply on the radiation effect. Following radiation incidence, cellular oxygen becomes ionized and hence being able to ionize DNA components and to induce DNA damages. Moreover, the interaction of oxygen and DNA “radicals“, e.g., at DNA breaks, prevent the binding of repair proteins; open DNA ends are not connected and the DNA damage is “fixed“. For continuous cell irradiation the dose delivery is in such an extent that oxygen consumption and replacement by means of diffusion are balanced on a certain level. By contrast, for (ultra-)short pulsed particle beams with high dose rates during the pulse, the cellular oxygen is considerably reduced during the pulse and the pulse frequency might be shorter than the time needed to replace the cellular oxygen. In consequence, less cellular oxygen is available for subsequent particle pulses, which result in a reduced amount of induced and fixed, i.e., not repaired, DNA damages. This in turn might lead to a higher cellular survival and lower biological effectiveness, respectively.

Nevertheless, the other physical parameters of the laser-accelerated electron beam can also be hypothesized as potential reasons for the reduced biological effectiveness obtained in the framework of the present work. Compared to the 200 kV X-ray reference, the JETI electrons exhibit a lower mean dose rate, averaged over the irradiation time, but a several orders of magnitude higher pulse dose rate within the electron pulse. In addition, the energy spectra of 200 kV X-rays ($\approx 40 - 200$ keV) and JETI electrons (3 - 20 MeV) are significantly different resulting in varying LET influences. The individual contributions of these beam parameters on the biological effectiveness of laser-accelerated electrons are investigated in running experiments initiated by the findings of this dissertation.

In summary, this particular issue of the present dissertation was also carried out successfully. The technological improvement of the JETI laser system towards stable and reproducible cell irradiations was performed in such an extent that the delivery of prescribed doses is possible. Applying this unique feature first systematic *in vitro* studies were realized providing not only useful radio-

biological results, but also a feedback and starting points for further improvements of the laser and auxiliary technique. Outstanding questions on the potential reasons for the reduced biological effectiveness of laser-driven electrons will be answered in future. In the end, it can be concluded that laser-accelerated electrons will not provide any disadvantage for radiotherapy, that means tumor cells are killed under sparing of the normal tissue. Based on the successful results obtained with laser-accelerated electrons in the present work, future experiments will be concentrated on laser-accelerated protons and their potential role in radiotherapy.

5 Literature

- [1] DIN 6800-2, Procedures of dosimetry with probe type detectors for photon and electron radiation - Part 2: Ionization chamber dosimetry of high energy photon and electron radiation. 2008.
- [2] L. Anderson, C. Henderson, and Y. Adachi. Phosphorylation and rapid relocalization of 53BP1 to nuclear foci upon DNA damage. *Mol. Cell. Biol.*, 21(5):1719–29, 2001.
- [3] B. Azadegan. Investigation of planar channeling radiation on diamond and quartz crystals at electron energies between 14 and 34 MeV and probing the influence of ultrasonic waves on Channeling Radiation. *Dissertation, Dresden University of Technology*, 2007.
- [4] M. J. Berger, J. S. Coursey, M. A. Zucker, and J. Chang. ESTAR, PSTAR and ASTAR: Computer Programs for Calculating Stopping-Power and Range Tables for Electrons, Protons and Helium Ions (Version 1.2.3). <http://physics.nist.gov/star>, 2009.
- [5] E. H. Berkowitz. Dose compensation by differential pattern scanning. *US Patent*, 4449051, 1984.
- [6] E. Beyreuther, W. Dörr, A. Lehnert, E. Lessmann, and J. Pawelke. Relative biological effectiveness of 25 and 10 kV X-rays for the induction of chromosomal aberrations in two human mammary epithelial cell lines. *Radiat. Environ. Biophys.*, 48(3):333–40, 2009.
- [7] E. Beyreuther, E. Lessmann, J. Pawelke, and S. Pieck. DNA double-strand break signalling: X-ray energy dependence of residual co-localised foci of γ -H2AX and 53BP1. *Int. J. Radiat. Biol.*, 85(11):1042–50, 2009.
- [8] D. Blöcher. DNA double-strand break repair determines the RBE of alpha-particles. *Int. J. Radiat. Biol.*, 54(5):761–71, 1988.
- [9] J. J. Boei, S. Vermeulen, J. Fomina, and A. T. Natarajan. Detection of incomplete exchanges and interstitial fragments in X-irradiated human lymphocytes using a telomeric PNA probe. *Int. J. Radiat. Biol.*, 73(6):599–603, 1998.
- [10] J. J. Boei, S. Vermeulen, and A. T. Natarajan. Detection of chromosomal aberrations by fluorescence in situ hybridization in the first three postirradiation divisions of human lymphocytes. *Mutat. Res.*, 349(1):127–35, 1996.
- [11] D. J. Brenner, S. G. Sawant, M. P. Hande, et al. Routine screening mammography: how important is the radiation-risk side of the benefit-risk equation? *Int. J. Radiat. Biol.*, 78(12):1065–67, 2002.

-
- [12] M. J. Butson, T. Cheung, and P. K. N. Yu. Weak energy dependence of EBT Gafchromic film dose response in the 50 kVp-10 MVp X-ray range. *Appl. Radiat. Isot.*, 64(1):60–62, 2006.
- [13] M. J. Butson, P. K. N. Yu, T. Cheung, and P. Metcalfe. Radiochromic film for medical radiation dosimetry. *Mater. Sci. Eng. R*, 41(3-5):61–120, 2003.
- [14] Center for ultrafast optical science, College of Engineering, University of Michigan, USA. Wakefield electron acceleration.
www.engin.umich.edu/research/cuos/ResearchGroups/HSF/Research/, 23.03.2010.
- [15] C. Chiu, M. Fomytskyi, F. Grigsby, et al. Laser electron accelerators for radiation medicine: A feasibility study. *Med. Phys.*, 31(7):2042–52, 2004.
- [16] S. T. Chiu-Tsao, Y. Ho, R. Shankar, L. Wang, and L. B. Harrison. Energy dependence of response of new high sensitivity radiochromic films for megavoltage and kilovoltage radiation energies. *Med. Phys.*, 32(11):3350–54, 2005.
- [17] Committee to Assess Health Risks from Exposure to low levels of Ionizing Radiation. Health risks from exposure to low levels of ionizing radiation. *BEIR VII Phase 2*, 2006.
- [18] J. Cygler, N. V. Klassen, C. K. Ross, T. J. Bichay, and G. P. Raaphorst. The survival of aerobic and anoxic human glioma and melanoma cells after irradiation at ultrahigh and clinical dose rates. *Radiat. Res.*, 140(1):79–84, 1994.
- [19] L. A. R. da Rosa, M. Seidenbusch, and D. F. Regulla. Dose profile assessment at gold-tissue interfaces by using TSEE. *Radiat. Prot. Dosimetry*, 85(1-4):433–36, 1999.
- [20] S. Devic, J. Seuntjens, G. Hegyi, et al. Dosimetric properties of improved GafChromic films for seven different digitizers. *Med. Phys.*, 31(9):2392–2401, 2004.
- [21] S. Devic, J. Seuntjens, E. Sham, et al. Precise radiochromic film dosimetry using a flat-bed document scanner. *Med. Phys.*, 32(7):2245–53, 2005.
- [22] F. Di Martino, M. Giannelli, A. C. Traino, and M. Lazzeri. Ion recombination correction for very high dose-per-pulse high-energy electron beams. *Med. Phys.*, 32(7):2204–10, 2005.
- [23] G. Dietze and W. G. Alberts. Why it is advisable to keep $w_R = 1$ and $Q = 1$ for photons and electrons. *Radiat. Prot. Dosimetry*, 109(4):297–302, 2004.
- [24] J. S. Durham, S. E. Merwin, and K. L. Swinth. Skin dose evaluations using exoelectron dosimeters. *Radiat. Prot. Dosimetry*, 39(1-3):67–70, 1991.
- [25] A. A. Edwards, D. C. Lloyd, and R. J. Purrott. Radiation induced chromosome aberrations and the poisson distribution. *Radiat. Environ. Biophys.*, 16(2):89–100, 1979.
- [26] H. Eichenmüller. Thermally stimulated exoelectron emission (TSEE) from metal and semiconductor surfaces. *Radiat. Prot. Dosimetry*, 4(3-4):281–85, 1983.

-
- [27] I. Eke, V. Sandfort, K. Storch, et al. Pharmacological inhibition of EGFR tyrosine kinase affects ILK-mediated cellular radiosensitization in vitro. *Int. J. Radiat. Biol.*, 83(11-12):793–802, 2007.
- [28] J. Fan, W. Luo, E. Fourkal, et al. Shielding design for a laser-accelerated proton therapy system. *Phys. Med. Biol.*, 52:3913–30, 2007.
- [29] J. Faure, Y. Glinec, A. Pukhov, et al. A laser-plasma accelerator producing monoenergetic electron beams. *Nature*, 431:541–44, 2004.
- [30] Forschungszentrum Dresden-Rossendorf. Radiation source ELBE.
<http://www.fzd.de>, 24.03.2010.
- [31] E. Fourkal, B. Shahine, M. Ding, et al. Particle in cell simulation of laser-accelerated proton beams for radiation therapy. *Med. Phys.*, 29(12):2788–98, 2002.
- [32] D. Frankenberg, K. Kelnhofer, K. Bär, and M. Frankenberg-Schwager. Enhanced neoplastic transformations by mammography X rays relative to 200 kVp X rays: indication for a strong dependence on photon energy of the RBE(M) for various end points. *Radiat. Res.*, 157(1):99–105, 2002. Erratum in: *Radiat. Res.* 158(1), 126 (2002).
- [33] M. Fuss, E. Sturtewagen, C. De Wagter, and D. Georg. Dosimetric characterization of Gaf-Chromic EBT film and its implication on film dosimetry quality assurance. *Phys. Med. Biol.*, 52:4211–25, 2007.
- [34] F. Gabriel, P. Gippner, E. Grosse, et al. The Rossendorf radiation source ELBE and its FEL projects. *Nucl. Instrum. Methods Phys. Res. B*, 161-63:1143–47, 2000.
- [35] GEANT4 collaboration. GEANT4 a simulation toolkit. *Nucl. Instrum. Methods Phys. Res. A*, 506(3):250–303, 2003.
- [36] C. G. R. Geddes, C. Toth, J. v. Tilborg, et al. High-quality electron beams from a laser wakefield accelerator using plasma-channel guiding. *Nature*, 431:538–41, 2004.
- [37] German Commission on Radiological Protection. Evaluation of the relative biological effectiveness of different types of ionizing radiation. Statement of the German Commission on Radiological Protection. *Bonn: Urban & Fischer*, Band 53, 2005.
- [38] German Commission on Radiological Protection. Summary and Assessment of the 2007 Retreat of the German Commission on Radiological Protection: Biological Effectiveness of low doses of ionizing radiation [in German]. www.ssk.de, 2007.
- [39] German Commission on Radiological Protection. Evaluation of the effectiveness of quality-assured mammography screening in Germany. Statement of the German Commission on Radiological Protection. [in German]. www.ssk.de, 2008.

-
- [40] W. Göggelmann, C. Jacobsen, W. Panzer, et al. Re-evaluation of the RBE of 29 kV x-rays (mammography x-rays) relative to 220 kV x-rays using neoplastic transformation of human hybrid CGL1-hybrid cells. *Radiat. Environ. Biophys.*, 42(3):175–82, 2003.
- [41] C. Guerrero-Carbajal, A. A. Edwards, and D. C. Lloyd. Induction of chromosome aberration in human lymphocytes and its dependence on X ray energy. *Radiat. Prot. Dosimetry*, 106(2):131–35, 2003.
- [42] S. L. Hammond, R. G. Ham, and M. R. Stampfer. Serum-free growth of human mammary epithelial cells: rapid clonal growth in defined medium and extended serial passage with pituitary extract. *Proc. Natl. Acad. Sci. U.S.A.*, 81(17):5435–39, 1984.
- [43] B. M. Hegelich, B. J. Albright, J. Cobble, et al. Laser acceleration of quasi-monoenergetic MeV ion beams. *Nature*, 439:441–44, 2006.
- [44] T. Herrmann and M. Baumann. *Klinische Strahlenbiologie. 3. Aufl. Gustav Fischer Verlag*, 1997.
- [45] G. J. Heyes and A. J. Mill. The neoplastic transformation potential of mammography x rays and atomic bomb spectrum radiation. *Radiat. Res.*, 162(2):120–27, 2004.
- [46] G. J. Heyes, A. J. Mill, and M. W. Charles. Enhanced biological effectiveness of low energy X-rays and implications for the UK breast screening program. *Br. J. Radiol.*, 79(939):195–200, 2006.
- [47] B. Hidding, K.-U. Amthor, B. Liesfeld, et al. Generation of quasimonoenergetic electron bunches with 80-fs laser pulses. *Phys. Rev. Lett.*, 96(10):105004, 2006.
- [48] M. A. Hill. The variation in biological effectiveness of X-rays and gamma rays with energy. *Radiat. Prot. Dosimetry*, 112(4):471–81, 2004.
- [49] M. A. Hill, D. L. Stevens, S. J. Marsden, et al. Is the increase in relative biological effectiveness of high LET particles due to spatial or temporal effects? Characterization and OER in V79-4 cells. *Phys. Med. Biol.*, 47(19):3543–55, 2002.
- [50] G. Holzapfel. Zur Exoelektronen-Emission (Kramer-Effekt) von Berylliumoxid. *Dissertation, Technische Universität Berlin*, 1968.
- [51] J. H. Hubbell and S. M. Seltzer. Tables of X-Ray Mass Attenuation Coefficients and Mass Energy-Absorption Coefficients (version 1.4). <http://physics.nist.gov/xaamdi>, 2004.
- [52] N. Hunter and C. R. Muirhead. Review of the relative biological effectiveness dependence on linear energy transfer for low-LET radiations. *J. Radiol. Prot.*, 29(1):5–21, 2009.
- [53] Y. Ichijima, R. Sakasai, N. Okita, et al. Phosphorylation of histone H2AX at M phase in human cells without DNA damage response. *Biochem. Biophys. Res. Commun.*, 336(3):807–12, 2005.

-
- [54] International Atomic Energy Agency. Biological Dosimetry: Chromosomal aberration analysis for dose assessment. *Technical Report Series No. 260*, 1986.
- [55] International Commission on Radiation Units and Measurements. Linear Energy Transfer. *ICRU Report*, 16, 1970.
- [56] International Commission on Radiological Protection. ICRP Publication 60: 1990 Recommendations of the International Commission on Radiological Protection. *Annals of the ICRP*, 21(1-3), 1991.
- [57] International Commission on Radiological Protection. ICRP Publication 92: Relative Biological Effectiveness (RBE), Quality Factor (Q), and Radiation Weighting Factor (w_R). *Annals of the ICRP*, 33(4), 2003.
- [58] International Commission on Radiological Protection. ICRP Publication 103: The 2007 Recommendations of the International Commission on Radiological Protection. *Annals of the ICRP*, 37(2-4), 2007.
- [59] International Specialty Products (ISP). Gafchromic® EBT: self-developing film for radiotherapy dosimetry. *International Specialty Products Inc., Wayne, NJ, USA*, 2007.
- [60] K. K. Kainz, K. R. Hogstrom, J. A. Antolak, et al. Dose properties of a laser accelerated electron beam and prospects for clinical application. *Med. Phys.*, 31(7):2053–67, 2004.
- [61] P. Kegel, E. Riballo, M. Kühne, P. A. Jeggo, and M. Löbrich. X-irradiation of cells on glass slides has a dose doubling impact. *DNA repair (Amst.)*, 6(11):1692–97, 2007.
- [62] A. Kinner, W. Wu, C. Staudt, and G. Iliakis. γ -H2AX in recognition and signaling of DNA double-strand breaks in the context of chromatin. *Nucleic Acids Res.*, 36(17):5678–94, 2008.
- [63] W. Kottler, D. Lerch, W. Kriegseis, A. Scharmann, and B. Wörner. Evaporated beryllium oxide films for TSEE dosimetry. *Nucl. Instrum. Methods Phys. Res.*, 175(1):101–03, 1980.
- [64] J. Kramer. Exoelektronen-Dosimeter für Röntgen- und Gammastrahlen. *Z. Angew. Phys.*, 20:411–17, 1966.
- [65] H. Krieger. *Grundlagen der Strahlungsphysik und des Strahlenschutzes. [in German]*. B.G. Teubner, Wiesbaden., 1 edition, 2004.
- [66] W. Kriegseis, M. Petel, A. Scharmann, and C. U. Wieters. Potentials of TSEE for beta ray dosimetry. *Radiat. Prot. Dosimetry*, 14(2):151–55, 1986.
- [67] W. Kriegseis, K. Rauber, A. Scharmann, et al. Dependence of the TSEE response of BeO thin films on photon energy and composition of cover materials. *Radiat. Prot. Dosimetry*, 47(1-4):143–46, 1993.

-
- [68] M. Krumrey, G. Ulm, and E. Schmid. Dicentric chromosomes in monolayers of human lymphocytes produced by monochromatized synchrotron radiation with photon energies from 1.83 keV to 17.4 keV. *Radiat. Environ. Biophys.*, 43(1):1–6, 2004.
- [69] M. Löbrich and P. A. Jeggo. The impact of negligent G2/M checkpoint on genomic instability and cancer induction. *Nat. Rev. Cancer*, 7(11):861–69, 2007.
- [70] E. L. Leatherbarrow, J. V. Harper, F. A. Cucinotta, and P. O’Neill. Induction and quantification of gamma-H2AX foci following low and high LET-irradiation. *Int. J. Radiat. Biol.*, 82(2):111–18, 2006.
- [71] K. W. D. Ledingham, W. Galster, and R. Sauerbrey. Laser-driven proton oncology - a unique new cancer therapy? *Br. J. Radiol.*, 80(959):855–58, 2007.
- [72] W. P. Leemans, B. Nagler, A. J. Gonsalves, et al. GeV electron beams from a centimetre-scale accelerator. *Nat. Phys.*, 2:696–99, 2006.
- [73] A. Lehnert. Establishment of the physical and technical prerequisites for the determination of the relative biological effectiveness of low-energy monochromatic X-rays. *Wiss.-Tech. Berichte*, FZR-441, 2005.
- [74] A. Lehnert, W. Dörr, E. Lessmann, and J. Pawelke. RBE of 10 kV X rays determined for the human mammary epithelial cell line MCF-12A. *Radiat. Res.*, 169(3):330–36, 2008.
- [75] A. Lehnert, E. Lessmann, J. Pawelke, and W. Dörr. RBE of 25 kV X-rays for the survival and induction of micronuclei in the human mammary epithelial cell line MCF-12A. *Radiat. Environ. Biophys.*, 45(4):253–60, 2006.
- [76] J. Lesz, A. Scharmann, and G. Holzapfel. Connected TSEE/OSEE readouts of BeO thin-film dosimeter. *Jpn. J. Appl. Phys.*, 24(Suppl. 24-4):259–61, 1985.
- [77] M. Fenech. The cytokinesis-block micronucleus technique: a detailed description of the method and its application to genotoxicity studies in human populations. *Mutat. Res.*, 285(1):35–44, 1993.
- [78] C.-M. Ma, I. Velchev, T. Lin, et al. Laser-proton acceleration for radiation therapy. *Medical Physics, 2007 AAPM Annual Meeting Program*, 34(6):2550, 2007.
- [79] S. H. MacPhail, J. P. Banáth, Y. Yu, E. Chu, and P. L. Olive. Cell cycle-dependent expression of phosphorylated histone H2AX: reduced expression in unirradiated but not X-irradiated G1-phase cells. *Radiat. Res.*, 159(6):759–67, 2003.
- [80] S. H. MacPhail, J. P. Banáth, Y. Yu, et al. Expression of phosphorylated histone H2AX in cultured cell lines following exposure to X-rays. *Int. J. Radiat. Biol.*, 79(5):351–58, 2003.
- [81] P. Maine, D. Strickland, P. Bado, M. Pessot, and G. Mourou. Generation of ultrahigh peak power pulses by chirped pulse amplification. *IEEE J. Quantum Electron.*, 24(2):398–403, 1988.

-
- [82] A. Maksimchuk, S. Gu, K. Flippo, D. Umstädter, and V. Bychenkov. Forward ion acceleration in thin films driven by a high-intensity laser. *Phys. Rev. Lett.*, 84(18):4108–11, 2000.
- [83] V. Malka, S. Fritzler, E. Lefebvre, E. d’Humières, and R. Ferrand. Practicability of proton-therapy using compact laser systems. *Med. Phys.*, 31(6):1587–92, 2004.
- [84] S. P. D. Mangles, C. D. Murphy, Z. Najmudin, et al. Monoenergetic beams of relativistic electrons from intense laser-plasma interactions. *Nature*, 431:535–38, 2004.
- [85] E. Marková, N. Schultz, and I. Y. Belyaev. Kinetics and dose-response of residual 53BP1/gamma-H2AX foci: co-localization, relationship with DSB repair and clonogenic survival. *Int. J. Radiat. Biol.*, 83(5):319–29, 2007.
- [86] M. Mestres, M. R. Caballín, L. Barrios, M. Ribas, and J. F. Barquinero. RBE of X rays of different energies: a cytogenetic evaluation by FISH. *Radiat. Res.*, 170(1):93–100, 2008.
- [87] H. B. Michaels, E. R. Epp, C. C. Ling, and E. C. Peterson. Oxygen sensitization of CHO cells at ultrahigh dose rates: Prelude to oxygen diffusion studies. *Radiat. Res.*, 76(3):510–21, 1978.
- [88] Nature Education. Chromatin-has-highly-complex-structure-with-several-levels of organization. <http://www.nature.com/scitable/content/Chromatin-has-highly-complex-structure-with-several-18847>, 06.04.2010.
- [89] W. Neubert, B. Azadegan, W. Enghardt, et al. Electron beam monitoring for channeling radiation measurements. *Nucl. Instrum. Methods Phys. Res. B*, 254(2):319–28, 2007.
- [90] W. Neubert, W. Enghardt, U. Lehnert, et al. *Advanced Monte Carlo for Radiation Physics, Particle Transport Simulation and Applications: Optimization of a tunable quasi-monochromatic x-ray source for cell irradiations. Monte Carlo 2000 Conference, Lisbon, Portugal*. Springer, Berlin - Heidelberg - New York, 2001.
- [91] A. Niroomand-Rad, C. R. Blackwell, B. M. Coursey, et al. Radiochromic film dosimetry: Recommendations of AAPM Radiation Therapy Committee Task Group 55. *Med. Phys.*, 25(11):2093–2115, 1998.
- [92] H. Norppa and G. C.-M. Falck. What do human micronuclei contain? *Mutagenesis*, 18(3):221–33, 2003.
- [93] A. Panteleeva, D. Slonina, K. Brankovic, et al. Clonogenic survival of human keratinocytes and rodent fibroblasts after irradiation with 25 kV x-rays. *Radiat. Environ. Biophys.*, 42(2):95–100, 2003.
- [94] R. J. Pauley, T. J. Paine, and H. D. Soule. Immortal human mammary epithelial cell sublines. *US Patent*, 5206165, 1993.
- [95] P. Perry and S. Wolff. New Giemsa method for the differential staining of sister chromatids. *Nature*, 251(5471):156–58, 1974.

-
- [96] L. M. Persson, B. K. Lind, M. R. Edgren, I. Hedlöf, and A. Brahme. RBE of 50 MV scanned bremsstrahlung beams determined using clonogenic assay. *Int. J. Radiat. Biol.*, 78(4):275–84, 2002.
- [97] S. M. Pfothenauer, O. Jäckel, A. Sachtleben, et al. Spectral shaping of laser generated proton beams. *New J. Phys.*, 10:033034, 2008.
- [98] A. L. Ponomarev, S. V. Costes, and F. A. Cucinotta. Stochastic properties of radiation-induced DSB: DSB distributions in large scale chromatin loops, the HPRT gene and within the visible volumes of DNA repair foci. *Int. J. Radiat. Biol.*, 84(11):916–29, 2008.
- [99] I. Rappold, K. Iwabuchi, T. Date, and J. Chen. Tumor suppressor p53 binding protein 1 (53BP1) is involved in DNA damage-signaling pathways. *J. Cell Biol.*, 153(3):613–20, 2001. Erratum in: *J. Cell Biol.* 154(2), 469 (2001).
- [100] D. F. Regulla and U. Leischner. Comparing interface dosimetry with conventional methods and TSEE. *Radiat. Prot. Dosimetry*, 4(3-4):174–76, 1983.
- [101] C. Richter, J. Woithe, L. Karsch, and J. Pawelke. Energy dependence of EBT-1 radiochromic film response for photon (10 kVp-15 MVp) and electron beams (6-18 MeV) readout by a flatbed scanner. *Med. Phys.*, 36(12):5506–14, 2009.
- [102] A. Rink, I. A. Vitkin, and D. A. Jaffray. Energy dependence (75 kVp to 18 MV) of radiochromic films assessed using a real-time optical densitometer. *Med. Phys.*, 34(2):458–63, 2007.
- [103] W. C. Röntgen. On a new kind of rays. *Nature*, 53(1369):274–76, 1896.
- [104] E. P. Rogakou, D. R. Pilch, A. H. Orr, V. S. Ivanova, and W. M. Bonner. DNA double-stranded breaks induce histone H2AX phosphorylation on serine 139. *J. Biol. Chem.*, 273(10):5858–68, 1998.
- [105] H. Roos and E. Schmid. Analysis of chromosome aberrations in human peripheral lymphocytes induced by 5.4 keV x-rays. *Radiat. Environ. Biophys.*, 36(4):251–54, 1998.
- [106] K. Rothkamm and M. Löbrich. Evidence for a lack of DNA double-strand break repair in human cells exposed to very low x-ray doses. *Proc. Natl. Acad. Sci. U.S.A.*, 100(9):5057–62, 2003.
- [107] M. S. Sasaki, S. Endo, Y. Ejima, et al. Effective dose of A-bomb radiation in Hiroshima and Nagasaki as assessed by chromosomal effectiveness of spectrum energy photons and neutrons. *Radiat. Environ. Biophys.*, 45(2):79–91, 2006.
- [108] M. S. Sasaki, K. Kobayashi, K. Hieda, et al. Induction of chromosome aberrations in human lymphocytes by monochromatic X-rays of quantum energy between 4.8 and 14.6 keV. *Int. J. Radiat. Biol.*, 56(6):975–88, 1989.
- [109] W. H. Scharf. Biomedical Particle Accelerators. *AIP Press, New York*, 1994.

-
- [110] H.-P. Schlenvoigt, K. Haupt, A. Debus, et al. A compact synchrotron radiation source driven by a laser-plasma wakefield accelerator. *Nat. Phys.*, 4(2):130–33, 2008.
- [111] E. Schmid. Verifizierung der unterschiedlichen biologischen Wirksamkeit von Photonen im Energiebereich von 10 keV - 6 MeV mittels onkogener Transformationsraten an Maus-Embryofibroblasten und in der menschlichen CGL 1 - Hybridzelllinie. *Schriftenreihe Reaktorsicherheit und Strahlenschutz*, BMU-2005-657, 2005.
- [112] E. Schmid, M. Krumrey, G. Ulm, H. Roos, and D. Regulla. The maximum low-dose RBE of 17.4 and 40 keV monochromatic X rays for the induction of dicentric chromosomes in human peripheral lymphocytes. *Radiat. Res.*, 160(5):499–504, 2003.
- [113] E. Schmid, D. Regulla, H.-M. Kramer, and D. Harder. The effect of 29 kV X rays on the dose response of chromosome aberrations in human lymphocytes. *Radiat. Res.*, 158(6):771–77, 2002.
- [114] E. Schmid, D. Schlegel, S. Guldbakke, R.-P. Kapsch, and D. Regulla. RBE of nearly monoenergetic neutrons at energies of 36 keV-14.6 MeV for induction of dicentrics in human lymphocytes. *Radiat. Environ. Biophys.*, 42(2):87–94, 2003.
- [115] R. J. Schulz, R. Nath, and J. R. Testa. The effects of ultra-high dose rates on survival and sublethal repair in Chinese-hamster cells. *Int. J. Radiat. Biol. Relat. Stud. Phys. Chem. Med.*, 33(1):81–88, 1978.
- [116] D. Schulz-Ertner, T. Haberer, O. Jäkel, et al. Radiotherapy for chordomas and low-grade chondrosarcomas of the skull base with carbon ions. *Int. J. Radiat. Oncol. Biol. Phys.*, 53(1):36–42, 2002.
- [117] H. Schwoerer, S. Pfoth, O. Jäkel, et al. Laser-plasma acceleration of quasi-monoenergetic protons from microstructured targets. *Nature*, 439:445–48, 2006.
- [118] K. Shinohara, H. Nakano, N. Miyazaki, M. Tago, and R. Kodama. Effects of single-pulse (≤ 1 ps) X-rays from laser-produced plasmas on mammalian cells. *J. Radiat. Res. (Tokyo)*, 45(4):509–14, 2004.
- [119] D. Slonina, K. Spekl, A. Panteleeva, et al. Induction of micronuclei in human fibroblasts and keratinocytes by 25 kV x-rays. *Radiat. Environ. Biophys.*, 42(1):55–61, 2003.
- [120] M. R. Stampfer and J. C. Bartley. Induction of transformation and continuous cell lines from normal human mammary epithelial cells after exposure to benzo[a]pyrene. *Proc. Natl. Acad. Sci. U.S.A.*, 82(8):2394–98, 1985.
- [121] M. R. Stampfer and P. Yaswen. Culture models of human mammary epithelial cell transformation. *J. Mammary Gland Biol. Neoplasia*, 5(4):365–78, 2000.

-
- [122] Strahlenschutzkommission des BMU. Brustkrebs- und Zervixkarzinom-Screening. *Berichte der Strahlenschutzkommission*, Heft 42, 2004.
- [123] R. Svensson, B. Lind, and A. Brahme. Beam characteristics and clinical possibilities of a new compact treatment unit design combining narrow pencil beam scanning and segmental multileaf collimation. *Med. Phys.*, 25(12):2358–69, 1998.
- [124] T. Tajima and J. M. Dawson. Laser electron-accelerator. *Phys. Rev. Lett.*, 43(4):267–70, 1979.
- [125] C. Tillman, G. Grafström, A.-C. Jonsson, et al. Survival of mammalian cells exposed to ultrahigh dose rates from a laser-produced plasma x-ray source. *Radiology*, 213(3):860–65, 1999.
- [126] N. Tomic, M. Gosselin, J. F. Wan, et al. Verification of cell irradiation dose deposition using a radiochromic film. *Phys. Med. Biol.*, 52(11):3121–31, 2007.
- [127] J. Torudd, M. Protopopova, R. Sarimov, et al. Dose-response for radiation-induced apoptosis, residual 53BP1 foci and DNA-loop relaxation in human lymphocytes. *Int. J. Radiat. Biol.*, 81(2):125–38, 2005.
- [128] University of Leicester. Genetics Education Networking for Innovation and Excellence (GENIE). <http://www.le.ac.uk/ge/genie/vgec/introduction/index.html>, 23.03.2010.
- [129] W. Wagner, B. Azadegan, M. Sobiella, et al. An intense channeling radiation source. *Nucl. Instrum. Methods Phys. Res. B*, 266(2):327–34, 2008.
- [130] B. Wang, S. Matsuoka, P. B. Carpenter, and S. J. Elledge. 53BP1, a mediator of the DNA damage checkpoint. *Science*, 298(5597):1435–38, 2002.
- [131] A. Yogo, K. Sato, M. Nishikino, et al. Application of laser-accelerated protons to the demonstration of DNA double-strand breaks in human cancer cells. *Appl. Phys. Lett.*, 94:181502, 2009.
- [132] K. Zeil, E. Beyreuther, E. Lessmann, W. Wagner, and J. Pawelke. Cell irradiation setup and dosimetry for radiobiological studies at ELBE. *Nucl. Instrum. Methods Phys. Res. B*, 267(14):2403–10, 2009.

Acknowledgments

The present dissertation is based on the research I have carried out at the Institute of Radiation Physics at the Forschungszentrum Dresden-Rossendorf in close cooperations with the other OncoRay partners, especially the University hospital Carl Gustav Carus at the Technische Universität Dresden. I am very grateful to all people that have contributed to the realization of this work. It is not possible to enumerate all of them, but I would like to thank some people in particular.

First of all I would like to thank Prof. Michael Schlömann, who gave me the possibility to carry out my Ph.D. graduation at the Technische Universität Bergakademie Freiberg. Thanks also to Prof. Sepp Unterricker for his efforts and his ongoing interest on my Ph.D. work. I acknowledge Prof. Wolfgang Enhardt for the possibility to carry out my doctoral studies in Rossendorf, for the scientific incentives and his support during the last years.

My most sincere thanks are addressed to my supervisor Dr. Jörg Pawelke, without whom the present dissertation would not have been possible. Dr. Pawelke not only introduced me in radiation physics, he also provided valuable scientific guidance, time for fruitful discussions and continuous motivation.

I am very grateful to Elisabeth Lessmann, whose assistance during the radiobiological studies was essential and who exercised great patience in introducing me to cellular work. Moreover, I thank Dr. Anna Lehnert for her guidance at the beginning of my Ph.D. time and her help and motivation during my research.

My thank goes also to the former and the present heads of the Institute of Radiation Physics at the Forschungszentrum Dresden-Rossendorf, Prof. Eckart Grosse and Prof. Thomas Cowan, which gave me the possibility to carry out my research. My colleagues Dr. Behnam Azadegan, Dr. Fine Fiedler, Dr. Daniela Kunath, Kristin Laube, Marlen Prieognitz, Jenny Philipp, Sebastian Schöne, Dr. Georgy Shakirin and Dr. Wolfgang Wagner from the Division of Radiation Physics I thank for the pleasant atmosphere and helpful suggestions. From the Laser Particle Acceleration group of the Forschungszentrum Dresden-Rossendorf I want to mention Karl Zeil, who has done much of the work associated with the EBT films. I thank Manfred Sobiella and the Technical Department for their assistance, and the ELBE crew for their interest and support.

I am also grateful to my colleagues of the onCOOPtics group, namely Dr. Leonhard Karsch, Lydia Laschinsky, Dr. Doreen Naumburger, Christian Richter, Michael Schürer and, again, Elisabeth Lessmann and Dr. Jörg Pawelke, for the successful laser experiments. Moreover I thank Dr. Hans-Peter Schlenvoigt, Prof. Malte Kaluza and Maria Nicolai from the Institut für Optik und Quantenelektronik at the Friedrich-Schiller-Universität in Jena for their operation and assistance at JETI. From the OncoRay groups I want to mention Katja Storch for introducing me in immunochemical detection and Prof. Michael Baumann for his motivation. I am also thankful to Prof. Wolfgang Dörr and his

Acknowledgments

group for the good cooperation.

My special thanks go to my family for their support and to my friends for their assistance and motivation during my Ph.D. time. Finally, I want to express my gratitude to my husband Markus for his lovingly attention and steady encouragement during the ups and downs of my Ph.D. time. Mathilda, thank you for giving me unlimited happiness and adding a new dimension to our life.

Declaration

Hiermit versichere ich, dass ich die vorliegende Arbeit ohne unzulässige Hilfe Dritter und ohne Benutzung anderer als der angegebenen Hilfsmittel angefertigt habe; die aus fremden Quellen direkt oder indirekt übernommenen Gedanken sind als solche kenntlich gemacht.

Bei der Auswahl und Auswertung des Materials sowie bei der Herstellung des Manuskripts habe ich Unterstützungsleistungen von folgenden Personen erhalten: siehe Danksagung

Weitere Personen waren an der Abfassung der vorliegenden Arbeit nicht beteiligt. Die Hilfe eines Promotionsberaters habe ich nicht in Anspruch genommen. Weitere Personen haben von mir keine geldwerten Leistungen für Arbeiten erhalten, die nicht als solche kenntlich gemacht worden sind.

Die Arbeit wurde bisher weder im Inland noch im Ausland in gleicher oder ähnlicher Form einer anderen Prüfungsbehörde vorgelegt.

Dresden,